12-21

SANDIA REPORT

SAND95–2730 • UC–721
Unlimited Release
Printed December 1995

Long-Term Modeling of Glass Waste in Portland Cement- and Clay-Based Matrics

H. W. Stockman, K. L. Nagy, C. E. Morris

Prepared by
Sandia National Laboratories
Albuquerque, New Mexico 87185 and Livermore, California 94550
for the United States Department of Energy
under Contract DE-AC04-94AL85000

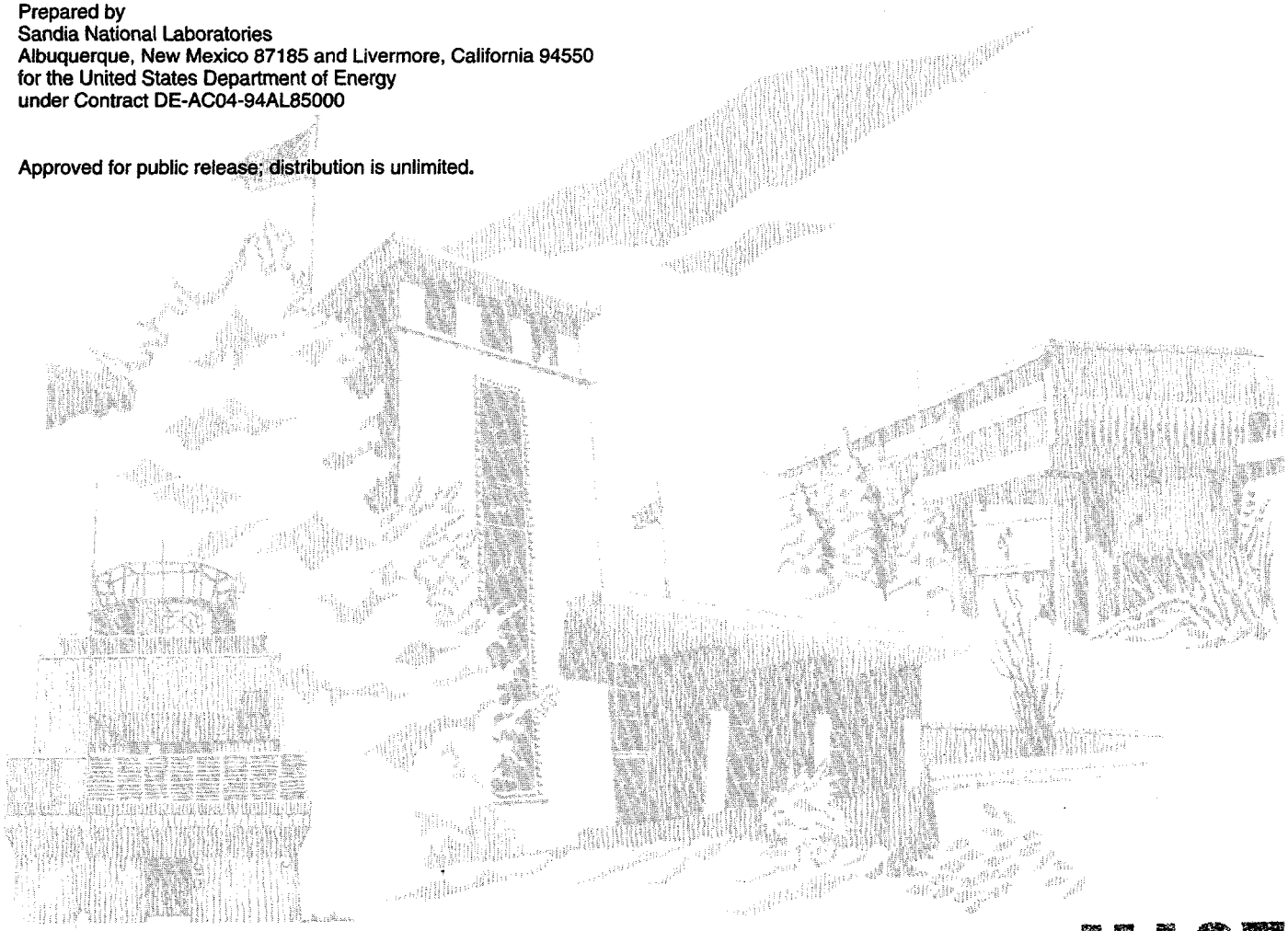

Issued by Sandia National Laboratories, operated for the United States Department of Energy by Sandia Corporation.

Available to DOE and DOE contractors from
Office of Scientific and Technical Information
PO Box 62
Oak Ridge, TN 37831

Prices available from (615) 576-8401, FTS 626-8401

Available to the public from
National Technical Information Service
US Department of Commerce
5285 Port Royal Rd
Springfield, VA 22161

NTIS price codes
Printed copy: A05
Microfiche copy: A01

Distribution
Category UC-721

SAND95-2730
Unlimited Release
Printed December 1995

Long-Term Modeling of Glass Waste in Portland Cement- and Clay-Based Matrices

H.W. Stockman and K.L. Nagy
Geochemistry Department 6118
Sandia National Laboratories
Albuquerque, NM 87185-0750

C.E. Morris
Dept. of Civil and Mining Engineering
University of Wollongong
Wollongong, NSW
Australia, 2522

Abstract

A set of "templates" was developed for modeling waste glass interactions with cement-based and clay-based matrices. The templates consist of a modified thermodynamic database, and input files for the EQ3/6 reaction path code, containing embedded rate models and compositions for waste glass, cement, and several pozzolanic materials. Significant modifications were made in the thermodynamic data for Th, Pb, Ra, Ba, cement phases, and aqueous silica species. It was found that the cement-containing matrices could increase glass corrosion rates by several orders of magnitude (over matrixless or clay matrix systems), but they also offered the lowest overall solubility for Pb, Ra, Th and U. Addition of pozzolans to cement decreased calculated glass corrosion rates by up to a factor of 30. It is shown that with current modeling capabilities, the "affinity effect" cannot be trusted to passivate glass if nuclei are available for precipitation of secondary phases that reduce silica activity.

Acknowledgments

The authors thank Tom Wolery, Bill Bourcier and Jim Johnson of Lawrence Livermore National Laboratory for helpful advice regarding EQ3/6 and the thermochemical database, and many personnel at the Fernald Environmental Restoration and Management Corporation (FERMCo) for information on the composition of waste glasses. L.A. Dawson provided insights on DOE waste streams in the early stages of the investigation, and Margaret S.Y. Chu initiated the project. This project was supported by the Laboratory Directed Research and Development Department at Sandia National Laboratories.

Contents

List of Tables

List of Figures

1. Introduction and Goals of Project

The primary goal of this project is to reduce the uncertainty inherent in modeling the long-term behavior of radioactive waste sites, including uncertainty in the release of radionuclides to the environment. Much of this uncertainty traces to the rate of degradation of the waste form, and the many factors that can affect radionuclide solubility in groundwater, once the waste form breaks down or dissolves. In this report, we focus on the degradation of glass-based waste forms. Our approach is to examine critically and improve the thermodynamic and kinetic data available for modeling, and to use reaction path runs to determine which factors have the greatest effect on the uncertainty of the calculated degradation rates and solubilities as functions of time. We recognize that our goal is a "moving target", since the design of waste sites and forms is constantly changing, and new rate and thermochemical data become available each year. To deal with inevitable change, we have developed a set of reaction path "templates" for modeling the interactions of glass waste forms with water and solid matrices based on clays, ash additives, and ordinary portland cement (OPC). Our ultimate intent is to anticipate DOE's plans for disposal of low level, orphan, and "special case" wastes, and to provide guidance for the choice of disposal configurations and matrix.

As this report will show, subtle changes in the composition of matrix materials can have dramatic effects on the predicted degradation rate of glass and radionuclide solubility. Perhaps more important, matrices that induce desirable behavior in the short-term (1 to 10 years period) may have such uncertain behavior in the long term, that they offer no real advantage from the point of view of performance assessment. It should also become apparent that modeling the long-term performance of glassy waste materials is not trivial, and requires careful selection of thermodynamic data, and care in setting up a problem that is both solvable and realistic. Yet the long-term modeling of such systems is absolutely necessary, because disposal of wastes from U.S. National Laboratories and former uranium processing and weapons production sites will likely generate large amounts of radioactive glass and related materials; the Hanford site alone is expected to produce over 421,000 tonnes (Orme, 1995).

This report discusses the development of the templates, documents the choice of thermodynamic and kinetic data, illustrates use of the templates with a wide range of sample matrices, and shows how uncertainty in key parameters affects the predictions of radionuclide solubility and glass degradation. All reaction path calculations were performed with a modified version of the EQ3/6 code suite v7.2a (Wolery, 1992). The calculations use a hypothetical glass, based on compositions proposed for disposal of wastes from the Fernald site in Ohio (DOE, 1993). The templates are essentially EQ3/6 input files (with the embedded rate laws) and the modified thermochemical database, and are available from the authors upon request. The results of the EQ3/6 runs are used to evaluate the relative merits of different matrices, and suggestions are made for specific experimental work that could reduce the uncertainty in long-term modeling.

2. Sample Problem: The Fernald Glasses

2.1 History and Glass Composition

The Fernald waste was produced in the 1940's and 1950's from processing of pitchblende ores from the Shinkolobwe mine in the Belgian Congo, and the Rum Jungle and Radium Hill mines in Australia (DOE, 1993). Some of the ore-processing wastes were converted to slurries and transferred to "Silos" 1 and 2 at the Fernald site, where excess water was decanted. Other wastes were calcined and pneumatically transferred to Silo 3. From a radiological standpoint, the principal isotopes in the waste are ^{210}Pb, ^{226}Ra, ^{228}Th, ^{230}Th (the parent of ^{226}Ra), ^{232}Th, ^{234}U, ^{235}U and ^{238}U. The wastes also contain substantial amounts of Pb, Ba, P and S from chemical processing (*e.g.*, $BaSO_4$ coprecipitation of Ra, or tributyl phosphate separation of Th), and lighter elements from the addition of clays and sorbants.

The glass compositions assumed for this study are given in Table 1, along with OPC and ash compositions. The glass data are idealizations of two extreme compositions (sequence A and sequence C; DOE, 1993). The idealized sequence A glass is typical of high-Na, moderate-Si glasses proposed for other waste streams (*e.g.* Bourcier, 1994), apart from the unusually high Pb and Ba contents. The idealized sequence C glass is not typical of any other proposed waste glasses we are aware of, and is characterized by low Si and high P contents. It must be noted that since DOE's 1993 study, new lower-Na compositions have been proposed for the sequence A glass (Merrill and Whittington, 1994). The new compositions have lower leach rates (a factor of $\approx 1/2$ for Si). Therefore, based on the compositions given in Table 1, results from the present study should conservatively overpredict the rate of glass degradation. After melting, the waste glasses are formed into flattened ellipsoids ("gems") massing approximately 4 to 5 grams; when closest-packed, the gems have $\approx$ 20 to 26% void space. The gems may subsequently be packed into concrete boxes with internal dimensions of 137 cm × 127 cm × 135 cm and wall thicknesses of 13 cm. At the time of burial, the gems may be emplaced in the boxes, or simply poured into trenches and backfilled with alluvium.

2.2 Likely Disposal Environment

Current plans (Cochran *et al.*, 1995) call for disposal of the Fernald glass at the Radioactive Waste Management Site (RWMS), located in the Nevada Test Site (NTS) in Southern Nevada. The waste may be placed either in 40 m deep boreholes, or 7 m deep trenches dug in the alluvium. This area is hot and arid ($\approx$10 cm precipitation/year), and there is evidence that the net flux of water (at depth below $\approx$ 10 m) is upward, reflecting gradual evaporation of water stored in the lower alluvium since the last ice age. The alluvium itself is derived from silicic to intermediate volcanics, consisting of quartz, feldspar and cristobalite in devitrified volcanic glass, swelling clays and sporadic clinoptilolite, and calcite and gypsum caliche (Jones, 1982; Stockman *et al.*, 1995). The water table is over 250 m below the surface, so there would be at least 210 m between the bottom of the proposed boreholes and the water table.

While the NTS site is arid, this does not mean that water can be excluded from the analysis of waste performance. Even in the desert, the humidity reaches nearly 100% within a meter of the surface, and our analyses show the alluvium contains up to 6%

Table 1. Idealized Compositions*.

Component	Wt % in Seq A Glass	Wt % in Seq C Glass	Wt % in OPC	Wt % in Fly Ash	Wt % in Fuel Ash
SiO_2	54.3	30.0	22.4	48.0	52.9
Na_2O	15.2	6.00	0.16	1.90	0.44
PbO	10.6	0.19	--	--	--
Fe_2O_3	4.90	9.40	3.05	15.8	7.07
MgO	1.50	10.2	1.23	1.10	1.71
Al_2O_3	3.20	20.0	5.58	19.1	31.3
BaO	5.40	0.03	--	--	--
P_2O_5	0.73	9.40	--	--	--
CaO	1.30	4.70	65.1	9.70	4.86
K_2O	0.75	1.80	0.24	1.90	0.88
UO_2	0.19	0.34	--	--	--
ThO_2	0.19	0.32	--	--	--
B_2O_3	0.00	5.00	--	--	--
RaO	3.16e-5	1.13e-7	--	--	--
S	1.00	1.00	0.85	1.00	0.33

*Because of varied assumptions about oxidation state of Fe and S, totals do not necessarily add to 100%. Sources: Seq A and Seq C glass, DOE (1993); OPC, Lea (1970), and Yilmaz *et al.* (1991) for typical Na and K content; Fly ash is a composite of rows 10 and 11 in Lea (1970) table 71, equimolar Na and K assumed; Fuel ash is a composite from Dhir and Byars (1993).

water (released at 60°C) at depths below ≈ 2 m. Performance assessment must consider the possibility that future climates will induce a greater (or at least downward) flux of water, due to lower temperatures or increased precipitation. Lastly, there is a strong possibility that future wastes of similar composition will be destined for burial in wetter, eastern climates, to satisfy political requirements.

2.3 Pros and Cons of Matrix Materials

There are good reasons to add matrix material, such as clays or cements, to granular waste forms. For fine powders produced by ashing or calcining, a cementitious matrix greatly

reduces the leachable surface area. Encasement in cement also decreases the risk of losing the finely powdered waste during transport from the generation site to the burial site. Monolithic waste forms are also easier to transport and retrieve, should retrievability be a condition of disposal. Cements and clays reduce the permeability of the bulk material, decreasing the risk of intrusion by liquid water, and decreasing the emanation rate of radon. Matrix materials such as zeolites and swelling clays strongly sorb some radionuclides, reducing the rate of loss to the accessible environment.

Unfortunately, there are negative aspects of matrix materials. When a coarsely granular material (such as glass waste pellets) is placed in a fine-grained alluvium, the interface between becomes a capillary barrier (Stormont, 1995), preventing flow of water into the coarse material. Adding an unconsolidated matrix removes this barrier, allowing water to be held against the waste. However, if the granular waste is simply poured into trenches or boreholes, sand and silt will eventually filter into the interstices, and some fraction of the capillary barrier will be lost anyway. OPC-based matrices can produce very high pH, which can degrade the glass, and pozzolanic reactions (reactions between fly ash, silica gel, or clays and OPC; Lea, 1970; Berry *et al.*, 1989) can expand and crack the monolithic waste form and eliminate retrievability. For the purpose of this study, we define pozzolans as fine-grained siliceous and/or aluminous materials (such as fly and fuel ash, silica fume or gel, and certain clays) which react with $Ca(OH)_2$ and Ca-silicates in OPC. Above pH 8, the rate of glass degradation increases by roughly an order of magnitude for each increase of two pH units at 25 °C (Knauss *et al.*, 1990). Thus the degradation rate in a concrete at pH 13 could be 100 times greater than the rate in an alkaline clayey soil at pH 9. As we will show, the reaction of the glass and OPC can itself increase the pH, producing an autocatalytic effect. However, we will also show that the products of degradation may be effective "getters" for the sorption and immobilization of radionuclides.

3. Code Capabilities and Modifications

The EQ3/6 code suite is quite capable, and well-suited to modeling interactions of waste forms with an aqueous environment. Unique features of EQ3/6 include the ability to handle solid solutions (critical for modeling Ra solubility) and its use of alternating 1st and 2nd order convergence corrections. Nonetheless, it is important to recognize the limitations of EQ3/6 (and most other reaction-path codes). This section describes modifications made to the code to increase its utility for modeling glass-cement interactions, as well as the problems we were unable to overcome. We include recommendations for future code modifications needed to address these issues. All modifications were made to the PC-based version of the code, which was compiled with the Lahey F77L3 and LF90 compilers. It is likely that some of these limitations will be removed in the next release of EQ3/6.

3.1 Binary Interface to the Graphics Post-Processor (PP)

The output of the standard version of EQ3/6, version 7.2a, is in the form of ASCII tables (the ".6o", ".6t" and ".6tx" files). Though well organized, the tables can be extremely large (up to 40 MB (megabytes) in some of our runs), and tend to overwhelm the user with information. Furthermore, the ".6o" files generally report concentrations and mineral amounts for roughly one in ten steps in a run, and this selectivity can cause plots to be jagged and irregular. We modified EQ6.FOR to produce a more compact binary file containing all the output points, and wrote a "point-and-click" graphics post-processor called PP (Stockman, 1994) to speed the interpretation and processing of the EQ3/6 data files.

3.2 Rate Laws

Typically, the rate of an overall reaction dissolution is considered to be partly a function of the degree of saturation of the solution with respect to the dissolving solid phase. This can be approximated by using a formulation based in transition state theory (TST):

$$\text{Rate (in moles/sec)} = k \cdot S \cdot a_{H^+}^{N} \cdot [1 - (Q/K)^{(1/\sigma)}] \quad (1)$$

where k is a rate coefficient (in moles·sec^{-1}·cm^{-2}), which incorporates effects of temperature and undefined rate inhibitors or catalysts, S is the surface area of the reacting solid (in cm^2), a_{H^+} is the activity of hydrogen ion in the aqueous phase, and N is the "reaction order" with respect to hydrogen ion activity. Q is the activity product:

$$Q = [\{F\}^f \times \{G\}^g \times \{H\}^h \times \ldots] / [\{A\}^a \times \{B\}^b \times \{C\}^c \times \ldots] \quad (2)$$

for dissolution of the solid *via* the reaction:

$$\text{solid} + a \cdot A + b \cdot B + c \cdot C + \ldots = f \cdot F + g \cdot G + h \cdot H + \ldots \quad (3)$$

where {A} represents the activity of species "A", *etc.* K is the value of Q at thermodynamic equilibrium. The ratio of Q to K is the saturation state of the solution with respect to the dissolving phase. The $[1 - (Q/K)^{(1/\sigma)}]$ term is sometimes called the "affinity" term, and the slowing of dissolution as Q approaches K is called the "affinity effect". The parameter $1/\sigma$ is the "order" of the overall reaction. Commonly, the rate is expressed as mol/(cm^2 sec) by normalizing to the total surface area S. One of the characteristics of the TST formulation is that it relates the dissolution rate to the precipitation rate through the inclusion of the Q/K, or "affinity" term. Thus, at equilibrium the reaction would have a net rate of zero.

Strictly, the TST formulation applies only to an elementary reaction. It cannot be applied rigorously to an overall reaction, *i.e.*, a reaction in which more than one step or mechanism controls the transition from reactants to products (*e.g.*, Nagy *et al.*, 1991). The reaction order $1/\sigma$ represents the stoichiometry of the "transition state complex" in the rate-limiting elementary reaction. For glass and minerals this rate-limiting step is generally unknown and can be obtained only by using experimental spectroscopic techniques. However, as an approximation, the TST formulation appears to work reasonably well for overall reactions involving some simple oxide mineral phases, *e.g.*, quartz (Rimstidt and Barnes, 1980). On the other hand, application to gibbsite ($Al(OH)_3$) shows that the TST formulation is inadequate to explain existing dissolution and precipitation rate data (Nagy and Lasaga, 1992). For more complex crystalline phases such as kaolinite (Nagy *et al.*, 1991; Devidal *et al.*, 1992), albite (Burch *et al.*, 1993; Oelkers *et al.*, 1994), and K-feldspar (Gautier *et al.*, 1994), a TST formulation may be used to model dissolution rates based on an overall reaction. However, in solutions with ~ 10^{-5} mol/kg Al, an additional term describing the inhibitory-effect of Al-adsorption is included (Oelkers *et al.*, 1994; Gautier *et al.*, 1994). The only silicate phases for which dissolution and precipitation rates have been related successfully are quartz (Rimstidt and Barnes, 1980), cristobalite (Rimstidt and Barnes, 1980; Renders *et al.*, 1995), amorphous silica (Carroll *et al.*, 1994), and kaolinite (Nagy *et al.*, 1991; Devidal *et al.*, 1992).

The application of equation (1) to glass dissolution is clearly tenuous because dissolution is incongruent and other chemical reactions occur nearly simultaneously. For example, secondary phases rapidly become supersaturated near the dissolving glass surface and precipitate by nucleating onto the surface, reducing reactive surface area. The pH of the solid/fluid interface can be buffered by these secondary reactions. Adsorption, as well, may alter the surface composition from that of the initial bulk glass. At the low temperatures of a waste repository it is questionable whether or not the equilibrium solubility of a high temperature phase such as glass would ever be attained in the surrounding solution. Therefore, the assignment of a value to K and the extent a value of Q/K (reaction affinity or saturation state) deviates from zero is uncertain. Nonetheless, approximations have been made in order to use the TST formulation for glass dissolution in reaction path models.

One approach to assigning a value to K is to calculate the free energy of the glass, and then the K for equation (3), from "hydration theory" (Jantzen and Plodinec, 1984).

However, since glasses are inherently unstable, this approach yields an affinity term that is nearly always close to 1, and does not accurately predict the dissolution rate. Another approach, which better fits experimental results, assumes dissolution of the bulk glass is controlled by the breakdown of the silica framework (Bourcier, 1994). In the latter approach, Q is simply $\{SiO_{2\,(aq)}\}$, and K is found by experiment to be (typically) between the K's for chalcedony and cristobalite.

Values for the kinetic components of equation (1) for glass dissolution have been determined by various researchers. The dissolution rate constant is generally determined from initial rates of Si release in batch dissolution experiments or steady-state rates in stirred-flow reactors at affinities that represent "far-from-equilibrium" solutions. It has been found that the value of k is a function of the initial composition of the glass (Bourcier, 1994). The dependence on pH or a_{H+} has been shown to reflect the same pattern observed for crystalline aluminosilicate phases (Knauss *et al.*, 1990), where N ranges from -1 to 0 at pH < 7 and from 0 to 0.5 at pH > 7. EQ3/6 allows one to sum up to 4 TST equations with different N and k, making it possible to span smoothly the entire pH range. The value of σ has been obtained from the Si-release rate data (Bourcier *et al.*, 1994; Berger *et al.*, 1994) and ranges from 1 to 10 depending on glass composition and the choice of K used for the fitting. However, it must be stressed again that this value of σ can be viewed only as a fitting parameter. No mechanistic information can be derived from σ because no elementary reaction mechanism has been determined for glass dissolution. Berger *et al.* (1994) suggested that when $\sigma > 1$ the overall glass dissolution reaction is controlled by more than one dissolution mechanisms acting in parallel. Thus, the various values of σ that have been observed may reflect differences in glass composition, solution pH, temperature, or other unidentified aspects of the experimental system's composition.

Unfortunately, in order to use the TST formulation for glass dissolution, EQ3/6 requires that the Q and K in equation (1) and the "solid" in equation (3) be associated with a single phase from the thermodynamic database (either a pure solid or a solid solution). It is not possible to assign the solid an arbitrary complex composition, and also have Q = $\{SiO_{2(aq)}\}$. However, there are two ways around this problem. The first is to recast the TST equation in terms of a sum of "activity law" equations:

$$k \cdot S \cdot a_{H^+}{}^N \cdot [1 - (Q/K)^{(1/\sigma)}] = k \cdot S \cdot a_{H^+}{}^N - k' \cdot S \cdot a_{H^+}{}^N \cdot a_{SiO2}{}^M \qquad (4)$$

where $k' = k/K^{(1/\sigma)}$ and $M = 1/\sigma$. Because of coding constraints, the glass composition must be entered in the database, either as a solid solution or a phase with fixed composition. The problem with this approach is that it tends to amplify numerical errors as the system nears saturation, particularly if the system is "stiff" (see section 3.3). In addition, EQ3/6 must still calculate reaction affinity, and if reaction affinity indicates dissolution, but equation (4) indicates precipitation, the calculation is terminated.

The second solution to the problem, used in this study, was to modify the EQ6.FOR source to add a new "parasitic" rate law to EQ3/6 (specified by setting `nrk = 5`). In the

parasitic rate law, the dissolution rate of the (n+1)th reactant equals a specified fraction (given by `rk1`) of the previously listed nth reactant. Thus, to model dissolution of a glass, yet have Q correspond to {SiO_2 (aq)}, one enters a silica phase (Quartz, Chalcedony, α-Cristobalite or SiO_2 (am)) as the nth reactant with its known TST rate law (`nrk = 2`), followed by an (n+1)th reactant (`nrk = 5`). The (n+1)th reactant is typically defined as a "special reactant" (`jcode = 2`) containing all other components of the glass. Note that several of these special reactants can be linked in series, as the (n+1)th, (n+2)th, *etc.* reactants, allowing one to mimic incongruent dissolution. If one sets `nrpk = 0`, then the (n+1)th component will not precipitate when the nth component precipitates, corresponding to the buildup of a silica-rich layer. When `nrpk = 5`, the (n+1)th reactant precipitates at the specified fraction of the rate of the nth reactant. We have found this approach to be far superior to the "activity law" approach described above because it allows one to change rapidly the silica species that controls K in equation (1). It also avoids the tedious recalculation of artificial solid solution "components" that is necessary any time one changes glass composition in the activity law approach. Most important, the parasitic rate law prevents the run-termination problem that plagued the activity law method.

We have explicitly included rate laws for glass, clays, silica phases, and feldspars. These are all minerals that react relatively slowly in laboratory experiments. Fast-reacting phases such as calcite or barite were allowed to equilibrate instantaneously with the rest of the system. For some minerals, we performed tests to check that kinetic and instantaneous rates produced no substantive differences in the path calculation results.

3.3 Stiff Systems

We have found EQ3/6 to be superior to some other reaction path codes in its ability to calculate through troublesome changes in phase assemblage, probably because of the advanced alternation of 1st-order and 2nd-order convergence methods. However, EQ3/6, like all other reaction path codes we know of, has difficulty with "stiff systems" when run in kinetic mode. Such systems typically involve several reactants with, in our experience, at least two orders of magnitude difference in rates of dissolution and precipitation, particularly as one or more reactants approaches equilibrium. The manifestation of the problem is that the code fails to meet its accuracy criteria (calculated by comparing the integrated differential equations against the predictions of the Newton-Raphson corrector term). As a result, the code reduces the step size more and more, until the reaction path progress effectively stalls out. We have not yet found a fool-proof solution to this problem, which often causes termination of a run in the most interesting part of a calculation. In some cases, we have been able to obtain satisfactory results by careful selection of the input file parameter `dlzmx1`, which sets the order-zero step size, or by limiting the number of reactants and minerals allowed to precipitate. Apart from completely recoding EQ3/6 to use a stiff ODE solver, it may be possible to enter fictive reactants into the database, with stoichiometries and $\log_{10}K$'s simply scaled by a factor of 100 or so, to make the rates appear to be more similar, thus easing the burden on the ODE solver.

3.4 Decay and Ingrowth (^{230}Th, ^{226}Ra)

A significant limitation on all widely-used reaction path codes is the failure to consider decay and ingrowth of radioactive isotopes. For example, the half-life of ^{226}Ra is 1600 years, yet our calculations must encompass periods up to 10,000 years. Our calculations assume the amount of radium in the system is constant; this would not be a problem if aqueous Ra concentrations were buffered by a pure, Ra-rich mineral. However, the calculations show that for many matrices, Ra solubility is controlled by the presence of a barite-$RaSO_4$ solid solution. Thus, to a first approximation aqueous Ra is proportional to the total amount of Ra in the system, and the concentrations reported in this study can be corrected with a simple $\exp(-t/\tau)$ term, where τ=1600 years. For the sequence C glasses, the problem is more complicated, because most of the ^{226}Ra is produced by decay of ^{230}Th with a half-life of 80,000 years. However, we cannot come up with a scenario where this complication causes our solubility calculations to be nonconservative. Only a small molar fraction of the total dissolved Th in the system is ^{230}Th. So, if the dissolved Th simply converted to ^{226}Ra by decay, and then stayed in solution without coprecipitation in barite, it would still not contribute significantly to the total dissolved Ra concentration. The latter conclusion is accurate, however, only if we use recent Th solubility data discussed in sections 4.1.5 - 4.1.8.

3.5 Compiler Bug Work-arounds

Working with Tom Wolery (at LLNL), we found several bugs in the Lahey compilers (versions F77L3 and LF90) used to compile EQ3/6. We must emphasize that these were not faults in the programming of EQ3/6, but rather flaws in the commercial programs that turn the source into executable code. For example, F77L3 contained an optimization bug that ultimately made EQ3/6 version 7.2a unable to hold a fixed fugacity. Version LF90 "optimized away" the test for the smallest positive number that could be used by the 80x86 floating point unit, causing runs to assume low precision (with subsequent early termination). To our knowledge, all of these problems have been resolved in the upcoming version 7.2b of EQ3/6. However, users with unmodified versions of the EQ3/6 7.2a binaries should be aware that they will not be able to reproduce the work reported in this document.

4. Database Modifications and Additions

4.1 Thermodynamic Data

The most extensive thermodynamic database available for EQ3/6, and the only one adequate for modeling radionuclide interactions with silicate minerals, cements, and glass is data0.com. The version of the database supplied with EQ3/6 7.2a was denoted data0.com.R22a (referred to hereafter as R22a). The most recent version supplied with EQ3/6 7.2b will probably be denoted data0.com.R1 (referred to hereafter as R1). This study was largely completed before EQ3/6 7.2b and the R1 database were shipped; however, LLNL supplied us with an advance version of R1 for testing purposes. The principal difference between R1 and R22a is a greater internal consistency for compounds that contain aluminum; for cement phases, this consistency can be very important, since R1 more closely matches the CHEMVAL data for $Al(OH)_4^-$, used extensively in calculations of cement thermodynamics (Atkins *et al.*, 1992). The LLNL staff made additional changes in R1 as a result of discrepancies discovered in the present study, particularly those related to the consistency of aqueous silica species. However, we found it necessary to further customize the R1 database. Our customizations are discussed below, along with the rationale for the changes, and the problems one would likely encounter with the raw R1 and R22a databases. We recognize the extreme difficulty in maintaining consistency in a thermodynamic compilation that includes nearly 2000 solids and aqueous species. However, we feel the added detail described in the sections below is necessary to justify our decisions, especially since some of our changes affect calculated solubilities by many orders of magnitude. This work illustrates why it is often difficult to do meaningful solubility calculations for a completely new system on short notice. We hope it is also obvious from this document why DOE should ensure adequate support for LLNL's efforts in database maintenance.

4.1.1 Silica species

Polynuclear aqueous silica species. The R22a version of the database contained a subtle inaccuracy in the stability constants for some polynuclear aqueous silica species, which had a dramatic effect on some calculations of silica solubility. For reference in the following discussion, Figures 1 and 2 show our "corrected" speciation of Si as a function of pH using both the "bdot" and Davies equations for determining activity coefficients. In general, Si solubility is accurately known up to pH of about 11 (Iler, 1979; Eikenberg, 1990). At pH slightly above 11, experimental measurements of total dissolved Si become much less accurate. In addition, both ionic strength corrections used for the EQ3/6 com (R1 and R22a) database (see section 4.3) become large and of doubtful accuracy, causing curvature in the species concentration curves. Suppression of the $H_4(H_2SiO_4)_4^{4-}$ aqueous species removes these perturbations (Fig. 3; section 4.3).

One source of the inaccuracy in the calculated silica solubility can be described as follows. In the original database, the stability constants for $H_6(H_2SiO_4)_4^{2-}$ and $H_4(H_2SiO_4)_4^{4-}$ were taken from the tabulation by Smith and Martell (1976), which was in turn derived from at

least 7 other studies. For example, Smith and Martell (1976) derived equilibrium constants consistent with the following reactions:

(A) $H_6(H_2SiO_4)_4^{2-}$	=	$4H_2SiO_4^{2-} + 6H^+$	($\log_{10}K_A = -78.2$)
(B) $4[H_2SiO_4^{2-} + 2H^+$	=	$SiO_{2\,(aq)} + 2H_2O]$	($\log_{10}K_B = 4\times22.96$)
(C) $H_6(H_2SiO_4)_4^{2-} + 2H^+$	=	$4SiO_{2\,(aq)} + 8H_2O$	$\log_{10}K_C = 13.64$.

It appears (*e.g.* Iler, 1979) that K_C was the primary measured constant (*via* the doppleganger $Si_4O_6(OH)_6^{2-}$) from experiments at high total silica concentrations. However, Smith and Martell (1976) chose to infer the intermediate formation constants K_A and K_B, such that $K_A \times K_B$ = the measured K_C. When the R22a database was reviewed, the authors apparently replaced the conditional (and purely formal) K_A with the more accurate $K_A' = 10^{21.1585}$ determined by Naumov *et al.* (1974), then erroneously recalculated $K_C' = K_A' \times K_B = 10^{6.434}$. (This mistake was easy to make, since the Smith and Martell (1976) review is far from clear on the origin of K_A and K_B.) The new K_C' caused EQ6 to calculate very high *total* aqueous Si (up to 0.5 M) at cristobalite and amorphous silica saturation, under conditions where the *total* aqueous Si concentration should have been ≈0.001 M. A similar error was made in the calculation of the stability constant for $H_4(H_2SiO_4)_4^{4-}$. A second source of inaccuracy in the stability constants for Si species arose because the R22a database included a "doppleganger" for $H_4(H_2SiO_4)_4^{4-}$; namely, $Si_4O_8(OH)_4^{4-}$. These two species designations differ only by the number of waters of hydration, and actually represent the same Si species. However, the code evaluated both species as if they were independent, effectively doubling the concentration of polynuclear silica. These errors will likely be corrected in the R1 database to be publicly released with EQ3/6 version 7.2b. All results presented in this report were obtained with the corrected stability constants.

Despite the fact that the stability constants for polynuclear silica species have been "corrected" in the new database, there are still large uncertainties in silica speciation at high pH. Figures 1 through 3 show the calculated aqueous silica speciation for three EQ3/6 runs with the new R1 database, using the bdot γ correction, the Davies γ correction, and the bdot correction with suppression of $H_4(H_2SiO_4)_4^{4-}$. The calculations were performed by titrating KOH into a system initially containing 1 kg water, 0.6 kg quartz, and enough HCl to induce initial pH = 4. In the later stages of the titration, the reaction paths curve back on themselves (to slightly lower pH) with both the bdot and Davies models (Figs. 1 and 2). This sort of behavior is not necessarily unrealistic, as the increasing ionic strength can rapidly drop the γ's for the silica tetramers, causing the proportion of tetramers to increase, resulting in consumption of OH^-, and ultimately buffering of pH. Figure 4 shows the total dissolved Si for all three EQ3/6 runs, along with Eikenberg's (1990) preferred model "1B"; the latter effectively falls between the EQ3/6 Davies calculation, and the EQ3/6 bdot calculation with the tetramer suppressed. There is uncertainty in Eikenberg's (1990) model as well, since it is based on numerous experiments of limited duration, and it is not clear if adequate time was allowed for the formation of silica polymers.

Ca,Mg aqueous silica species. The R22a database also contained several aqueous Mg and Ca silicate species, again from the compendium by Smith and Martell (1976), which showed up in surprisingly high concentrations in calculations involving cement phases. This anomaly was noticed by Atkins *et al.* (1992), who recommended the species be removed from cement calculations. Jim Johnson of LLNL (personal communication, November 10, 1994) suggests that the stability constants for these species were not properly corrected back to infinite dilution, and it appears they have been removed from recent versions of the database.

Aqueous SiO_2 at high pH, ionic strength, Na concentrations. It is inevitable that some calculations with cement phases will push the limits of the extended Debye-Hückel activity coefficient corrections by reaching conditions of high pH, and high dissolved Na and Si. The study by Eikenberg (1990) casts doubt on silica speciation calculated under such conditions, even when ionic strengths are below 1 m. In particular, it is questionable whether the high concentrations of aqueous $NaHSiO_3$ calculated by EQ3/6 are realistic, since the thermodynamic data for this species were extrapolated from hydrothermal experiments at 300°C. This species was not considered by Atkins *et al.* (1992), and did not appear in earlier versions of the com database. In our calculations, we have suppressed the formation of $NaHSiO_3$(aq).

4.1.2 Cement phases

The R22a and R1 databases contain entries for a number of cement phases, principally from the review by Sarkar *et al.* (1982). We have replaced the Sarkar *et al.* (1982) data for ettringite, gehlenite-hydrate, hydrotalcite and katoite with the work of Atkins *et al.* (1992). The Atkins *et al.* (1992) studies were performed at high pH where aqueous Al is dominantly $Al(OH)_4^-$, and were converted to the Al^{3+} basis assuming $\log_{10} K = 22.90$ (25°C) for the reaction $Al(OH)_4^- + 4H^+ = Al^{3+} + 4H_2O$. This $\log_{10}K$ is sufficiently close to the R1 database value of 22.883, that the Atkins *et al.* (1992) data were added directly to our database without further modification. The Sarkar *et al.* (1982) K's for tobermorite were close to the Atkins *et al.* (1992) values, and were not changed.

4.1.3 $BaCO_3$-$RaCO_3$ and $BaSO_4$-$RaSO_4$ solid solutions

The molar amounts of radium in low-level and orphan wastes are typically small, so that saturation with pure $RaCO_3$ and $RaSO_4$ is unlikely to occur. However, these wastes often contain substantial amounts of Ba, from separation of Ra *via* coprecipitation. The chemistry and ionic radii of Ba^{2+} and Ra^{2+} are extremely similar (Bloss, 1994); $BaCO_3$ (witherite) is isostructural with $RaCO_3$, and $BaSO_4$ (barite) is isostructural with $RaSO_4$, so some solid solution is inevitable. We have therefore added ideal $(Ba,Sr,Ra)SO_4$ and $(Ba,Sr,Ra)CO_3$ solid solutions in the R1 database. The "danger" is that the solid solution of Ra in $BaCO_3$ (*e.g.*) may prove to be non-ideal, like the solution of trace Sr in $CaCO_3$ (aragonite), where $\gamma_{Sr} \approx 100$ at 25°C under conditions of slow precipitation (Plummer and Busenberg, 1987). In such case, a calculation assuming ideality would underestimate the aqueous Ra concentration by a factor of 100. However, when aragonite precipitates from sea water, the Sr/Ca ratio of the solid is much higher than predicted by slow, reversible lab

studies, and is closer to the value predicted by ideal solution. Perhaps more important, the difference in ionic radii is much smaller for the Ra^{2+}-Ba^{2+} pair (0.06 Å) than for the Sr^{2+}-Ca^{2+} pair (> 0.2 Å), so we feel the Ra-Ba solid solutions are far more likely to be ideal.

The $BaCO_3$ (witherite) entries in the R22a and R1 databases trace to Helgeson *et al.* (1978), which in turn trace to the study by Adami and Conway (1966), and imply a high degree of stability. If these witherite data were correct, one would expect spontaneous conversion of barite to witherite in near-surface environments. There is reason to doubt the accuracy of the ΔH measurements made by Adami and Conway (1966), as there is typically a problem with incomplete or slow CO_2 degassing in low temperature acid calorimetry (personal comm., William H. Casey, Feb. 22, 1995). We have recalculated the $BaCO_3$ stability constants in our modified version of the R1 database, using free energies from Wagman *et al.* (1982); the latter are consistent with recent analysis by Sverjensky and Molling (1992), and the careful experimental study by Kiseleva *et al.* (1994). The effect of this change is to decrease the calculated stability field for $(Ba,Ra)CO_3$ relative to $(Ba,Ra)SO_4$, and ultimately to lower the calculated Ra solubility for the conditions considered in this study by several orders of magnitude.

The EQ3/6 database contains entries for alstonite ($CaBa(CO_3)_2$) and barytocalcite. We have suppressed the formation of these minerals, since we have no data on the solid solution of Ra in these phases (which are not isostructural with witherite and $RaCO_3$).

4.1.4 Pb solids and complexes

The raw R22a and R1 files contain very few carbonate and hydroxyl aqueous Pb species. Consequently, calculations at high pH tend to underpredict Pb solubility relative to the studies of Phillips *et al.* (1988) and Taylor and Lopata (1984). We have added stability constants for aqueous Pb hydroxyl, carbonate, and hydroxyl-carbonate species, as well as hydrocerussite, calculated from the free energy and K data in Phillips *et al.* (1988) and Neher-Neumann (1992). With these new data, we are able to reproduce the results in Taylor and Lopata (1984) to within a factor of two. Figure 5 shows that without the new Pb complex data, models of glass degradation in a cement matrix can underestimate Pb solubility by up to 13 orders of magnitude.

4.1.5 Th phosphate solids and complexes

Initial calculations with "sequence C" glass showed a high dissolved Th concentration due primarily to the formation of an aqueous phosphate complex. It was suspected that this high solubility was due, in part, to lack of data for the solid phase $Th_3(PO_4)_4$ in the EQ3/6 com database. Therefore, we calculated stability constants for $Th_3(PO_4)_4$ using free energies from Wagman *et al.* (1982). However, the calculated solubility product of the solid orthophosphate was large and did not counteract the stability of aqueous Th complexes, particularly the phosphate complexes.

Because addition of a solid Th-phosphate did not effect a decrease in the dissolved Th concentration, we examined more carefully the EQ3/6 database for Th complexes. The "com" data for Th phosphate complexes are largely derived from the study by Langmuir

and Hermann (1980), and ultimately trace to a brief report by Moskvin *et al.* (1967). Use of these data can result in extremely high calculated Th solubilities (as will be discussed in section 4.1.8), and can have serious consequences for predicting safety of Th disposal options.

Three recent studies (Östhols, 1995; Baglan *et al.*, 1994; Fourest *et al.*, 1994) suggest the R22a and R1 databases grossly overestimate the stability of the Th phosphate complexes, and the Wagman *et al.* (1982) data probably underestimate the stability of solid $Th_3(PO_4)_4$. Östhols (1995) examined the solubility of microcrystalline ThO_2 in phosphate solutions, and found extremely high phosphate concentrations were required to increase solubility above levels for phosphate-free solutions at the same pH. It was inferred that the only likely Th phosphate complex was $Th(OH)_4PO_4^{3-}$, with a rather weak $\log_{10}K = -14.9 \pm 0.36$ for the reaction:

$$Th^{4+} + 4H_2O + PO_4^{3-} = Th(OH)_4PO_4^{3-} + 4H^+ . \quad (5)$$

These results are questionable because the "ThO_2" in the system contained significant P, and may have been undergoing kinetically-controlled transformation to $Th_3(PO_4)_4$. Thus, it is possible that the formation of aqueous Th phosphate complexes was balanced by precipitation of relatively insoluble $Th_3(PO_4)_4$, causing the total Th concentration to remain nearly constant. The study by Baglan *et al.* (1994) gives the $\log_{10}$ solubility product for $Th_3(PO_4)_4$ as -112 ± 2.1, at least 15 orders of magnitude smaller than the value inferred from Wagman *et al.* (1982). However, the study by Fourest *et al.* (1994) leaves little doubt that the Moskvin *et al.* (1967) data are wrong, and consequently, the current "com" database causes gross overestimation of Th solubility *via* phosphate complexes. Fourest *et al.* (1994) found that the solubility of $Th_3(PO_4)_4$ at near-neutral pH is less than 10^{-8} mol/L at 0.3 mol/L total phosphate, and decreases rapidly with decreasing phosphate concentration. It can be inferred from figure 1 in Fourest *et al.* (1994) that the solubility is less than 10^{-10} mol/L at total phosphate concentrations of 0.025 mol/L. Using the data from Moskvin *et al.* (1967), one calculates Th solubilities well over 10^{-4} mol/kg for the same conditions.

Based on these recent studies, we have added Bagman *et al.*'s (1994) $Th_3(PO_4)_4$ data and the $Th(OH)_4PO_4^{3-}$ stability constant calculated by Östhols (1995) to the EQ3/6 database. We also have removed the aqueous Th phosphate complexes that trace back to the Moskvin *et al.* (1967) study.

4.1.6 Mg phosphates; effect on Th

Many phosphate-rich waste glasses are relatively Ca-poor. When such glasses decompose, there is insufficient Ca to precipitate the released P as apatite or other Ca phosphates. The Fernald sequence C glasses are Ca-poor, but have significant Mg which also might be expected to precipitate Mg phosphates. However, the EQ3/6 "com" database contains no solid Mg phosphates. Thus, the calculated fluid composition can become unrealistically enriched in HPO_4^{2-} and PO_4^{3-} as the glass dissolves, consequently predicting high concentrations of U and Th aqueous phosphate complexes. To make the

calculations more realistic, we added $Mg_3(PO_4)_2$ to the "com" database, using the free energies from Wagman *et al.* (1982).

4.1.7 ThO_2(am) *vs.* ThO_2 *vs.* $Th(OH)_4$

Under the conditions of this study, thorianite (crystalline ThO_2) is often predicted to be the most stable Th-containing solid. However, it is difficult to precipitate thorianite from solutions at low temperature; a hydrous, microcrystalline phase, sometimes described as $Th(OH)_4$ or $ThO_{2(act)}$, precipitates instead (Östhols *et al.*, 1994). The latter phase may be orders of magnitude more soluble than thorianite, and seems to persist metastably for years, with no indication of transformation to the more stable phase. Thus, a conservative and defensible solubility calculation should suppress the precipitation of thorianite in favor of the metastable phase. Östhols *et al.* (1994) calculated a solubility product for this phase, and also estimated stability constants for various coexisting Th carbonate complexes. We have added the latter data to the EQ3/6 "com" file, calling the metastable phase $ThO_{2(am)}$ ("amorphous") for consistency with EQ3/6 nomenclature.

4.1.8 Overall effect of changes in Th data

Figure 6 compares Th release during degradation of glass in water, without a solid matrix, and at a PCO_2 of $10^{-3.5}$ atm. Under these conditions, use of the com database with the Moskvin *et al.* (1967) Th phosphate complexes, and the $Th(OH)_4$ instead of the $ThO_{2(am)}$ data, can cause EQ3/6 to overestimate Th solubility by up to 8 orders of magnitude.

4.1.9 Clays

The clay stability constants in the EQ3/6 R22a and R1 databases are based both on measured clay solubilities as well as an algorithm to predict the Gibbs energy of formation of a clay phase based on the mineral's component oxides (Wolery, 1978). This algorithm is based primarily on that of Tardy and Garrels (1974) in which the Gibbs energy of formation of oxide and hydroxide components of layer silicates were derived from a set of reasonably well-known mineral solubility data. These component Gibbs free energies do not necessarily equal those obtained for the single oxide phase, if it exists. The strength of such an approach is that theoretically one can "predict" the solubility of complex layer silicates including phases with exchangeable interlayer cations by simple summation of the component Gibbs free energies. Clay phases in general have poorly-defined experimental solubilities at low temperatures because of the tendency for incongruent dissolution and back reactions to occur. These problems are similar to those that take place during glass dissolution resulting in poor knowledge of a glass' equilibrium solubility.

Refinements of the Tardy and Garrels (1974) modeling approach have been made in the past 20 years (see Chermak and Rimstidt (1989) for summary). We selected the recent model of Chermak and Rimstidt (1989, 1990) for comparison to the EQ3/6 model for illite ($K_{0.6}Mg_{0.25}Al_{1.8}Al_{0.5}Si_{3.5}O_{10}(OH)_2$) and for Fe-Mg smectite ($Ca_{0.025}Na_{0.1}K_{0.2}Fe^{2+}{}_{0.5}Fe^{3+}{}_{0.2}Mg_{1.15}Al_{1.25}Si_{3.5}O_{10}(OH)_2$) at 25°C. The two calculation schemes yield the same Gibbs free energy of formation for illite in units of kJ/mol (-5455.0_{CR1989} vs. $-5455.8_{EQ3/6}$ at 25°C). There appears to be a significant difference between the smectite Gibbs free energy of formation at 25°C calculated using the two

models (-5352.7_{CR1989} vs. $-5280.7_{EQ3/6}$) that is outside the uncertainty typically assumed for experimental determination of such reactions (4 - 8 kJ/mol). However, part of this difference is due to the manner of handling Fe^{2+} *vs.* Fe^{3+} in the correlations. As it turns out, a difference of 72 kJ/mol in smectite solubility has little effect in our calculations because the formation of high-Fe-Mg smectite never achieves steady-state in the presence of glass. The high-Fe-Mg smectite mainly acts as a source of components for precipitation of new, more stable clays.

Various smectite and oxide phases are the main clays that form at the dissolving glass surface (Mazer et al., 1992a,b,c; Ebert et al., 1993; Tomita et al., 1993; Abdelouas et al., 1994). Alteration layers formed on glass at 90°C can be quite complex in composition and texture (Mazer et al., 1992a). Mazer et al. (1992a,b,c) proposed that degree of hydration of the glass, time, and solution composition all control the composition and extent of the altered surface layer. Despite these observations, general mathematical formulations describing the kinetics of nucleation and growth of these secondary phases on glass surfaces are not yet available. Therefore, we suspect that the existing formulation for predicting their solubilities in EQ3/6 is adequate until more experimental data are obtained. Ransom and Helgeson (1994, 1995) recently pointed out that it is necessary to account for the effect of interlayer water in determining Gibbs free energies of formation for smectites. They suggest carrying out experimental correlation of XRD d-spacing for specific smectite compositions as a function of humidity. They then proposed a scheme for estimating the amount of interlayer H_2O that would account for the measured d-spacing. For fully-hydrated smectites, the effect is to increase the ΔS_f° by about a factor of two. This would alter a ΔG_f° at 25°C by about 75 kJ/mol. Such an error is the same as that between the calculated values using the EQ3/6 code and the model of Chermak and Rimstidt (1989). Therefore, we did not include the effect of hydration in our EQ3/6 runs.

Imogolite. The conditions for stability of this phase ($Al_2SiO_3(OH)_4$) are controversial; however, there is growing evidence that imogolite forms easily in soils, and the failure to consider this phase may result in unrealistic dominance of hydrous alumina phases in reaction path calculations (Su and Harsh, 1994). Su and Harsh (1994) calculated K's for decomposition of synthetic and natural imogolite; however, the free energies implicitly assumed for Al^{3+} and gibbsite ($Al(OH)_3$) differ substantially from those assumed in the rest of the EQ3/6 databases. We have used their experimental data for the reaction:

$$Al_2SiO_3(OH)_4 + H_2O = 2AlO(OH) + H_4SiO_{4(aq)} \qquad (6)$$

which required measurement of aqueous silica alone, and did not involve assumptions about the speciation of aluminum. The R1 data for decomposition of boehmite (AlO(OH)) was then used to calculate K's for the decomposition of imogolite to Al^{3+} and $SiO_{2(aq)}$, for both synthetic and natural varieties. A second reason for using this indirect approach is that it allows us to calculate a temperature dependence; the imogolite-boehmite reaction is the only one for which Su and Harsh (1994) give full temperature data. To date, imogolite has shown up only intermittently in our calculations.

4.2 Silicate Suppressions

In general, if a reaction path calculation predicted the formation of extremely improbable silicate phases, these phases were suppressed with the EQ3/6 `nxmod` option and the code was rerun. By "improbable" we mean phases such as muscovite which has not been identified as forming at 25°C in geologic environments (Newman and Brown, 1987; Velde and Meunier, 1987). Often the thermodynamic data for such minerals have been extrapolated from high temperatures and are of dubious accuracy at 25°C. The suppression of muscovite in the calculations led to the formation of celadonite. For phases such as celadonite the decision to suppress is less clear; there are examples of celadonite apparently formed in basalts at seafloor temperatures (Odom, 1984). However, in our calculations the suppression of celadonite had remarkably little effect on the system pH, silica activity, glass degradation rates, or solubilities of radionuclides, as smectite clays simply formed in its place. A similar situation was found with the suppression of epidote minerals and prehnite; suppression of these minerals caused somewhat greater amounts of zeolites to form in their stead, with little effect on the glass degradation rate or solubilities. We note, however, that if we were modeling the solubility of Cs and Sr, the formation of additional zeolites would be significant because zeolites provide additional sites for Cs and Sr sorption.

4.3 Activity Coefficient or Ionic Strength Corrections

Nearly all calculations performed in this study used the "bdot" activity coefficient model (EQ3/6 option `iopg1 = 0`) which provides reasonable corrections up to an ionic strength of $\approx$ 1 m. However, a few of the calculations reached ionic strengths exceeding 3 mol/kg, typically near the end of the run (at times ranging from 10 to 5000 years). An extreme example is the calculation involving OPC and "sequence A" glass ((1) in Table 2; no pozzolan, no CO_2 buffering), which reached ionic strengths of $\approx$4 mol/kg after approximately 10 years, and an ionic strength of $\approx$10 mol/kg at termination. By the end of the run, the activity coefficient (γ) for the dominant Si species $H_4(H_2SiO_4)_4^{4-}$ had decreased to a questionably low value of 10^{-6}. We suspect that this γ is grossly underestimated. If so, the error might cause a "runaway" dissolution artifact; *i.e.*, increasingly lower γ would cause SiO_2(aq) to convert to $H_4(H_2SiO_4)_4^{4-}$, inducing more glass to dissolve (per the affinity term in equation (1) which is written using the SiO_2(aq) species). Glass dissolution, in turn, would increase ionic strength by releasing more cations to solution such as Na^+, *etc.*, decreasing the activity coefficient even further. In reality, the role of $H_4(H_2SiO_4)_4^{4-}$ proves to be relatively insignificant in the calculations. In fact, complete suppression of $H_4(H_2SiO_4)_4^{4-}$ actually causes a slight *increase* in the calculated degradation rate for "sequence A" glass (Fig. 7) and a calculated maximum ionic strength of only $\approx$ 3 m. The reason why $H_4(H_2SiO_4)_4^{4-}$ is insignificant in the actual EQ3/6 run is that by the late stages of the calculation, the system contains numerous solid silicates that buffer aqueous silica activity. Because all of the Si-speciation reactions are written as dissociation of SiO_2(aq), suppression of the tetramers simply serves to redistribute dissolved silica among SiO_2 (aq), $HSiO_3^-$, $H_2SiO_4^{2-}$, *etc.*

We also used the Davies equation to calculate ionic strength (EQ3/6 option

`iopg1 = -1`) for a few runs, as a comparison. For runs at I < 1 mol/kg, the results were insignificantly different. For the run with just OPC and "sequence A" glass (Run (1) described in the previous paragraph), the use of the Davies equation gave virtually the same result as that obtained using the "bdot" equation with suppression of the Si-tetramer; *i.e.*, the Davies equation curve was nearly identical to the upper curve in Figure 8. Also, using the Davies equation, the maximum ionic strength was ≈ 3 mol/kg and γ for $H_4(H_2SiO_4)_4^{4-}$ was never less than 10^{-2}, which kept the Si-tetramer concentration at a low value.

Only two runs ((1) and (2) in Table 2) reached high ionic strength in less than 50 years. In these runs, the SiO_2 (aq) activity remained low, rendering the affinity term relatively insignificant, and leaving the rate of glass dissolution controlled largely by pH. The results of these runs must be interpreted with caution, however, particularly when they predict high solubility of a species with a large negative charge such as the Si-tetramer. On the other hand, the overall amount of glass degradation and the solubilities of U, Th, Ra and Pb are essentially unaffected by changing the activity correction model and suppressing highly charged species. Thus, we conclude that our results are qualitatively correct and can be used to delineate conditions leading to rapid glass degradation.

4.4 Kinetic Data

4.4.1 Glass

As stated in section 3.2 we used values of k and N in equation (1) for glass dissolution from Knauss *et al.* (1990). The k value is roughly consistent with results from Fernald glass dissolution studies (DOE, 1993; Merrill and Whittington, 1994). Under basic conditions, the value of N seems to vary little for a given temperature; for example, Gin *et al.* (1994), Grambow and Strachan (1988) and Knauss *et al.* (1990) all report values near 0.4 at 90°C. Based on data in Grambow and Strachan (1988), the equilibrium solubility of the glass (K) was taken to be in the range from chalcedony to cristobalite solubilities. The value of σ in the affinity term ranged from 1, for a true TST-equation for a single elementary reaction (*e.g.*, Laidler, 1987), to 3, obtained for basalt glass dissolution at T of 150°-300°C (Berger *et al.*, 1994), to 10, obtained for dissolution of CSG borosilicate glass at 100°C (Bourcier *et al.*, 1994). We note however that Bourcier *et al.* (1994) obtained $\sigma = 10$ while simultaneously obtaining a best-fit value of K equal to quartz solubility. While quartz precipitation from seawater at 25°C has been reported (MacKenzie, 1971), the process required a large specific surface area of quartz nuclei to obtain measurable precipitation on the scale of years. It is questionable whether nucleation and growth of quartz would be controlling Si activity in a repository at low temperature, particularly in the early stages of glass degradation and in the absence of nuclei. Initial dissolution of glass would most likely result in aqueous Si activities that rapidly overshoot quartz solubility and lie at least above chalcedony solubility. In this case, kinetic barriers would exist to inhibit quartz nucleation and silica activity would be controlled by a metastable silica phase (*e.g.*, Williams and Crerar, 1985). Most calculations in this study were performed with $\sigma = 10$ and a K corresponding to chalcedony, since our intent was to err on the side of overestimating the affinity effect for non-OPC matrices. (Section 6.5 and

Figs. 21 through 25 discuss the effects of varying σ and K on the overall glass corrosion rate.)

4.4.2 Clays

Kinetic parameters for equation (1) describing specific clay mineral dissolution and precipitation were taken from the review by Nagy (1995). For the run conditions of interest, we also approximated illite dissolution by using available data for muscovite dissolution (Knauss and Wolery, 1989) because no reliable illite data exist. All clays were assumed to have a specific surface area of 2.5×10^8 cm^2/mole. This specific area corresponds closely to the surface area for kaolinite determined by Ganor *et al.* (1995) of 7.5 m^2/g. However, it is too low for smectite which has a greater formula weight. Also, natural clays will not be carefully sized as are pretreated materials used in experiments. Thus, in an actual disposal scenario with added clay, the specific surface area of the clay would be expected to be much larger due to the presence of fines. Since we intend to show that the presence and reaction rate of smectite are sufficient to accelerate the corrosion rate of glass, we have erred on the side of underestimating surface area, and thus the total reaction rate.

4.4.3 Quartz and SiO_2(am)

Kinetic data for quartz dissolution at 25°C as a function of pH were taken from Brady and Walther (1990). These data agree to within a factor of two with those of Knauss and Wolery (1988) at 70°C when extrapolated to 25°C using the E_a suggested by Knauss and Wolery (1988). At neutral pH, the data also agree with the earlier kinetic data set of Rimstidt and Barnes (1980) which validated the application of the TST equation with σ = 1 to the dissolution and growth of silica phases. Recently, Renders *et al.* (1995) confirmed the application of TST to cristobalite as well.

The rate data for SiO_2 (am) were taken from Carroll *et al.* (1994). "Amorphous silica" added to OPC-pozzolan blends is assumed to represent silica fume (also called silica gel in this report), a common additive.

4.4.4 Feldspar

Kinetic data for feldspar dissolution were obtained from the review of Blum (1994) and the study by Schweda (1989).

5. Description of Systems Considered

Table 2 summarizes the systems used to create Figures 5 to 27. The run numbers, in column 1 of Table 2, will be used as a shorthand notation throughout the text and figures, and will be denoted as run (1), run (2)... (10 CO2), *etc.* We have used the idealized compositions in Table 1 for glass, OPC and ash, and have also added stoichiometric amorphous silica ("fume" or "gel") and kaolinite to two runs. We used the illite composition

$K_{0.6}Mg_{0.25}Al_{1.8}Al_{0.5}Si_{3.5}O_{10}(OH)_2$

and smectite composition ("Smectite-high-Fe-Mg")

$Ca_{0.025}Na_{0.1}K_{0.2}Fe^{+2}{}_{0.5}Fe^{+3}{}_{0.2}Mg_{1.15}Al_{1.25}Si_{3.5}H_2O_{12}$

which are taken directly from the EQ3/6 R1 database.

All systems initially contain 1 kg water and 16.4 kg glass. The starting water composition is a composite from our leaching tests of NTS alluvium (Stockman *et al.*, 1995), with added traces of U, Th, Pb and Ra. Apart from the small amount of initial HCO_3^- in the water, which forms a small amount of calcite in the OPC runs, and precipitation of chloride in pyromorphite ($Pb_5(PO_4)_3Cl$), the trace constituents seem to have no significant effect on the reaction paths. With an assumed density of 2.87 g/cm^3, the glass occupies 5714 cm^3; closest packing of spheres would yield ≈26% void space, or 2008 cm^3. Thus, in systems that contain no matrix material between the glass gems ((6), (6 CO2), (8) and (8 CO2)), the water would occupy half the void space. Recent studies (personal comm., Bob Vogel of FERMCo, May 10, 1995) indicates the gems pack with only 20% void space, which implies that 1 kg water would occupy 70% of the void space and air the rest.

The runs that include OPC also start with 985 grams of dry portland cement. We allow the dry OPC to hydrate before initiating the reaction with the pozzolans and clays; thus we have skipped approximately the first year of the cement hydration process. Hydration of the OPC reduces the free water mass to 0.755 kg, and increases the cement mass to 1.23 kg. When pozzolans and clays are present, the weight ratio of additives to OPC is 2.3 to 5.2. These ratios are high, but quite reasonable for grouts (Bowen, 1981). The fly ash and fuel ash particles are assumed to exist as 10 μm diameter spheres and to have the same TST parameters as the waste glass. The SiO_2 (am) in run (5) is assumed to be 1 μm diameter spheres, and dissolves with the TST parameters described in section 4.4.3. In effect, the high surface area of the pozzolans makes them sacrificial materials, reacting and consuming the corrosive agents in the OPC, before the corrosive agents attack the waste glass itself. In run 7, the OPC was also allowed to pre-react with $10^{-3.5}$ atm CO_2 (nominally the ambient for the earth's surface), and the fugacity of CO_2 was maintained at this level throughout the run, to simulate the degradation in the carbonated skin of a cast concrete block. While the outer skin of a concrete structure carbonates quickly (Walton

et al., 1990; Ohga and Nagataki, 1989), the rate decreases with the square root of time; the outer mm is typically converted within 0.1 years, but it can take 1000 years to reach a depth of 10 cm. Carbonation consumes Ca in portlandite and CSH (calcium silicate-hydrate) to produce calcite, and can reduce pH to near the Calcite-Gypsum-air buffer (≈ 7.8), thereby greatly increasing the activity of SiO_2(aq) relative to other aqueous silica species. This has the effect of slowing the glass degradation rate according to the affinity term. It could be argued that in a normal repository, groundwater would see only the carbonated skin of a waste form. However, the glass and matrix deep inside a cemented block will still follow the reaction paths defined for runs (1)-(5), which will produce a different set of minerals than simple carbonation.

Two types of CO_2 constraints were applied to the runs that do *not* contain OPC. In (6), (8), (9) and (10), the only source of CO_2 was the small amount of HCO_3^- initially dissolved in the aqueous phase. In (6 CO2) through (10 CO2), the fugacity of CO_2 was fixed at $10^{-3.5}$ atm. We believe the latter conditions are more realistic, since uncemented matrices tend to be highly permeable, and the soils at NTS "breathe" to tens of meters (Lindstrom *et al.*, 1993). The CO_2 pressure in NTS soils approaches the surface ambient ($\approx 10^{-3.5}$ atm) in the dry winter months, but may be several times this value during the rainy season (Terhune and Harden, 1991). The effect of even this modest fixed CO_2 fugacity can be quite significant. The breakdown of the glass produces a great deal of sodium, which allows maintenance of both high pH and high aqueous CO_3^{2-} and HCO_3^-, and encourages the formation of soluble hydroxy-carbonate complexes of U and Th.

All runs reported in this study used a fixed O_2 fugacity of 0.2 atm. In general, the choice of such a high O_2 pressure is conservative for U solubility (*i.e.*, tends to overestimate solubility). Test runs at lower fO_2 (down to 10^{-40} atm) showed little effect on the solubility of Pb, Ra and Th, and virtually no effect on the glass degradation rate; the principal effect was the replacement of some solid oxides with sulfides (*e.g.* galena, PbS, replaced plattnerite). In most groundwater systems, the rate of conversion of sulfate to sulfide is quite slow (Goldhaber and Kaplan, 1974), in the absence of bacteria and organic matter. Sulfate-reducing bacteria generally live at neutral pH in the absence of oxygen. These conditions are unlikely to be found in cement environments. Therefore, the instantaneous conversion assumed by EQ3/6 at low fO_2 may be quite unrealistic. The inherent fO_2 of OPC-pozzolan-waste glass systems can vary tremendously, as reductants are sometimes used in glass processing to suppress formation of a separate sulfate phase (DOE, 1993).

Table 2. EQ3/6 Run Conditions.						
Run	**Glass**	**OPC**	**Pozzolan**	**Clay**	**CO_2 buff.**	**TST precipitation**
(1)	16.4 kg A	1 kg	0	0	--	--
(2)	16.4 kg A	1 kg	2.5 kg fly ash	0	--	--
(3)	16.4 kg A	1 kg	2.5 kg fly ash	2.6 kg Kaol	--	--
(4)	16.4 kg A	1 kg	2.3 kg FUEL ash	0	--	--
(5)	16.4 kg A	1 kg	2.5 kg fly ash 0.3 kg SiO_2 gel	0	--	--
(6)	16.4 kg A	0	0	0	--	Qtz
(6 CO2)	16.4 kg A	0	0	0	$10^{-3.5}$ atm	Qtz
(7)	16.4 kg A	1 kg	0	0	$10^{-3.5}$ atm	Qtz
(8)	16.4 kg A	0	0	0	--	--
(8 CO2)	16.4 kg A	0	0	0	$10^{-3.5}$ atm	--
(8C CO2)	16.4 kg C	0	0	0	$10^{-3.5}$ atm	--
(9)	16.4 kg A	0	0	4 kg Smec	--	Qtz, K-spar, Kaol
(9 CO2)	16.4 kg A	0	0	4 kg Smec	$10^{-3.5}$ atm	Qtz, K-spar, Kaol
(10)	16.4 kg A	0	0	3.4 kg Illite	--	Qtz, K-spar, Kaol
(10 CO2)	16.4 kg A	0	0	3.4 kg Illite	$10^{-3.5}$ atm	Qtz, K-spar, Kaol

The rightmost column in Table 2 indicates additional phases, initially present in trace quantities, that were allowed to precipitate and redissolve according to TST rate laws. In the (6), (7) and (6 CO2) runs, a small amount of quartz seed (1 g / 267 g of glass) was added to the system; the assumed surface area of the quartz corresponds to grains 0.4 mm in diameter. For the (6) and (6 CO2) runs, the quartz seed is intended to represent the fine sand that would invariably filter in among the glass gems if the latter were simply poured into the trenches; for the (7) run, it represents the fine sand that is invariably in cement. Runs (9) through (10 CO2) initially predicted the precipitation of K-feldspar (maximum microcline) and kaolinite. Because these phases can artificially lower $\{K^+\}$ and $\{SiO_2(aq)\}$ if allowed to precipitate instantaneously, we chose to constrain their precipitation with a TST rate law inferred from dissolution studies. The amounts assumed to be initially present correspond to $\approx$ 1 g K-feldspar and 1 g kaolinite per 60 g glass. The K-feldspar grains are assumed to be $\approx$ 0.8 mm in diameter, and the specific surface area of the kaolinite is as described in section 4.4.2.

6. Results and Discussion

6.1 Overview

Figure 8 shows the results of eight EQ3/6 calculations for the systems summarized in Table 2, plotted as the "moles" of waste glass consumed *vs.* time, for a system containing a total of approximately 10^2 moles (a "mole" of waste glass is $\approx$ 160 g). The top 5 curves are all for systems containing some uncarbonated OPC in the matrix; the topmost curve (1) is for a system with a pure OPC matrix, and curves (2)-(5) represent blends of various pozzolonic additives with the OPC. In the lower portion of the plot, curve (8) is for a system with no matrix material except water occupying 1/2 the volume of the interstices between the glass pellets. The calculation for curve (8) was restricted to suppress formation of any silica polymorphs more stable than cristobalite; most of the silicate phases formed in the course of the calculation are smectite clays. The calculation for curve (6) is very similar to (8), except the system contains fine-grained quartz "sand" in the interstices of the glass pellets, as described in the previous section. Curve (7) is for the same initial composition as curve (1), except the OPC was allowed to carbonate, and the calculation was maintained at $PCO_2 = 10^{-3.5}$ (the ambient) throughout the calculation. Thus curve (7) represents the path taken by the carbonated skin on the outside of a cast OPC/glass block.

While the addition of pozzolans does decrease the corrosion rate of glass in OPC blends, the maximum reduction between curves (1) and (5) is a factor of $\approx$ 30. In comparison, the reduction offered by simple carbonation (curve (7)) is up to 4 orders of magnitude. Thus it does not seem practical to rely solely on the pozzolanic effect to eliminate glass corrosion. However, we will later show that the OPC-containing matrices may be effective in reducing radionuclide solubility.

Figure 9 shows the effects of using clays as matrix materials, and reprises curves (6) and (8) on an expanded vertical scale, for the case of no CO_2 buffering. Both the high-Fe-Mg smectite (9) and illite (10) clays enhance glass corrosion at some point in the calculation. For the former, the enhancement occurs as Fe-Mg-rich smectite converts to more stable, silica- and Fe-rich clays (nontronite and saponite); for the latter, the enhancement correlates with the precipitation of K-feldspar and smectites. Figure 10 shows results from the same set of matrices, but with CO_2 fugacity buffered to $10^{-3.5}$ atm. The additional CO_2 mainly slows the corrosion rate for run (6 CO2), where the matrix is a small amount of quartz "seed"; the principal reason is that the CO_2 lowers the pH, decreasing the overall glass dissolution rate. The added CO_2 also seems to stabilize the system numerically, allowing the illite calculation (10 CO2) to extend to much longer times (see section 3.3).

The variation of pH with time for 5 matrix/environment combinations is shown in Figure 11. The upper two curves are for non-carbonated OPC; the lower three curves all represent cases where the system is buffered to atmospheric CO_2. Figures 12-16 show the

calculated minerals assemblages for the 5 cases shown in Figure 11; the ties between system pH and the minerals formed will be discussed in the following sections. Figures 17-20 show Pb, Ra, Th, and U solubilities as a function of time. Ties between these solubilities and mineral assemblages will also be made.

6.2 Trusting the "Affinity Effect"

The contrast between curves (6) and (8) in Figure 8 shows the problem with trusting the "affinity effect" to keep corrosion rates low. The calculations were intentionally biased toward early silica saturation (and cessation of glass corrosion) by using the Bourcier *et al.* (1994) value of $\sigma = 10$, and by assuming the K for silica saturation (equation 1) corresponded to chalcedony (on the low end of the K's measured for glass dissolution). Curve (6), with quartz precipitation, follows the course of curve (8) until about 10 years, then begins to climb rapidly. The calculation of (6) was stopped because the differential equation system became "stiff", and required extremely small time steps for convergence. However, mere extrapolation of the trend suggests that within 1000 years, the amount of glass corroded would reach the levels found in curves (1)-(5), the systems with OPC matrices. The cause of the runaway degradation is simple; quartz precipitation lowers the concentration of $SiO_{2\,(aq)}$ in solution, potentially below the "saturation" K for the glass. This increases the surface area of quartz available for precipitation, causing more glass to dissolve, increasing the rate of removal of $SiO_{2\,(aq)}$ from solution, which increases the rate of glass degradation, *etc.* There are many assumptions in the calculation of (6). The most questionable assumption may be the validity of using the dissolution rates to infer precipitation rates *via* the TST equation. Uncertainties also arise by assuming that most of the surface area of the quartz grains is available for precipitation; and that there will be no inhibitors to the precipitation of quartz (such as Fe hydroxide coatings or adsorption of phosphate on mineral surfaces). However, Renders *et al.* (1995) have shown that precipitation rates for cristobalite apparently can be inferred from TST dissolution rates, and Rimstidt and Barnes (1980) showed quartz precipitation and dissolution rates were consistent with TST. The alluvium at the RWMS is low in Fe, and there is no evidence for development of extensive Fe coatings on the existing quartz grains. Therefore a conservative conclusion is that the "affinity effect" may cease to protect the glass from corrosion after as little as 10 years.

In parts of the NTS, not far from the RWMS, the ground waters are supersaturated with respect to quartz. In fact, the dissolved silica concentrations are closer to equilibrium with cristobalite and even amorphous silica (Guzowski *et al.*, 1983; Yang *et al.*, 1990). Such high silica concentrations are probably maintained by dissolution of abundant, very fine-grained cristobalite in the devitrified tuff, and by breakdown of volcanic glass in the vitric tuffs. However, there is currently no evidence for such silica saturation in the RWMS-area pore waters.

6.3 pH Effects

In the absence of a strong affinity effect, the most reliable control on the rate of glass degradation is pH. As shown in Figure 11, CO_2-buffered systems (6 CO2, 7 and 8 CO2) generally maintain a lower pH than the unbuffered, OPC-containing systems (1 and 5).

However, the generalization is not perfect. For run (8 CO2), the pH is nearly constant at 8.2. Since precipitation of stable silica polymorphs is suppressed in this run, very little glass dissolves, so the aqueous Na content is never very high. The principal alteration mineral, smectite (Fig. 12), contains OH in its formula and offers some pH control. In contrast, in run (6 CO2), where quartz is allowed to precipitate, the pH rises as the glass dissolves. Smectite and quartz are the principal minerals formed (Fig. 13), but together do not offer enough buffering to offset the Na released from the glass. The CO_2 pressure has a limited effect in lowering the pH, mainly because the aqueous phase is low in alkaline earths that could precipitate insoluble carbonates. Therefore, ultimately the pH rises even higher than in run (5), an unbuffered OPC run. In contrast, run (7) maintains a pH of 7.7 for most of the calculation, controlled by the buffering capacity of the calcite-gypsum couple (Fig. 14).

To understand the contrast between cases (1) and (5) in Figure 11, it is necessary to examine the phases that form as a function of time (Figs. 15 and 16). In OPC and OPC/fly ash mixes, it is common for pH to rise from 13.2 to 13.8 in the first 30 days of curing (Berry *et al.*, 1989). This increase is attributed to reactions of the type:

$$Na_2SO_4 + Ca(OH)_2 + 2H_2O = CaSO_4{\cdot}2H_2O + 2NaOH, \quad (7)$$

and in fact, the increase in pH generally corresponds to a decrease in solution sulfate concentration. This pH increase starts immediately during the setting of the cement, and in our calculations, such reactions are assumed to have occurred before the clock is started for the glass-matrix reaction path. However, the interaction of the sodic component of glass can have a similar effect, *via* creation of hillebrandite:

$$Na_2SiO_3 + 2Ca(OH)_2 = Ca_2SiO_3(OH)_2 + 2NaOH; \quad (8)$$

and similarly, *via* creation of tobermorite from hillebrandite:

$$5(Ca_2SiO_3(OH)_2) + 7Na_2SiO_3 + 23H_2O = 2(Ca_5Si_6O_{17}{\cdot}10.5H_2O) + 14NaOH. \quad (9)$$

A strategy for lessening the effects of reactions (8) and (9) is to add siliceous and aluminous material with lower Na contents, and thus effect the conversion of portlandite by (for example):

$$SiO_2 + 2Ca(OH)_2 = Ca_2SiO_3(OH)_2 + H_2O\,. \quad (10)$$

The initial pH rise for run (5) is less dramatic than for run (1), mainly because the silica gel, and then the fly ash, consume $Ca(OH)_2$ by reactions that produce little base. There are additional contributions to pH control in the early stages. For example, the greater aluminum content of the fly ash for (5) encourages formation of ettringite ($Ca_6Al_2(SO_4)_3(OH)_{12}{\cdot}26H_2O$), which consumes hydroxyl. In the latter stages of reaction, production of saponite (nominally $Ca_{0.165}Mg_3Al_{0.33}Si_{3.67}O_{10}(OH)_2$) also consumes OH^-. The fly ash/silica gel-containing system is also predicted to produce numerous zeolites

early in its evolution. In our experience, the specific type of zeolite and relative abundances, predicted by EQ3/6, depend on subtleties in the Ca/Na/Al/Si ratios of the system. While zeolites were long ignored in the cement literature, numerous recent studies (Cole *et al.*, 1981; Hoyle and Grutzeck, 1989; Larosa *et al.*, 1992a,b; Marfil and Maiza, 1993) show that they do indeed form, but require relatively high Si/Ca and/or Al/Ca for the matrix blend. In real cements, an effectively high$\{SiO_2\ (aq)\}/\{Ca^{2+}\}$ can also be achieved through carbonation, which may explain the production of high-silica zeolites in the study by Cole *et al.* (1981). It is interesting that the zeolite-producing compositions in Hoyle and Grutzeck (1989) fall outside the compositional range of most American OPC/fly ash blends (Atkins *et al.*, 1989), but are closer to our OPC/fuel ash and OPC/fly ash/silica gel blends (Fig. 8, curves (4) and (5)). The growth of zeolites in the cement matrix greatly reduces the leachability of Cs (Hoyle and Grutzeck, 1989), so it may be worthwhile to tailor matrix composition to encourage zeolite formation.

6.4 Solubility of Radionuclides

Figures 17 through 20 show the calculated solubilities of Pb, Ra, Th and U as functions of time for cases (1), (5), (7) and (8 CO2) (the corresponding mineral assemblages can be found in Figures 12 and 14-16). The most striking conclusion to be drawn from these calculations is that the matrices associated with the lowest glass corrosion rates (*e.g.* (7) and (8 CO2)) generally *do not* engender the lowest solubilities. Thus, it will be very important for those designing repositories to carefully weigh the benefits of minimizing glass degradation, such as structural integrity and retrievability, against those of minimizing the release and transport of radionuclides.

Lead solubility (Fig. 17) in the OPC blends ((1) and (5)) is largely due to the formation of aqueous $Pb(OH)_3^-$ with plattnerite (PbO_2) as the solubility-limiting phase. The peak solubility for run (1) at about 10 years corresponds to the sharp pH maximum seen in Figure 11. For run (8 CO2), the dominant solution complex is $PbCO_3$ (aq), but in run (7), Pb^{2+} dominates for over 1000 years before being replaced by $PbCO_3$ (aq). In both of the latter cases, pyromorphite ($Pb_5(PO_4)_3Cl$) joins plattnerite as a solubility-limiting phase. In experiments at moderate PCO_2, hydrocerussite generally forms in preference to plattnerite; however, the Q/K for hydrocerussite is $\approx$0.8 in our CO_2-buffered runs, so within the error of the thermodynamic data, either phase might form. Pyromorphite is stabilized in the CO_2-buffered systems, because the low Ca^{2+} prevents precipitation of apatite, and allows solution phosphate concentrations to reach higher levels. The small amount of Cl comes from the initial pore waters. Overall, the lowest Pb solubility is for run (5), the OPC-fly ash-SiO_2 gel blend.

Radium solubility (Fig. 18) is dominantly from Ra^{2+} for all cases. The highest Ra solubility is for run (8 CO2), which never develops a solid Ra-containing phase, mainly because glass dissolution terminates before the release of significant sulfate. For the other three cases, formation of the barite ($(Ba,Ra)SO_4$) solid solution maintains low Ra solubility.

Thorium solubility (Fig. 19) is highest for the two CO_2-buffered systems. For run (8 CO2), the dominant dissolved species is $Th(OH)_3CO_3^-$, and no solubility-limiting solid

ever forms. The plateau in Th solubility merely reflects cessation of glass dissolution. For (7), $Th(OH)_3CO_3^-$ also dominates, but $Th(OH)_4$ (aq) is also significant, and solubility is ultimately controlled by ThO_2 (am). For the two systems *without* CO_2 buffering, (1) and (5), the $Th(OH)_4$ (aq) complex dominates, and ThO_2 (am) is the solubility-limiting solid.

Uranium solubility (Fig. 20) is also highest in the CO_2-buffered systems, where haiweeite ($Ca(UO_2)_2(Si_2O_5)_3 \cdot 5H_2O$) is ultimately the solubility-limiting solid. In (8 CO2), the highest solubilities occur when the $UO_2(CO_3)_2^{2-}$ aqueous complex is preponderant. For run (7), $UO_2(OH)_2$ (aq) dominates until ≈ 2000 years, when $UO_2(CO_3)_3^{4-}$ becomes the major aqueous species. In the runs with OPC and *no* CO_2 buffering, $CaUO_4$ is the solubility-limiting solid, and hydroxide complexes dominate; for (1), $UO_2(OH)_4^{2-}$ initially dominates, then gives way to $UO_2(OH)_3^-$, and for (5), $UO_2(OH)_3^-$ and $UO_2(OH)_2$ (aq) are of similar importance. While $CaUO_4$ is unknown in purely natural systems, unspecified calcium uranium oxides have reportedly formed in uranium-contaminated soils at the Fernald site over a time frame of 50 years (Buck *et al.*, 1994). The very high Ca/phosphate of the OPC blends undoubtedly increases the stability of the simple Ca-U^{+6} -oxides over the Ca-U^{+6}-phosphate minerals, such as autunite, which commonly form in nature. No thermodynamic data were available for becquerelite ($Ca[(UO_2)_6O_4(OH)_6] \cdot 8H_2O$; Pagoaga *et al.*, 1987), which is found in nature as an alteration mineral at uranium deposits.

6.5 Sensitivity Study: Effects of Varying Affinity Term Parameters

We have shown that the precipitation of secondary silicate minerals can cause {SiO_2 (aq)} to drop, effectively removing the passivating effect of the affinity term in equation (1) in as little as 100 years. This occurs even when there is no matrix other than a small amount of "seed" quartz (section 6.2, and curves (6) and (6 CO2) in Figs. 9 and 10) that provides an initial surface area for SiO_2 precipitation. However, there is another reason not to trust the affinity effect; the K and σ parameters are essentially obtained by curve fits, and their evaluation from experiments depends heavily on assumptions about the effective surface area of the glass, the precipitation of secondary phases, and the speciation of aqueous silica. In this section, we consider how the uncertainty in these parameters affects the uncertainty in the estimates of glass corrosion rate. Figures 21 through 25 compare calculations for 5 systems for three sets of conditions: (a) K = chalcedony, and σ = 10; (b) K = α-cristobalite and σ = 10; and (c) K = chalcedony and σ = 1. The $\log_{10}K$ for chalcedony is -3.723 at 25°C (-2.862 at 100°C), and the $\log_{10}K$ for cristobalite is -3.449 at 25°C (-2.660 at 100°C). Though this difference may seem trivial, it can be quite significant for some calculations. We focus on cases with no matrix or with clay matrices, where the affinity effect has been proposed to be a significant cause of passivation (Godon *et al.*, 1992). The affinity effect is relatively unimportant for most systems with OPC and *no* CO_2 buffering, since {SiO_2 (aq)} is kept low by the high Ca/Si of solid OPC. The only unbuffered OPC matrix considered in the following discussion is run (5), where the added SiO_2 gel and fly ash significantly increase {SiO_2 (aq)}. It is important to emphasize that the conclusions below apply *only* to uncertainty in the rate of glass corrosion; the calculated solubilities of Pb, Ra, Th and U are little affected by the uncertainty in K and σ.

For run (8 CO2), the effects of varying K and σ are relatively small. At times greater than 10 years, the maximum difference in moles of glass dissolved varies only by a factor of 2.5. This is insignificant, given that less than 0.0005% of the total glass is corroded (Fig. 21). In contrast, for run (6 CO2), where quartz is allowed to precipitate (Fig. 22), the effect of varying K is more than a factor of 10 after 100 years, and the discrepancy grows with time. By 1000 years, about 0.5% of the glass has corroded for the run with K = cristobalite.

The calculations with the two clay matrices (Figs. 23 and 24) show similar effects. For illite, the value of σ seems to have the greatest effect, though the early termination of the run after about 3 years (due to the "stiff system" problem described in section 3.3) makes a firm conclusion impossible. For the high-Fe-Mg smectite matrix, the value of σ definitely makes the greatest difference, causing nearly a factor of 10 discrepancy after 200 years; the effect of varying K is insignificant.

The effect of varying σ is also much more significant than the effect of varying K for run (5), the OPC-fly ash-SiO_2 gel matrix (Fig. 25). After 100 years, the run with K = cristobalite has 3 times the amount of glass corrosion as the run with K = chalcedony. The gap widens even further at 300 years, indicating corrosion of about 5% of the total glass for the K = cristobalite case.

6.6 Reality Check: Comparison with Experiments

Our reaction path calculations assume that the dissolution of pozzolans and waste glass is not hindered by diffusion and the "armoring" of the glass surface by secondary minerals. The calculations also make implicit assumptions about the rates of precipitation of some alteration minerals, about the phases that control solubility, and about the amount of surface area available for precipitation of secondary phases. While these assumptions are clearly important, they cannot all be tested independently within the scope of the current study. However, it is possible and useful to compare the predictions of our work against the degradation rates and solubilities observed for cement- and glass-containing systems.

6.6.1 Rates of pozzolan reaction

There is conflicting evidence in the literature on the reaction rate between pozzolans and OPC. Diamond *et al.* (1989) found no evidence for extensive reaction between OPC and various Al-rich fly ashes, based on the apparent constancy of portlandite ($Ca(OH)_2$) abundance over a year period. The fly ash grains were ≈ 10 μm in diameter (approximately the same size assumed in our calculations), and from SEM examination, appeared to be only slightly altered in year-old cements. In contrast, Lea (1970) documents clear evidence of pozzolanic reactions occurring over year-long periods, particularly for cements with relatively high (4:1) pozzolan:OPC weight ratios. In the latter case, up to 97% of the $Ca(OH)_2$ was consumed within a year. Atkins *et al.* (1989) also provided evidence for significant pozzolonic reactions in OPC-blends. In a mix of 20% fly ash and 80% OPC, they showed that 40% of the fly ash was consumed within 4 months. For OPC with 30 to 85% blast furnace slag, 40% of the slag was consumed within one month, with no apparent dependence an the amount of slag in that time period.

The latter results are more consistent with our calculations (Figs. 26 and 27), which indicate 40% of the fly ash consumed within 3 to 5 months. It is possible that some fly ashes have much lower primary rate constants. Hrma *et al.* (1992) found that higher Al_2O_3 contents greatly increased glass durability in the MCC-1 and PCT tests, while higher SiO_2 and CaO contents had more modest effects. According to their correlation, an Al_2O_3 increase from 20% to 25% by weight could lower leach rate by a factor of 4.

It is tempting to compare the predictions of this study against the experimental work of Andriambololona *et al.* (1992), who measured the corrosion of waste glass in the presence of mortar and various pozzolanic admixtures. However, Andriambololona *et al.* (1992) employed relatively small pozzolan/cement ratios, typically less than 0.25, and performed the tests at 90°C. The current study used pozzolan/OPC up to 4, and all calculations were performed at 25°C. Use of such high pozzolon/OPC material is common in grouting practice, and such grouts can achieve half the strength of structural OPC mixes (Bowen, 1981).

There is an extensive literature on the degradation of glass fibers in OPC (*e.g.* Larner *et al.*, 1976; Yilmaz, 1992). The fibers are ≈ 5 μm in diameter, and are added to strengthen the cement, but typically react almost completely within a year at 55°C. From the photomicrographs and activation energies given by Larner *et al.* (1976), we estimate a degradation rate of 0.5 μm/year at 25°C for "A" glass (73% SiO_2, 1% Al_2O_3, 13% Na_2O, 4% MgO, 8% CaO). Thus, it is conceivable that 10 μm spheres of silica-rich fly ash could take $\approx$ 10 years to react completely with OPC at 25°C.

6.6.2 Rates of clay formation

In our calculations, clays can form in two ways. In the first, clays form in the absence of clay "seeds." The rate of clay formation is governed solely by the attainment of saturation with respect to a particular clay. Clay nucleation and growth is instantaneous once saturation is reached. In the second, clays form according to precipitation rates derived from the TST rate law, and when an arbitrary concentration of initial "seed" surface area is present. These two modeling approaches raise two important questions. First, in the absence of clay seeds, are we modeling the nucleation and growth of clays on glass surfaces correctly? Second, in the case where seeds are initially present, is dissolution of one clay and precipitation of a new clay truly a "thermodynamically-driven" transformation, or in reality is Si concentration reduced by adsorption onto existing mineral surfaces?

To answer the first question we can look at data for smectite formation rates from glass in experiments and in nature. Various researchers have shown that smectites can form from gels, which may represent to some extent a hydrated glass surface, at 25°C in time frames of months to years (Nagy, 1995). In glass dissolution experiments at 90° to 225°C, Mazer et al. (1992a,b,c) correlated semi-quantitatively time, solution composition, and degree of hydration to the composition and extent of formation of clay/oxide alteration layers. They found evidence for formation of 7, 10, and more rarely 14 Å clay minerals after 22 days at 175°C. At T = 90°C (Ebert *et al.*, 1993) smectites form during glass degradation in near-

neutral dilute solutions in a year and in three to seven days in ≥ 1 mol/kg NaOH solutions (Tomita *et al.*, 1993). At 190°C, saponite forms on altered basaltic glass surfaces after a few months (Abdelouas *et al.*, 1994). However, at all these temperatures, the amounts of smectite that form during laboratory glass dissolution are small and consequently, their identification can be ambiguous. Smectites are thought to form during weathering of glasses buried in soils at 25°C for 1650 years (Cox and Ford, 1993); however, the dominant alteration product in these cases is amorphous. Although these lines of evidence point to nucleation and growth of smectites on glass as likely processes for our modeling approach, it is clear that more research is needed to determine unambiguously the quantity and rate of smectite formation from glass in waste repository environments. The hypothesized role of clays in reducing reactive glass surface area also must be evaluated (*e.g.*, Bates *et al.*, 1992).

The second question is addressed by considering both adsorption and dissolution/reprecipitation processes. Although it is true that Si adsorbs onto clay surfaces at 25°C (see review by Nagy, 1995), this may be the dominating process only at short times. However, when adsorption is viewed as the precursor step to subsequent nucleation and growth, the question becomes broader and is related to the fluid composition. If there are enough other components available for coadsorption, then nucleation and growth of secondary clays is likely to predominate. Within the longer span of time represented in our calculations, dissolution and reprecipitation are not unreasonable to expect, given that clay dissolution and precipitation reactions are accelerated in basic alkaline solutions in both the laboratory (Carroll-Webb and Walther, 1988) and in nature (*e.g.*, Banfield *et al.*, 1991a,b; Yuretich and Cerling, 1983).

6.6.3 Effect of clays on rate of glass degradation

Godon *et al.* (1992) showed that some smectites enhance glass degradation rates by a factor of ≈ 10 over "bentonite" at 90°C. We calculated up to a factor of 10 variation in the rate of glass degradation for illite *vs.* smectite matrices at 25°C. We have performed calculations with other clay compositions (not described in this report, at both 25°C and 90°C), and the Fe-Mg-rich clays seems to enhance corrosion of glass the most. It is unclear if the cause is an inherent lowering of silica activity, or the occurrence of reactions that drive the formation of Fe-Mg-rich silicates from the glass.

6.6.4 Cement phases: hillebrandite/tobermorite *vs.* CSH gel

In the classification of Atkins *et al.* (1992), the OPC used in this study is in the compositional region for portlandite, high Ca/Si CSH (calcium silicate hydrogel), gehlenite, and hydrotalcite. Our model currently lacks a capability to model the CSH solid solution, so calculations typically predict an admixture of hillebrandite (Ca/Si = 2) and lesser tobermorite (Ca/Si = 0.833) rather than a single CSH phase with Ca/Si ≈ 1.7. We are aware that CSH, though metastable relative to hillebrandite and tobermorite, may persist for thousands of years (Atkins *et al.*; 1991, 1992). However, the Ca silicates in our model perform mainly as a Ca-rich titrant for the much slower-reacting glass component, and it is not critical that we exactly match the phase assemblage found in real cements. Nonetheless, the hillebrandite-portlandite assemblage in our model system seems to do a

remarkably good job matching the aqueous Ca and Si concentrations measured in equilibrium with high Ca/Si CSH. Table 5.14 from Atkins *et al.* (1992) gives, for system Ca/Si = 1.9 and 0.4 mol/L NaOH, *measured* $[Ca_{tot}] = 1.3 \cdot 10^{-3}$ mol/kg, and *measured* $[Si_{tot}] = 2.4 \cdot 10^{-5}$; the EQ3/6 runs with the hillebrandite-portlandite assemblage give calculated $[Ca_{tot}] = 1.7 \cdot 10^{-3}$ mol/kg, and calculated $[Si_{tot}] = 2.4 \cdot 10^{-5}$. It is notable that the CSH thermodynamic model of Atkins *et al.* predicts Ca concentrations slightly better than our hillebrandite-portlandite model, but overpredicts the *measured* Si concentrations by two orders of magnitude.

Our model does a respectable job predicting U solubilities in cement matrices. Atkins *et al.* (1991) examined U concentration in equilibrium with OPC matrices, and obtained a maximum measured value of $\leq 10^{-6}$ to 10^{-7} mol/L, *vs.* a predicted value of $\approx 10^{-4}$ mol/L using then-available thermodynamic data. For run (1), most analogous to the Atkins *et al.* (1991) study, we obtain a predicted maximum of $\approx 10^{-8.6}$ m. The greater agreement may be fortuitous, but may also reflect our improvements in the thermodynamic database.

7. Conclusions and Recommendations

We have shown that reaction path calculations provide a framework for assessing the merits of proposed waste form-matrix combinations. The calculations provide reasonable matches to observed and experimental rates of fly ash reaction and observed solute concentrations in OPC matrices. The minerals predicted from the calculations are reasonably close to those found in real cements and glass corrosion studies. We have developed a set of templates for modeling glass-matrix interactions, and use of these templates should speed future work.

The most obvious conclusion from this study is that the lowering of radionuclide solubility, and the reduction of glass corrosion, are not necessarily compatible goals (Figs. 8-11 and 17-20). The OPC-containing matrices clearly increase the predicted corrosion rate of waste glass, but the OPC-fly ash-silica blend provides the overall lowest predicted solubilities for Pb, Ra, Th and U. Performance assessment calculations are often driven by solubilities, so there is a clear need for modelers and engineers to weigh the consequences of using matrix materials that may significantly degrade the waste form. It appears from Figure 8 that the OPC-glass reaction can be substantially slowed through judicious use of pozzolans, but long-term and accelerated experiments must be performed to determine if there are other negative effects, such as excessive expansion and cracking of the cemented waste form.

If the cessation of glass corrosion is the intended goal, the simple carbonation of the concrete (curve (7) in Fig. 8) will accomplish this task. However, carbonation rates decrease dramatically with time, and the glass-OPC reactions inside cast meter-sized blocks will likely continue for hundreds, if not thousands of years. A more complete assessment of carbonation would couple reaction path calculations with flow models that include effects of the entire repository environment. If a repository is massive enough, water reaching waste may pass through large amounts of concrete and be depleted in CO_2, making carbonation unlikely. It is also important to recognize that the reaction path taken by waste forms that are immediately exposed to atmospheric CO_2 could be quite different from a path that involves glass-OPC reactions in a massive concrete block for hundreds of years. This would be especially true if cracking and exposure to CO_2 occurred at a time when the glass is already largely degraded.

With current modeling capabilities, we cannot trust the "affinity effect" to ensure long-term passivation of glass waste forms (curves (6) and (6 CO2) in Figs. 9 and 10). Experiments that determine the TST k, K, N and σ parameters (equation 1) are carefully designed to avoid the "artifacts" contributed by precipitation of secondary minerals. However, such artifacts would be omnipresent if glass waste pellets are simply dumped into trenches, and fine-grained alluvium fills the pore spaces. Our calculations may be overly conservative, because they do not include the armoring effects of secondary minerals, which may passivate both the surface of the waste glass and the quartz and feldspar grains in the alluvium. It should be possible to approximate such effects, through

modeling and judicious long-term experiments. Based on the calculations shown in Figures 8-10, up to 20 years would be required to detect the failure of the affinity effect at 25°C; however, the time could be shortened substantially by increasing temperature and the surface area of the seed minerals. However, the presence of seed minerals in the calculations may not represent the actual mode of formation of clays on degrading glass surfaces in the repository environment. Clays likely nucleate by adsorption of metals onto local linked-SiO_2 structural units in the glass surface that then form precursor nuclei for continued clay growth. Little is known about clay nucleation mechanisms and kinetics on glass and much more research in this area is necessary before accurate modeling can be conducted. In the absence of experiments, studies of analogues such as glasses buried for hundreds of years in moist sediments (*e.g.* Cox and Ford, 1993) may be adequate to test the affinity effect.

We are confident that our modifications to the thermochemical database have improved the accuracy of our calculations. Nonetheless, the many-orders-of-magnitude variations seen in Figures 5 and 6 are disturbing, and underline the need for scrutiny and diligence in any calculation involving a very different waste form or radionuclide. The task of maintaining a self-consistent database is enormous, and our experiences should serve as warning to those who believe solubility calculations are straightforward.

8. Abbreviations

80x86	A processor based on Intel 80x86 architecture; *e.g.* iAPX486 or Pentium.
CSH	Amorphous, hydrous Ca-silicate gel formed in hydrated portland cement.
DOE	U. S. Department of Energy.
EQ3/6	A set of thermodynamic modeling codes. EQ3 sets initial speciation and EQ6 calculates reaction paths.
F77L3	FORTRAN 77 compiler produced by Lahey Computer Systems, Inc.
LF90	FORTRAN 90 compiler produced by Lahey Computer Systems, Inc.
LLNL	Lawrence Livermore National Laboratory.
MCC-1	Materials Characterization Center - 1 Test.
NTS	Nevada Test Site.
ODE	Ordinary Differential Equation.
OPC	Ordinary Portland Cement.
PC	Personal Computer.
PCT	Product Compatibility Test.
PP	Post Processor, a data interpretation/graphics code for EQ3/6.
PNL	Pacific Northwest Laboratory.
RWMS	Radioactive Waste Management Site.
TST	Transition State Theory (rate law).

9. References

Abdelouas A., Crovisier J. L., Lutze W., Fritz B., Mosser A., and Muller R. (1994) Formation of hydrotalcite-like compounds during R7T7 nuclear waste glass and basaltic glass alteration. *Clays Clay Min.* **42**, 526-533.

Adami L. H. and Conway K. C. (1966) Heats and free energies of formation of anhydrous carbonates of barium, strontium, and lead. *U. S. Bur. Mines Report Invest.* **6822**, 7 pp.

Andriambololona Z., Godon N., and Vernaz E. (1992) R7T7 Glass alteration in the presence of mortar: effect of the cement grade, in: C. G. Sombret (ed.) *Scientific Basis for Nuclear Waste Management XV*, Mat. Res. Soc. Symp. Proc. **247**, 151-158.

Atkins M., Glasser F. P., and Moroni L. P. (1991) The long-term properties of cement and concretes, in: T. Abrajano and L. H. Johnson (eds.), *Scientific Basis for Nuclear Waste Management XVII*, Mat. Res. Soc. Symp. Proc. **212**, 373-386.

Atkins M., Macphee D. E., and Glasser F. P. (1989) Chemical modelling in blended cement systems, in: V. M. Malhotra (ed.), *Fly Ash, Silica Fume, Slag, and Natural Pozzolans in Concrete*, Proceedings Third International Conference, Trondheim, Norway, 1989, American Concrete Institute, 73-95.

Atkins M., Bennett D., Dawes A., Glasser G., Kindness A., and Read, D. (1992) *A Thermodynamic Model for Blended Cements*, DOE-HMIP-RR-92.005.

Baglan N., Fourest B., Guillaumont R., Blain G., LeDu J.-F., and Genet M. (1994) Solubility of thorium orthophosphate, *New Jour. Chemistry* **18**, 809-816.

Banfield J. F., Jones B. F., and Veblen D. R. (1991a) An AEM-TEM study of weathering and diagenesis, Abert Lake, Oregon: I. Weathering reactions in the volcanics, *Geochim. Cosmochim. Acta* **55**, 2781-2793.

Banfield J. F., Jones B. F., and Veblen D. R. (1991b) An AEM-TEM study of weathering and diagenesis, Abert Lake, Oregon: II. Diagenetic modification of the sedimentary assemblage, *Geochim. Cosmochim. Acta* **55**, 2795-2810.

Bates J. K., Ebert W. L., Feng X., and Bourcier W. L. (1992) Issues affecting the prediction of glass reactivity in an unsaturated environment, *Jour. Nuclear Materials* **190**, 198-227.

Berger G., Claparols C., Guy C., and Daux V. (1994) Dissolution rate of a basalt glass in silica-rich solutions: implications for long-term alteration, *Geochim. Cosmochim. Acta* **58**, 4875-4886.

Berry E. E., Hemmings R. T., Langley W. S., and Carette G. G. (1989) Beneficiated fly ash: hydration, microstructure, and strength development in portland cement systems, in: V. M. Malhotra (ed.), *Fly Ash, Silica Fume, Slag, and Natural Pozzolans in Concrete*, Proceedings Third International Conference, Trondheim, Norway, 1989, American Concrete Institute, 241-273.

Bloss F. D. (1994) *Crystallography and Crystal Chemistry (An Introduction)*, Mineralogical Soc. America, 206-207, 209, 214, and 215.

Blum, A. E. (1994) Feldspars in Weathering, in: I. Parson (ed.), *Feldspars and Their Reactions*, Kluwer Academic Publishers, 595-630.

Bourcier W. L. (1994) *Critical Review of Glass Performance Modeling* ANL-94/17, Argonne National Laboratory, Argonne, IL 60439.

Bourcier W. L., Carroll S. A., and Phillips B. L. (1994) Constraints on the affinity term for modeling long-term glass dissolution rates, in: A. Barkatt and R. A. Van Konynenberg (eds.), *Scientific Basis for Nuclear Waste Management XVII*, Mat. Res. Soc. Symp. Proc. **333**, 507-512.

Bowen R. (1981) *Grouting in Engineering Practice* (Second Edition). Applied Science Publishers LTD. John Wiley & Sons, New York p. 285.

Brady P. V. and Walther J. V. (1990) Kinetics of Quartz Dissolution at Low Temperatures, *Chem. Geol.* **82**, 253-264.

Buck E.C., Brown N.R. and Dietz N.L. (1994) Distribution of uranium-bearing phases in soils from Fernald, in: A. Barkatt and R. A. Van Konynenberg (eds.), *Scientific Basis for Nuclear Waste Management XVII*, Mat. Res. Soc. Symp. Proc. **333**, 437-444.

Burch T. E., Nagy K. L., and Lasaga A. C. (1993) Free energy dependence of albite dissolution kinetics at 80°C and pH 8.8. *Chem. Geol.* **105**, 137-162.

Carroll S. A., Bourcier W. L., and Phillips B. L. (1994) *Surface Chemistry and Durability of Borosilicate Glass*, in: A. Barkatt and R. A. Van Konynenberg (eds.), *Scientific Basis for Nuclear Waste Management XVII*, Mat. Res. Soc. Symp. Proc. **333**, 533-540.

Carroll-Webb S. A. and Walther, J. V. (1988) A surface complex reaction model for the pH-dependence of corundum and kaolinite dissolution rates, *Geochim. Cosmochim. Acta* **52**, 2609-2623.

Chermak J. A. and Rimstidt J. D. (1989) Estimating the thermodynamic properties (ΔG_f° and ΔH_f°) of silicate minerals @ 298 K from the sum of polyhedral contributions, *Amer. Mineral.* **74**, 1023-1031.

Chermak J. A. and Rimstidt J. D. (1990) Estimating the free energy of formation of silicate minerals at high temperatures from the sum of polyhedral contributions, *Amer. Mineral.* **75**, 1376-1380.

Cochran J. R., Brown T. J., Price L. L., Stockman H. W., Gallegos D. P., and Conrad S. H. (1995) *Preliminary Evaluation of the Use of the Greater Confinement Disposal Concept for the Disposal of Fernald 11e(2) Byproduct Material at the Nevada Test Site*. Prepared by Sandia National Laboratories Safety and Risk Assessment Dept. for the U.S. Department of Energy, March 1995.

Cole W. F., Lancucki C. J., and Sandy M. J. (1981) Products formed in an aged concrete, *Cement and Concrete Research* **11**, 443-454.

Cox G. A. and Ford B. A. (1992) The long-term corrosion of glass by ground-water, *Jour. Mat. Sci.* **38**, 5637-5647.

Devidal J. L., Dandurand J. L., Schott J. (1992) Dissolution and precipitation kinetics of kaolinite as a function of chemical affinity (T = 150°C, pH = 2 and 7.8). In Y. K. Kharaka and A. S. Maest (eds.) Water Rock Interactions, 93-96, AA Balkema, Rotterdam.

Dhir R. K. and Byars E. A. (1993) Pulverized fuel-ash concrete: intrinsic permeability, *ACI Mat. Jour.* **90**, #6, 571-580.

Diamond S., Sheng Q., and Olek J. (1989) Evidence for minimal pozzolanic reaction in a fly ash cement during the period of major strength development, in: L. R. Roberts and J. P. Skalny (eds.), Mat. Res. Soc. Symp. Proc. **137**, *Pore Structure and Permeability of Cementitious Materials*, 437-445.

DOE, Fernald Office (1993) *Operable Unit 4 Treatability Study Report for the Vitrification of Residues from Silos 1,2, and 3.* Fernald Environmental Management Project, Fernald, OH, May 1993.

Ebert W. L., Bates J. K., Buck, E. C., and Bradley C. R. (1993) Accelerated glass reaction under PCT conditions. *Mat. Res. Soc. Proc.* **294**, 569-577.

Eikenberg J. (1990) *On the Problem of Silica Solubility at High pH,* PSIBericht Nr. 74 (Paul Scherrer Institut).

Fourest B., Baglan N., Guillaumont R., Blain G., and Legoux Y. (1994) Speciation of thorium in phosphate-containing solutions. *Jour. of Alloys and Compounds* **213/214**, 219-225.

Ganor J., Mogollon J.L., and Lasaga A.C. (1995) The effect of pH on kaolinite dissolution rate and on activation energy, *Geochim. Cosmochim. Acta* **59**, 1037-1052.

Gautier J.-M., Oelkers E. H., and Schott J. (1994) Experimental study of K-feldspar dissolution rates as a function of chemical affinity at 150C and pH 9, *Geochim. Cosmochim. Acta* **58**, 4549-4560.

Gin S, Godon N, Mestre J. P. and Vernaz E. Y. (1994) Experimental Investigations of Aqueous Corrosion of R7T7 Nuclear Glass at 90°C in the Presence of Organic Species, *Applied Geochemistry* **9**, 255-269.

Godon N., Andriambololona Z., and Vernaz E. (1992) Effect of a siliceous additive in a clay engineered barrier on aqueous corrosion of R7T7 nuclear waste glass, in: C. G. Sombret (ed.) *Scientific Basis for Nuclear Waste Management XV*, Mat. Res. Soc. Symp. Proc. **247**, 135-141.

Goldhaber M. B. and Kaplan I. R. (1974) The sulfur cycle, in: E. D. Goldberg (ed.) The Sea, Vol. 5 Marine Chemistry, John Wiley & Sons, New York, 569-655.

Grambow B. and Strachan D. M. (1988) A Comparison of the Performance of Nuclear Waste Glasses by modeling, in: M. J. Apted and R. E. Westerman (eds.) Materials Research Society Symposium Proc., V. 112, *Scientific Basis for Nuclear Waste Management XI*, 713-724.

Guzowski R.V., Nimick F.B., Siegel M.D., and Finley N.C. (1983) *Repository Site Data Report for Tuff: Yucca Mountain, Nevada*, NUREG/CR-2937 (SAND82-2105), Sandia National Laboratories, Albuquerque, NM 87185.

Helgeson H. C., Delaney J. M., Nesbitt H. W., and Bird D. K. (1978) Summary and critique of the thermodynamic properties of rock-forming minerals, *Amer. Jour. Sci.* **278-A**, 195 pp.

Hoyle S. L. and Grutzeck M. W. (1989) Incorporation of cesium by hydrating calcium aluminosilicates, *Jour. Amer. Ceramic Soc.* **72**, 1938-1947.

Hrma P. R., Piepel G. F., Schweiger M. J., and Smith D. E. (1992) First-order model for durability of Hanford waste glasses as a function of composition, in: *High Level*

Radioactive Waste Management, Proceedings of the Third International Conference, American Nuclear Society and American Society of Civil Engineers, 1236-1243.

Iler R.K. (1979) *The Chemistry of Silica*, John Wiley and Sons, New York, 866 pp.

Jantzen C. M. and Plodinec, M. J. (1984) Thermodynamic model of natural, medieval, and nuclear waste glass durability, *Jour. Non-Crystalline Solids* **67**, 207-223.

Jones B. F. (1982) Mineralogy of fine-grained alluvium from borehole U11G, Expl. 1, Northern Frenchman Flat area, Nevada Test Site, U.S.G.S. Open-File Report **82-765**, 10 pp.

Kiseleva I. A., Kotelnikov A. R., Martynov K. V., Ogorodova L. P., and Kabalov J. K. (1994) Thermodynamic properties of strontianite-witherite solid solution $(Sr,Ba)CO_3$, *Phys. Chem. Minerals* **21**, 392-400.

Knauss K.G., Bourcier W.L., McKeegan K.D., Merzbacher C.I., Nguyen S.N., Ryerson F. J., Smith D. K., Weed H. C., and Newton L. (1990) Dissolution kinetics of a simple analogue nuclear waste glass as a function of pH, time and temperature, in: V. M. Oversby and P. W. Brow (eds.), *Scientific Basis for Nuclear Waste Management XIII, Mat. Res. Soc. Symp. Proc.* **176**, 371-381.

Knauss K.G. and Wolery T.J. (1988) The dissolution kinetics of quartz as a function of pH and time at 70°C, *Geochim. Cosmochim. Acta* **52**, 42-43.

Knauss K. G. and Wolery T. J. (1989) Muscovite dissolution kinetics as a function of pH and time at 70°C, *Geochim. Cosmochim. Acta* **53**, 1493-1501.

Laidler K. J. (1987) *Chemical Kinetics, Third Edition*, Harper and Row, 531 pp.

Langmuir D. and Herman J. S. (1980) The mobility of thorium in natural waters at low temperatures, *Geochim. Cosmochim. Acta* **44**, 1753-1766.

Larner L. J., Speakman K., and Majumdar A. J. (1976) Chemical interactions between glass fibres and cement, *Jour. Non-Cryst. Solids* **20**, 43-74.

Larosa J. L., Kwan S., and Grutzeck M. W. (1992a) Self-generating zeolite-cement composites, *Materials Research Society Symp. Proc.* **245**, 211-216.

Larosa J. L., Kwan S., and Grutzeck M. W. (1992b) Zeolite formation in class F fly ash blended cement pastes, *Jour. Amer. Ceramic Soc.* **75**, 1574-1580.

Lea F. M. (1970) *The Chemistry of Cement and Concrete*, 3rd Ed., Edward Arnold (Publishers) Ltd, Surrey , 727 pp.

Lindstrom F.T., Cawfield D.E., Donahue M.E., Emer D.F. and Shott G.J. (1993) *A Simulation of the Transport and Fate of Radon-222 Derived from Thorium-230 Low Level Waste in the Near-Surface Zone of the Radioactive Waste Management Site in Area 5 of the Nevada Test Site*, DOE/NV/10630-58, Reynolds Electrical and Engineering Co. Inc., Las Vegas, NV.

MacKenzie F. T. (1971) Quartz synthesis at Earth-surface conditions, *Science* **173**, 533-535.

Marfil S. A. and Maiza P. J. (1993) Zeolite crystallization in portland cement concrete due to alkali-aggregate reaction, *Cement and Concrete Research* **23**, 1283-1288.

Mazer J.J., Bates J.K., Biwer B.M. and Bradley C.R. (1992a) AEM analyses of SRL 131 glass altered as a function of SA/V, *Materials Res. Soc. Symp. Proc.* **257, 73-81**.

Mazer J.J., Bates J.K., Stevenson, C.M., Bradley J.P., Bradley C.R. and Stevenson C.M. (1992b) Alteration of tektite to form weathering products, *Nature* **357**, 573-576.

Mazer J.J., Bates J.K., Stevenson, C.M. and Bradley C.R. (1992c) Obsidians and tektites: natural analogues for water diffusion in nuclear waste glasses, *Materials Res. Soc. Symp. Proc.* **257**, 513-519.

Merrill R. A. and Whittington, K. F. (1994) *Final Report of Vitrification Development Studies for Fernald CRU-4 Silo Wastes*, contract # PO625151, Battelle-Pacific Northwest Laboratory, Richland, WA 99352, April 1994.

Moskvin A. I., Essen L. N., and Bukhtiyarova T. N. (1967) Complexing of tetravalent thorium and uranium in phosphate solutions, *Zh. Neorp. Khim.* **12**, 3390-3392.

Nagy K. L. (1995) Dissolution and precipitation kinetics of sheet silicates, in: S. L. Brantley and A. F. White (eds.), Chemical Weathering Rates of Silicate Minerals, *Reviews in Mineralogy* **31**, Mineralogical Society of America, 173-233.

Nagy K. L. and Lasaga A. C. (1992) Dissolution and precipitation kinetics of gibbsite at 80°C and pH 3: The dependence on solution saturation state. *Geochim. Cosmochim. Acta* **56**, 3093-3111.

Nagy K. L., Blum A. E., and Lasaga A. C. (1991) Dissolution and precipitation kinetics of kaolinite at 80°C and pH 3: The dependence on solution saturation state. *Amer. Jour. Sci.* **291**, 649-686.

Naumov G. B., Ryzhenko B. N., and Khodakovsky I. L. (1974) *Handbook of Thermodynamic Data*, U.S.G.S. WRD-74-001, 328 pp.

Neher-Neumann E. (1992) Studies on metal carbonate equilibria 24. The hydrogen carbonate and carbonate complexes of the lead (II) and cadmium (II) ions in acid solutions and a 3 M (Na)ClO_4 ionic medium at 25°C, *Acta Chemica Scandinavica* **46**, 231-239.

Newman A. C. D. and Brown G. (1987) The chemical constitution of clays, in: A. C. D. Newman (ed.) "Chemistry of Clays and Clay Minerals", *Minerological Society Monograph No. 6, Longman Scientific & Technical*, 1-128.

Odom I. E. (1984) Glauconite and celadonite minerals, in: S. W. Bailey (ed.) Micas, *Reviews in Mineralogy* **13**, 545-572.

Oelkers E. H, Schott J. , Devidal J. L. (1994) The effect of aluminum, pH, and chemical affinity on the rates of aluminosilicate dissolution reactions. *Geochim. Cosmochim. Acta* **58**, 2011-2024

Ohga H. and Nagataki S. (1989) Prediction of carbonation depth of concrete with fly ash, in: V. M. Malhotra (copy rest of citation from Atkins and Macphee), 275-294.

Orme R. (1995) *TWRS Process Flowsheet*, WHC-SD-WM-TI-613 Rev. 1, Westinghouse Hanford Co., Richland, Washington 99352, 345 pp.

Östhols E, Bruno J. and Grenthe, I. (1994) "On the influence of carbonate and mineral dissolution: III. the solubility of microcrystalline ThO_2 in CO_2-H_2O media, *Geochim. Cosmochim. Acta* **58**, 613-623.

Östhols E. (1995) The solubility of microcrystalline ThO_2 in phosphate media, *Radiochimica Acta* **68**, 185-190.

Pagoaga M.K., Appleman D.E. and Stewart J.M. (1987) Crystal structures and crystal chemistry of the uranyl oxide hydrates becquerelite, billietite, protasite, *American Mineralogist* **72**, 1230-1238.

Phillips S. L., Hale F. V., Silvester L. F. and Siegel M. D. (1988) *Thermodynamic Tables for Nuclear Waste Isolation (Aqueous Solutions Database)*, NUREG/CR-4864 (LBL-22860, SAND87-0323) Vol. 1. 181 pp.

Plummer L. N. and Busenberg E. (1987) Thermodynamics of aragonite--strontianite solid solutions: results from stoichiometric solubility at 25 and 76°C, *Geochim. Cosmochim. Acta.* **51**, 1393-1411.

Ransom B. and Helgeson H. C. (1994) Estimation of the standard molal heat capacities, entropies, and volumes of 2:1 clay minerals. *Geochim. Cosmochim. Acta* **58**, 4537-4547.

Ransom B. and Helgeson H. C. (1995) A chemical and thermodynamic model of dioctahedral 2:1 layer clay minerals in diagenetic processes: dehydration of dioctahedral aluminous smectite as a function of temperature and depth in sedimentary basins. *Amer. Jour. Sci.* **295**, 245-281.

Renders,P. J. N, Gammons C. H., and Barnes H. L. (1995) Precipitation and dissolution rate constants for cristobalite from 150 to 300°C, *Geochim. Cosmochim. Acta* **59**, 77-86.

Rimstidt J. D. and Barnes H. L. (1980) The kinetics of silica-water reactions, *Geochim. Cosmochim. Acta* **44**, 1683-1700.

Sarkar A. K., Barnes M. W., and Roy D. M. (1982) Longevity of borehole and shaft sealing materials: Thermodynamic properties of cements and related phases applied to repository sealing. ONWI-201 (DE 83 000731).

Schweda P. (1989) Kinetics of alkali feldspar dissolution at low temperature, in: D. L. Miles (ed.), *Proc. of the 6th International Symposium on Water-Rock Interaction, AA Balkema, Rotterdam*, 639-642.

Smith R.M. and Martell A.E. (1976) *Critical Stability Constants, Vol. 4: Inorganic Complexes*, Plenum, New York, 257 pp.

Stockman H.W. (1994) *PP: a Graphics Post-Processor for the EQ3/6 Reaction Path Code*. SAND94–1955, Sandia National Laboratories, Albuquerque, NM 87185.

Stockman H. W., Anderson H. L., and Krumhansl J. L. (1995) Characterization of alluvium near the GCD site: Implications for geochemical modeling. SAND93-2737, Sandia National Laboratories, Albuquerque, NM 87185.

Stormont J. C. (1995) The effect of constant anisotropy on capillary barrier performance, *Water Resources Res.* **31**, 783-785.

Su C. and Harsh J. B. (1994) Gibbs free energies of formation at 298K for imogolite and gibbsite from solubility measurements, *Geochim. Cosmochim. Acta* **58**, 1667-1677.

Sverjensky D. A. and Molling P. A. (1992) A linear free energy relationship for crystalline solids and aqueous ions, *Nature* **356**, 231-233.

Tardy Y. and Garrels R. M. (1974) A method of estimating the Gibbs energies of formation of layer silicates, *Geochim. Cosmochim. Acta* **38**, 1101-1116.

Taylor P. and Lopata V. J. (1984) Stability and solubility relationships between some solids in the system PbO-CO_2-H_2O, *Can. J. Chem.* **62**, 395-402.

Terhune C. L. and Harden J. W. (1991) Seasonal variations of carbon dioxide concentrations in stony, coarse-textured desert soils of southern Nevada, USA, *Soil Science* **151**, 417-429.

Tomita K., Yamane, H., and Kawano, M. (1993) Synthesis of smectite from volcanic glass at low temperature. *Clays Clay Min.* **41**, 655-661.

Velde, B. and Meunier, A. (1987) Petrologic phase equilibria in natural clay systems, in: A. C. D. Newman (ed.) Chemistry of Clays and Clay Minerals, Mineralogical Society Monograph 6, Longman Scientific and Technical, 423-458.

Wagman D. D., Evans W. H., Parker V. B., Schumm R. H., Halow I., Bailey S. M., Churney K. L., and Nuttall R. L. (1982) The NBS tables of Chemical Thermodynamic Properties, *Journal of Physics and Chemistry Reference Data* **11**, Supplemental #2, 392 pp.

Walton J. C.; Plansky L. E.; Smith R. W. (1990) *Models of Estimation of Service Life of Concrete Barriers in Low-Level Radioactive Waste Disposal*, NUREG/CR-5542 (TI91000576), p 21.

Williams L. A. and Crerar D. A. (1985) Silica diagenesis, II. General mechanisms, *Jour. Sedimentary Petrol.* **55**, 312-321.

Wolery T.J. (1992) *EQ3/6, a Software Package for Geochemical Modeling of Aqueous Systems: Package Overview and Installation Guide (Version 7.0)* UCRL-MA-110662 PT I, Lawrence Livermore National Laboratory, Livermore, CA.

Wolery, T.J. (1978) *Some Chemical Aspects of Hydrothermal Processes at Mid-Ocean Ridges – A Theoretical Study*, Ph.D. thesis, Northwestern University, Evanston, IL.

Yang I.C., Davis J.S. and Sayre T.M. (1990) Comparison of pore-water extraction by triaxial compression methods and high speed centrifugation methods, in: Proc. of Conf. on Minimizing Risk to the Environment, Amer. Inst. of Hydrology, 250-259.

Yilmaz V. T. (1992) Chemical attack on alkali-resistant glass fibres in a hydrating cement matrix: characterization of corrosion products, *Jour. Non-Cryst. Solids* **51**, 236-244.

Yilmaz V. T., Lachowski E. E., and Glasser F. P. (1991) Chemical and microstructural changes at alkali-resistant glass fiber-cement interfaces, *Jour. Amer. Ceram. Soc.* **74**, 3054-3060.

Yuretich R. F. and Cerling T. E. (1983) Hydrogeochemistry of Lake Turkana, Kenya: Mass balance and mineral reactions in an alkaline lake, *Geochim. Cosmochim. Acta* **47**, 1099-1109.

10. Figures

For a summary of the "run" or "case" numbers described in the figures, see Table 2.

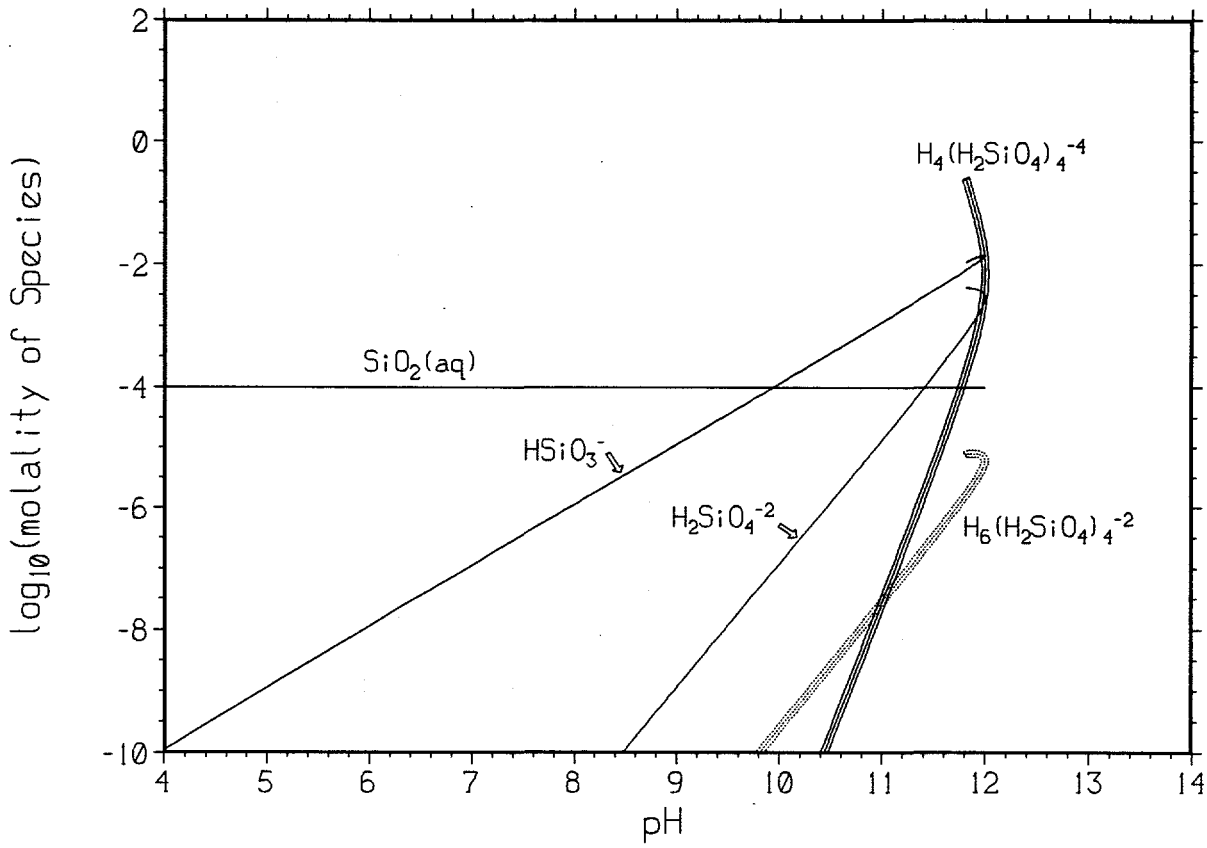

Figure 1. Calculated Si speciation, bdot γ correction, titrate KOH into water+quartz.

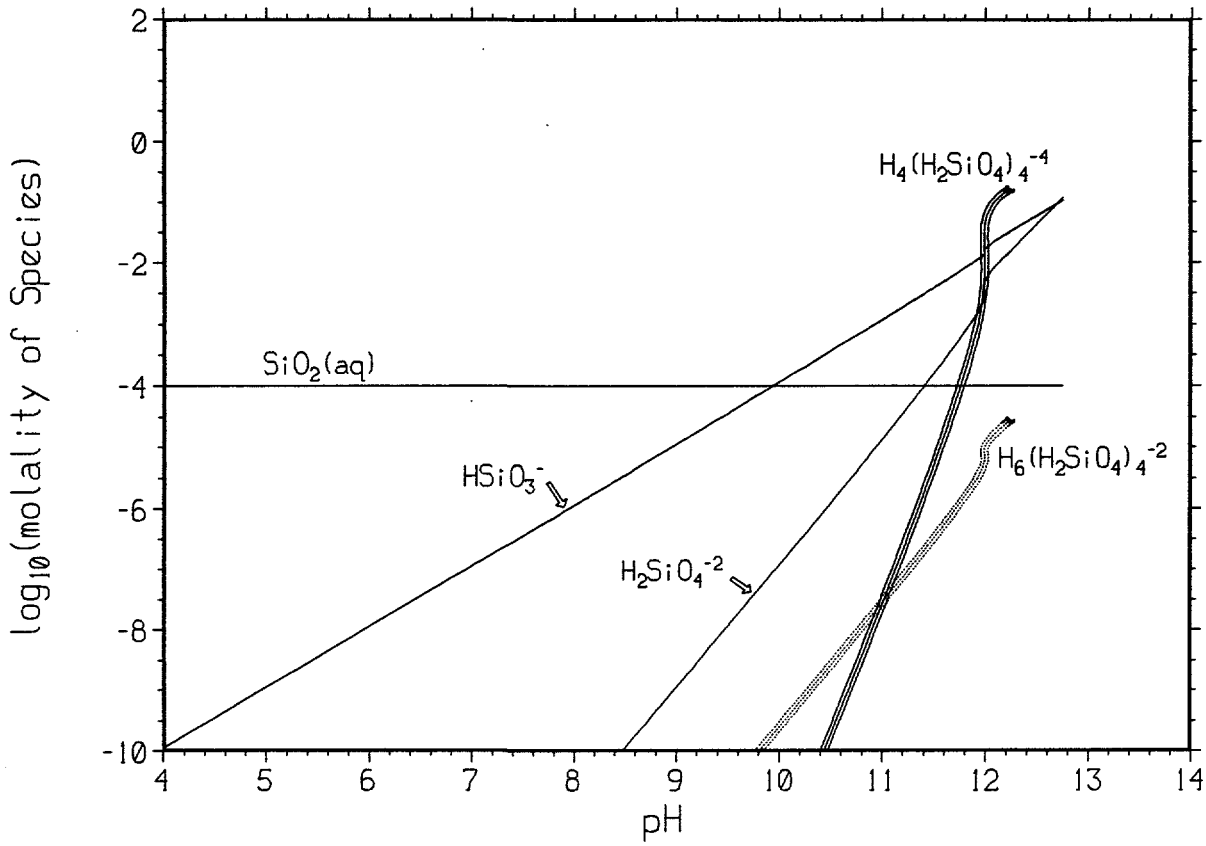

Figure 2. Calculated Si speciation, Davies γ correction, titrate KOH into water+quartz.

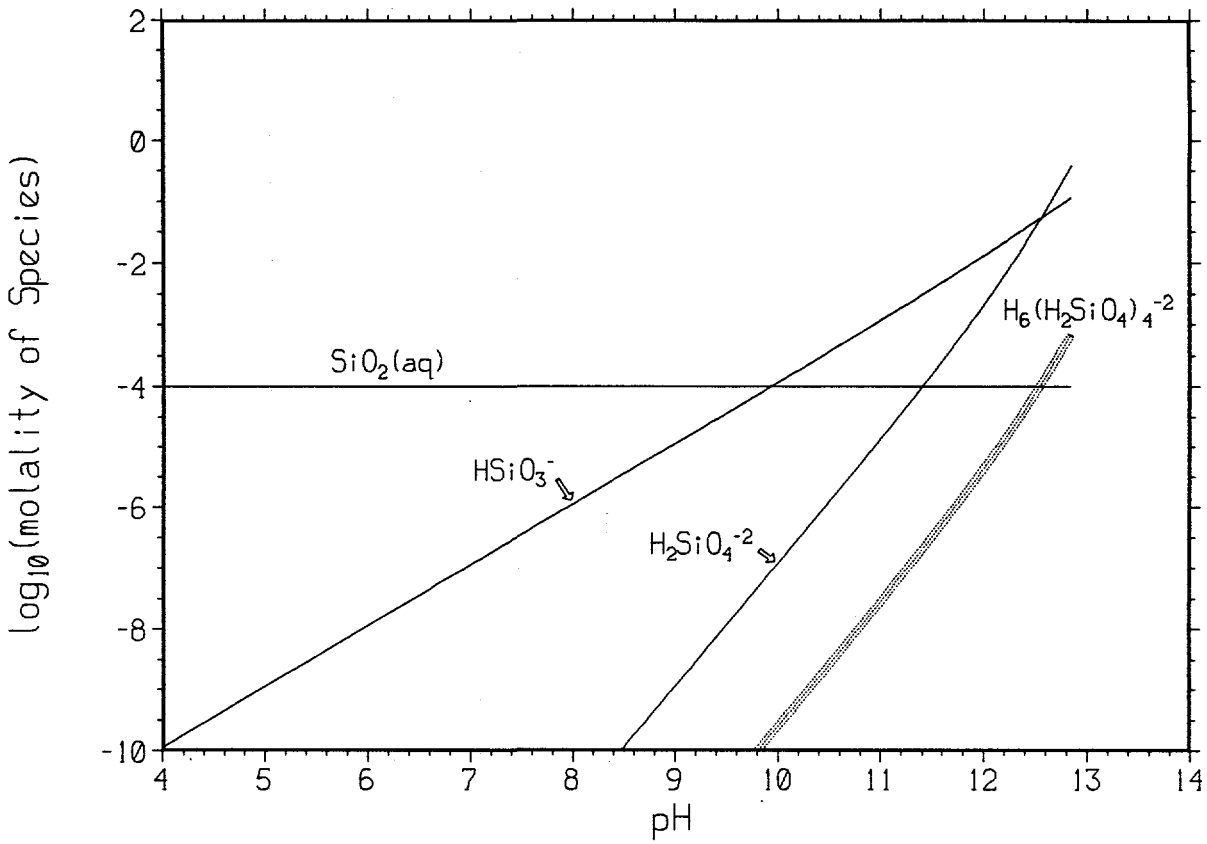

Figure 3. Calculated Si speciation, bdot γ correction, $H_4(H_2SiO_4)_4^{-}$ suppressed, titration of KOH into water+quartz.

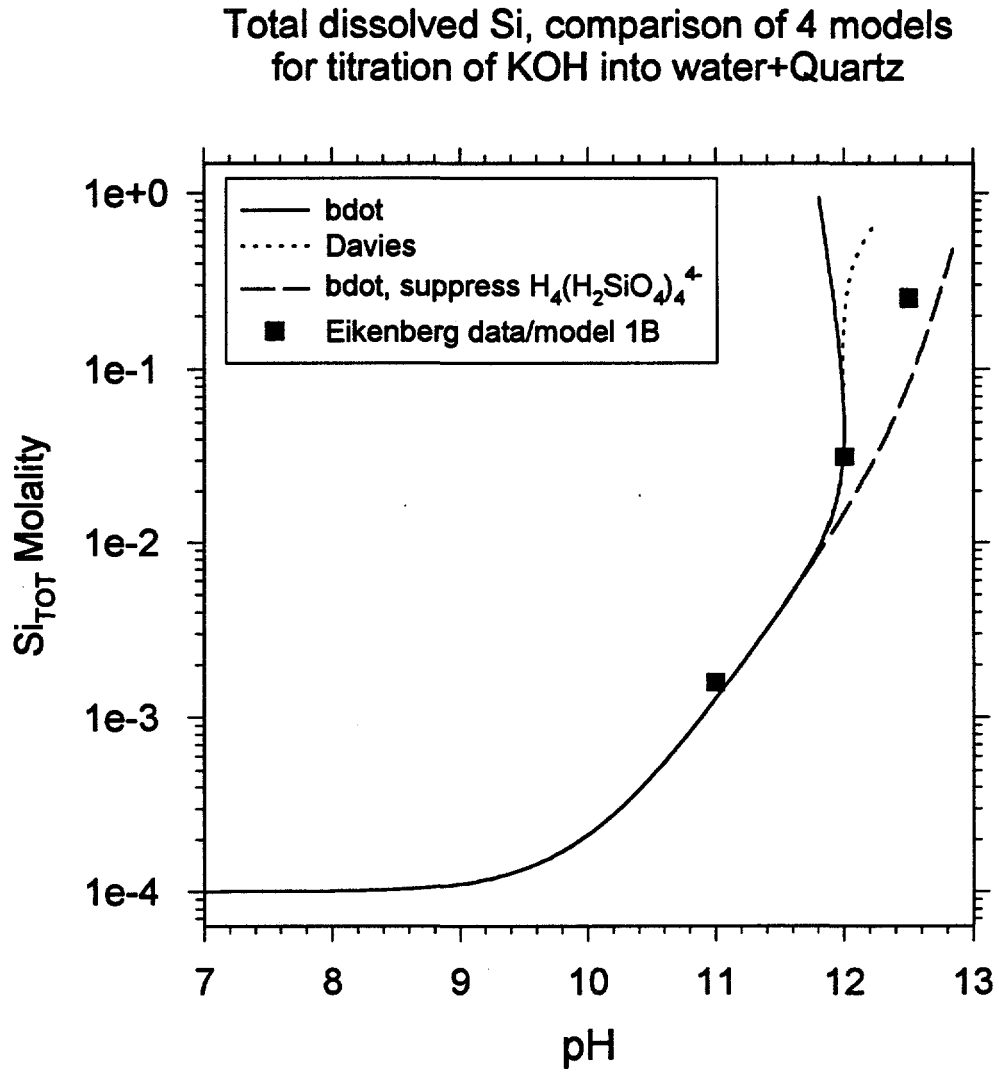

Figure 4. Calculated total Si molality for Figures 1-3, and Eikenberg's (1990) model 1B.

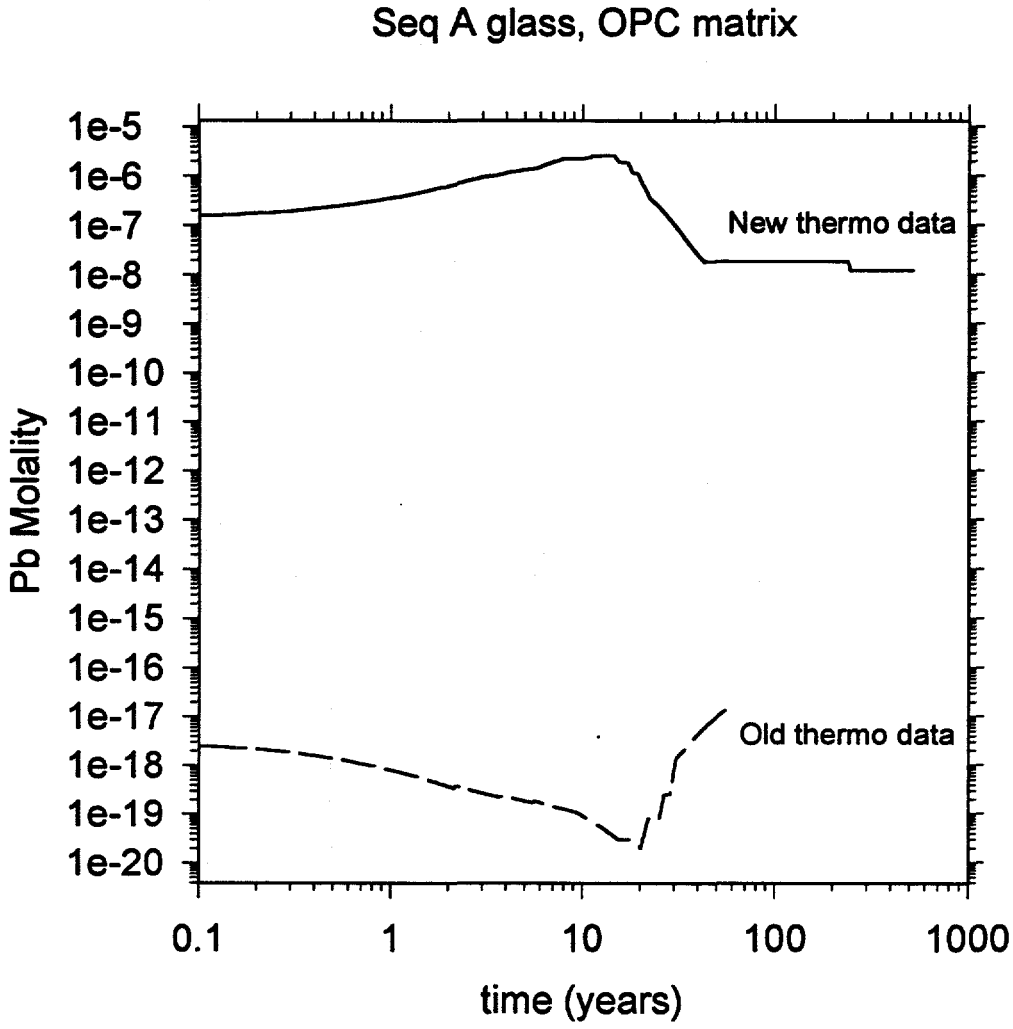

Figure 5. Effect of adding thermochemical data for Pb hydroxide complexes ("New" thermo data) to R1 database, for run (1), where matrix is OPC alone.

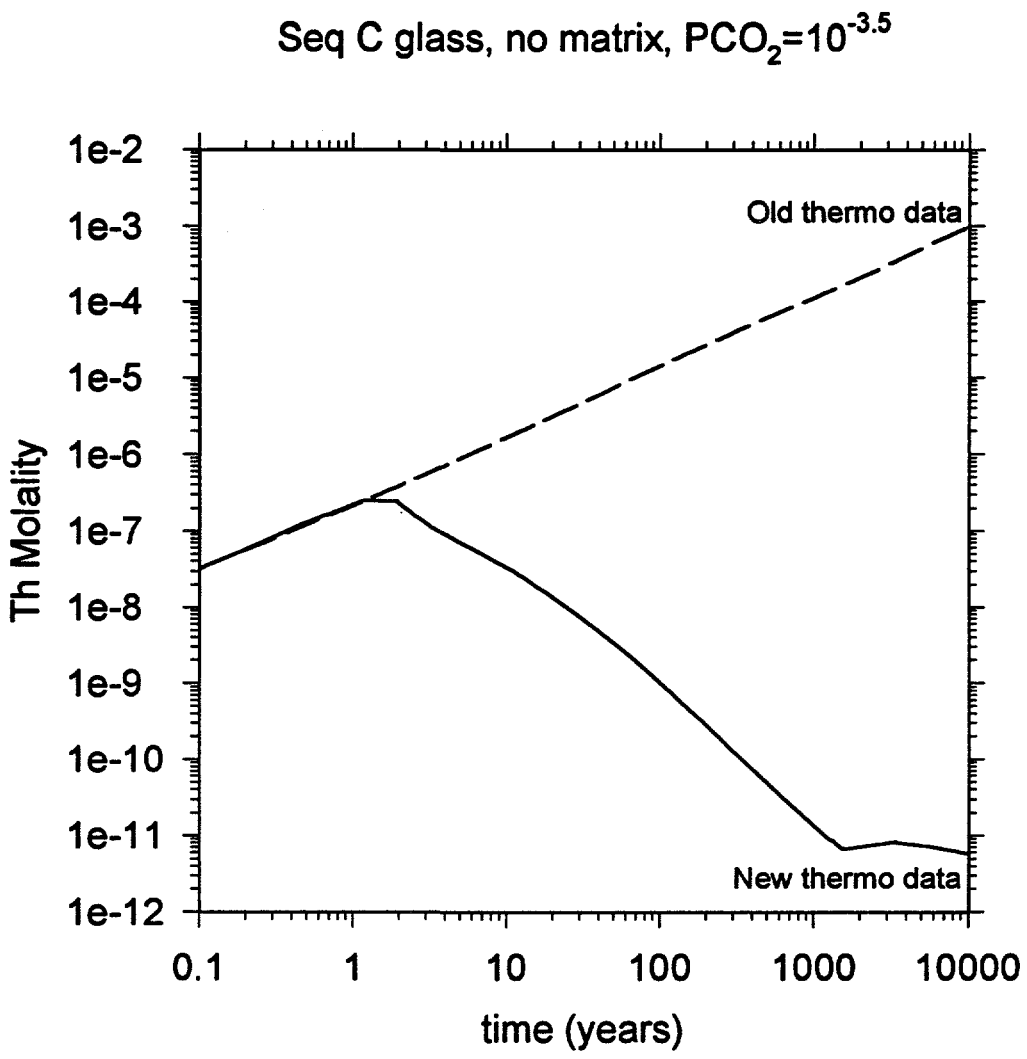

Figure 6. Effect of using "New" (correct) thermochemical data for Th phosphate complexes and solids for run (8 C CO2), where there is no matrix, but half of the pore space is filled with water at ambient CO_2 pressure. The "Old" data include the Moskvin *et al.* (1967) stability constants. Sequence C glass is very high in phosphate, and has insufficient Ca and Mg to precipitate all PO_4^{-3} as minerals.

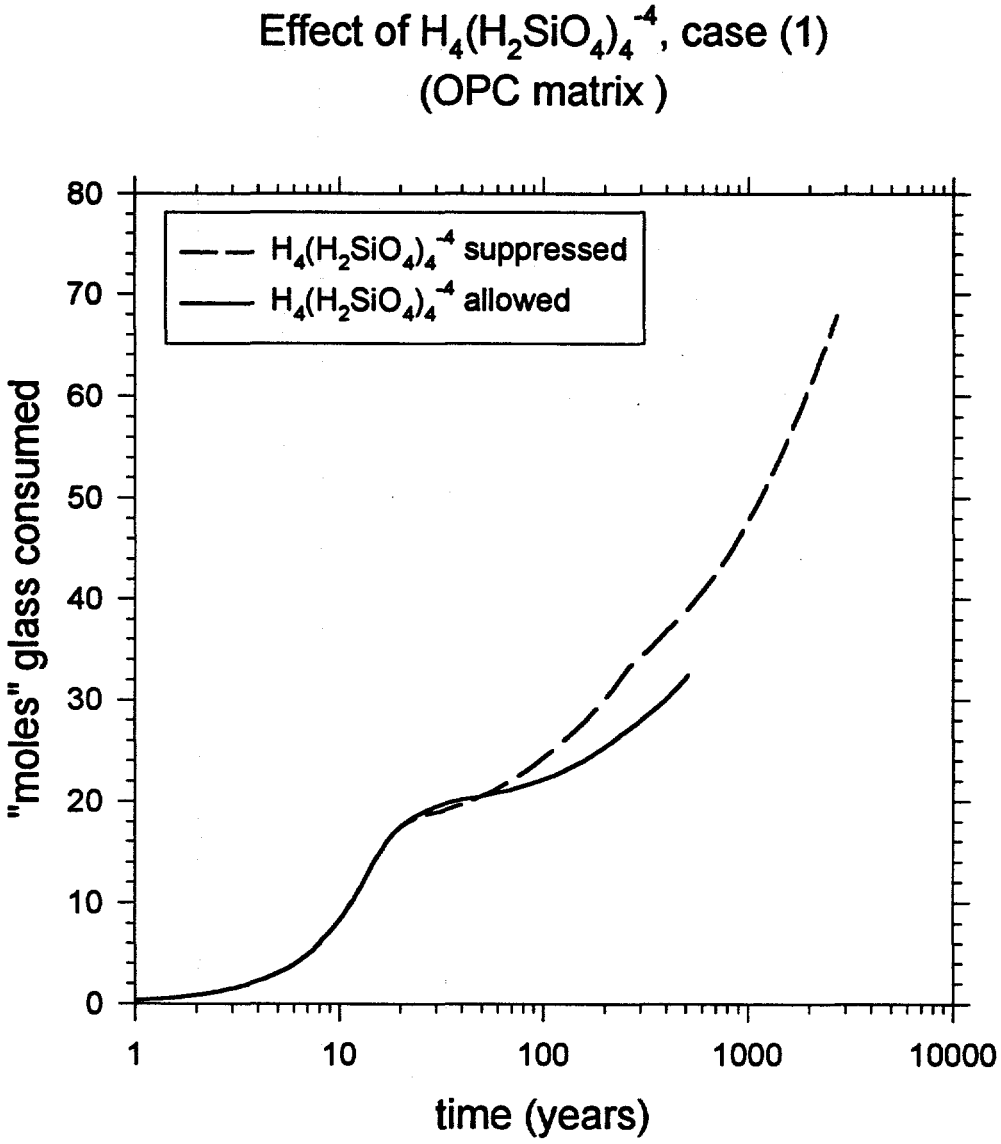

Figure 7. Suppression of the highly charged silica tetramer increases the calculated degradation rate. Case (1), sequence A glass with OPC matrix; this run achieves high ionic strength and likely has very inaccurate corrections for the $H_4(H_2SiO_4)_4^{-4}$ activity coefficient. Note linear scale on vertical axis.

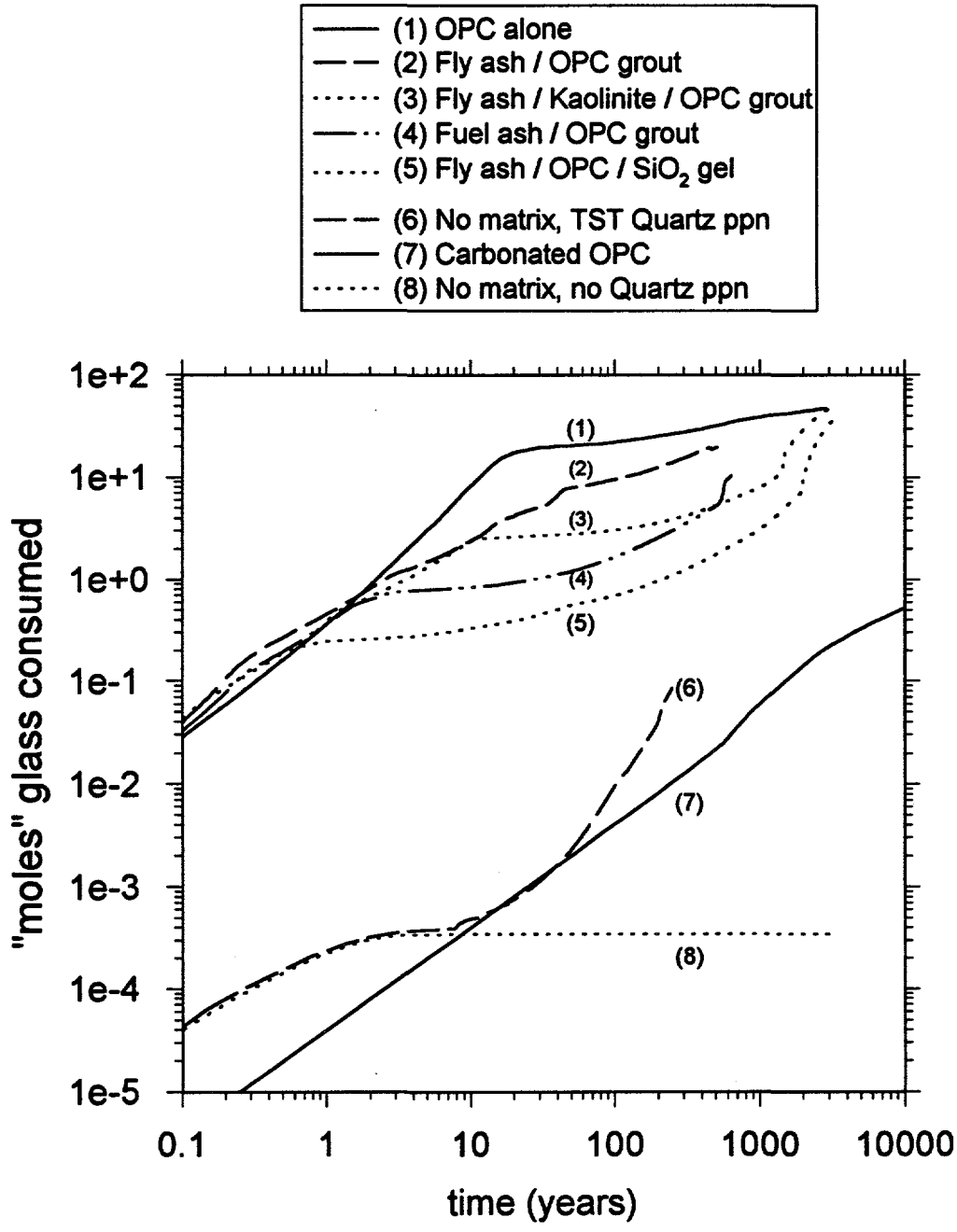

Figure 8. "Moles" of sequence A glass consumed for eight of the matrix combinations given in table 2. The top 5 all contain uncarbonated OPC. A "mole" of glass is ≈160 g.

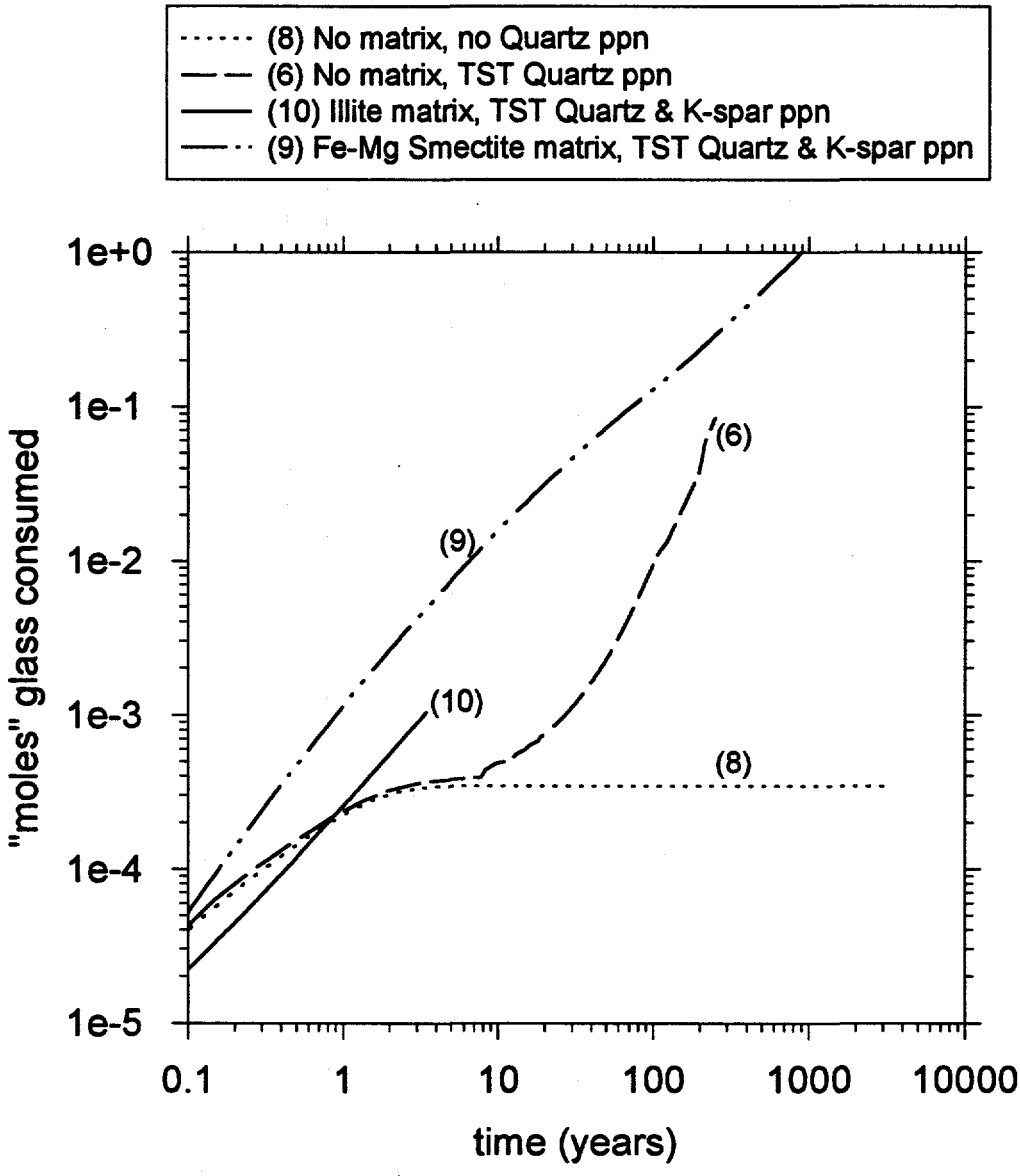

Figure 9. "Moles" of sequence A glass consumed for some non-OPC matrices, where the only CO_2 in the system is from the initial (50 ppm) HCO_3^- content of the pore water.

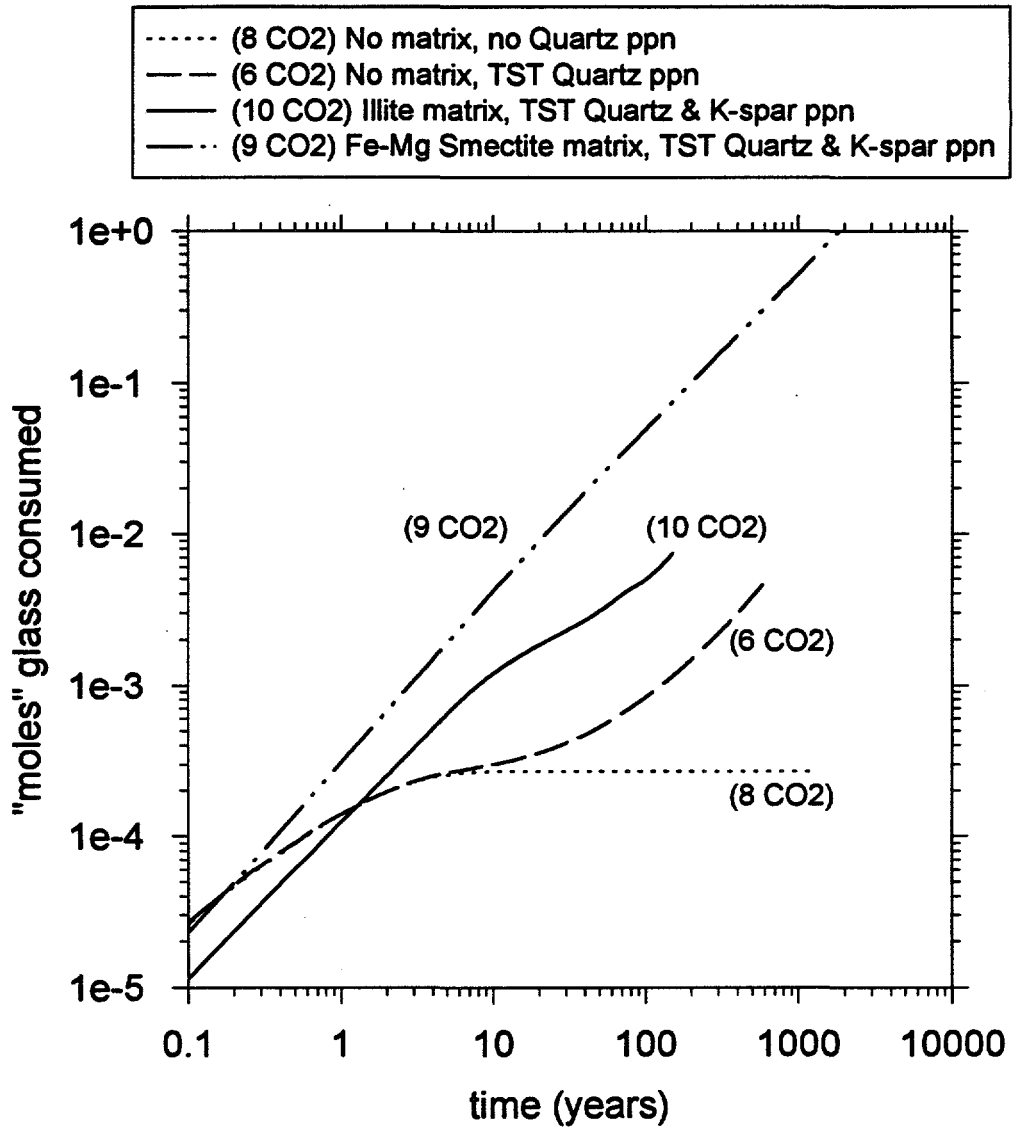

Figure 10. "Moles" of sequence A glass consumed for some non-OPC matrices, where the CO_2 pressure is buffered to an ambient of $10^{-3.5}$ atm (compare with Figure 4).

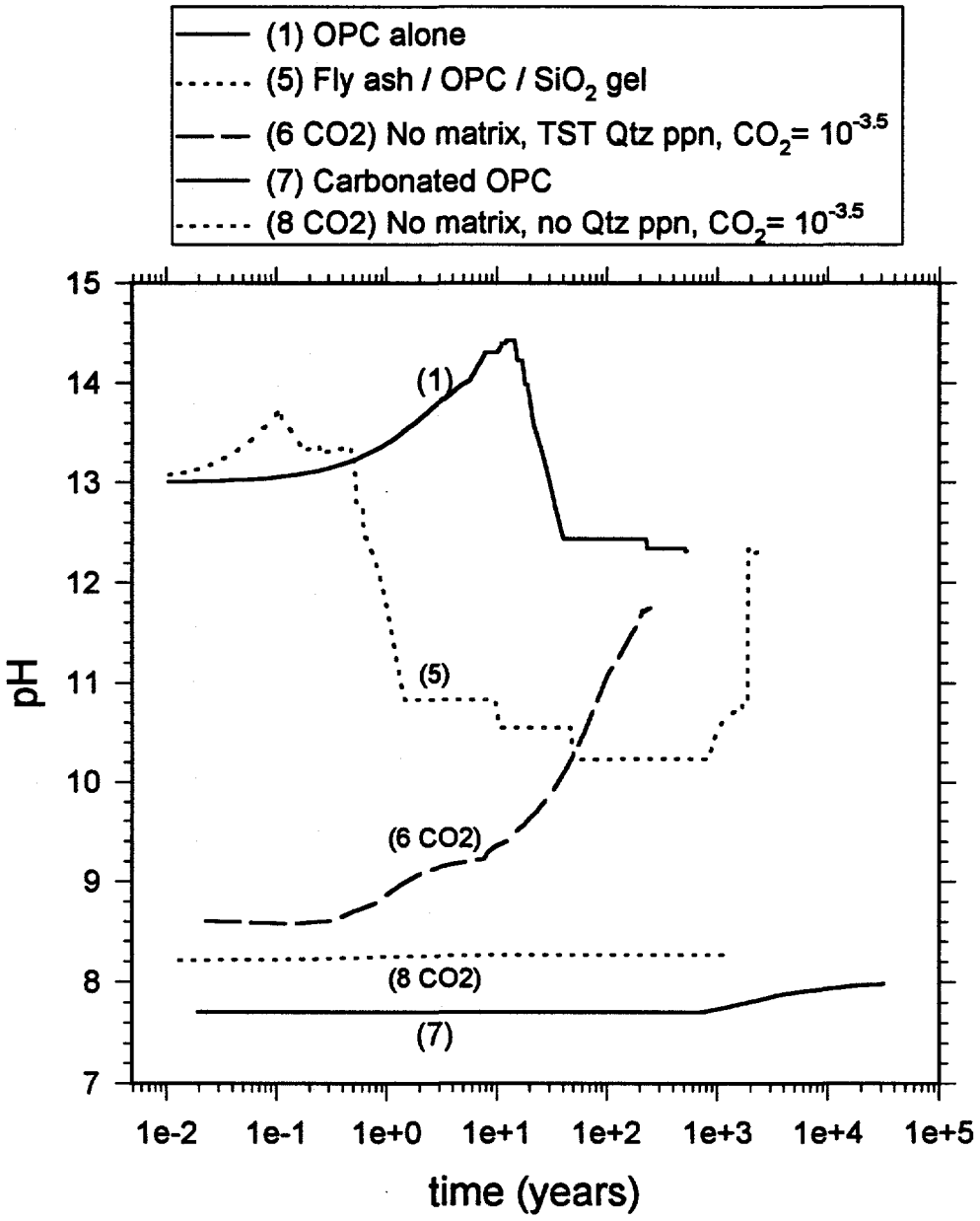

Figure 11. Variation of pH with time for 5 of the conditions given in table 2. For ≈ 800 years, (7) is held at the Calcite-Gypsum-ambient pH buffer.

shs

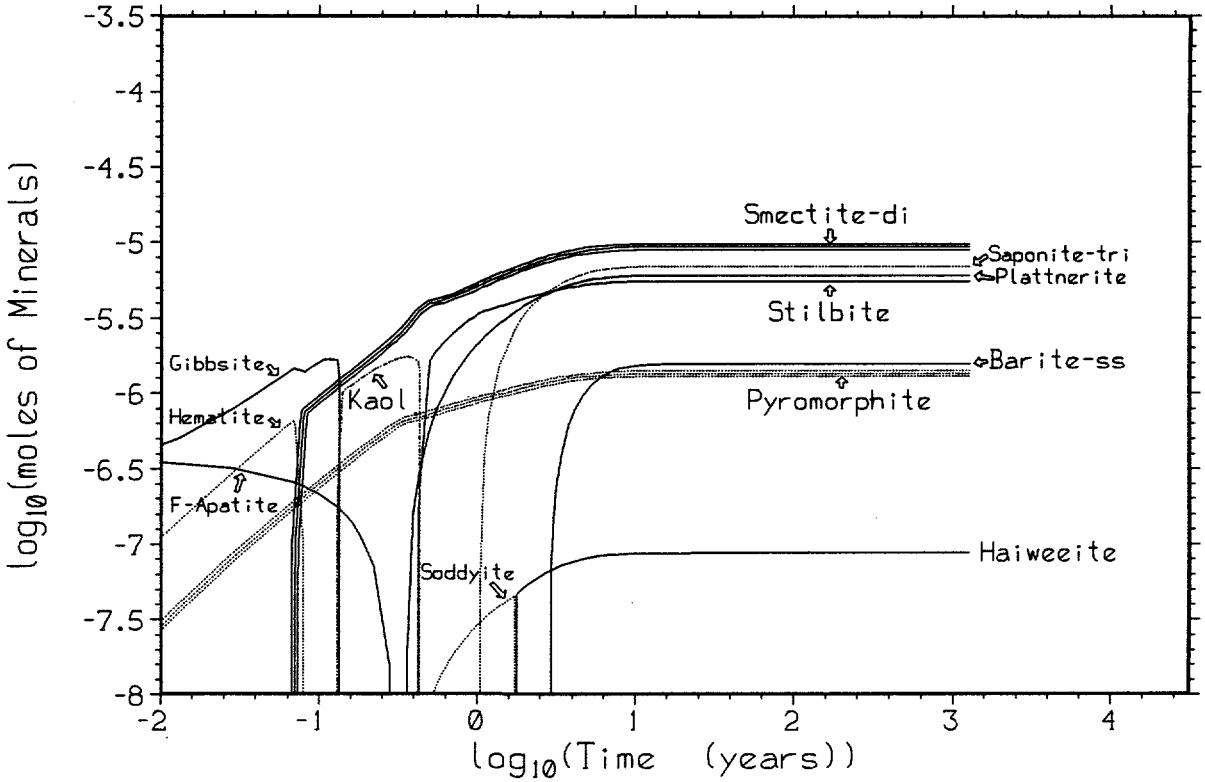

Figure 12. Minerals formed for run (8 CO2), no matrix, no quartz precipitation, and $PCO_2 = 10^{-3.5}$.

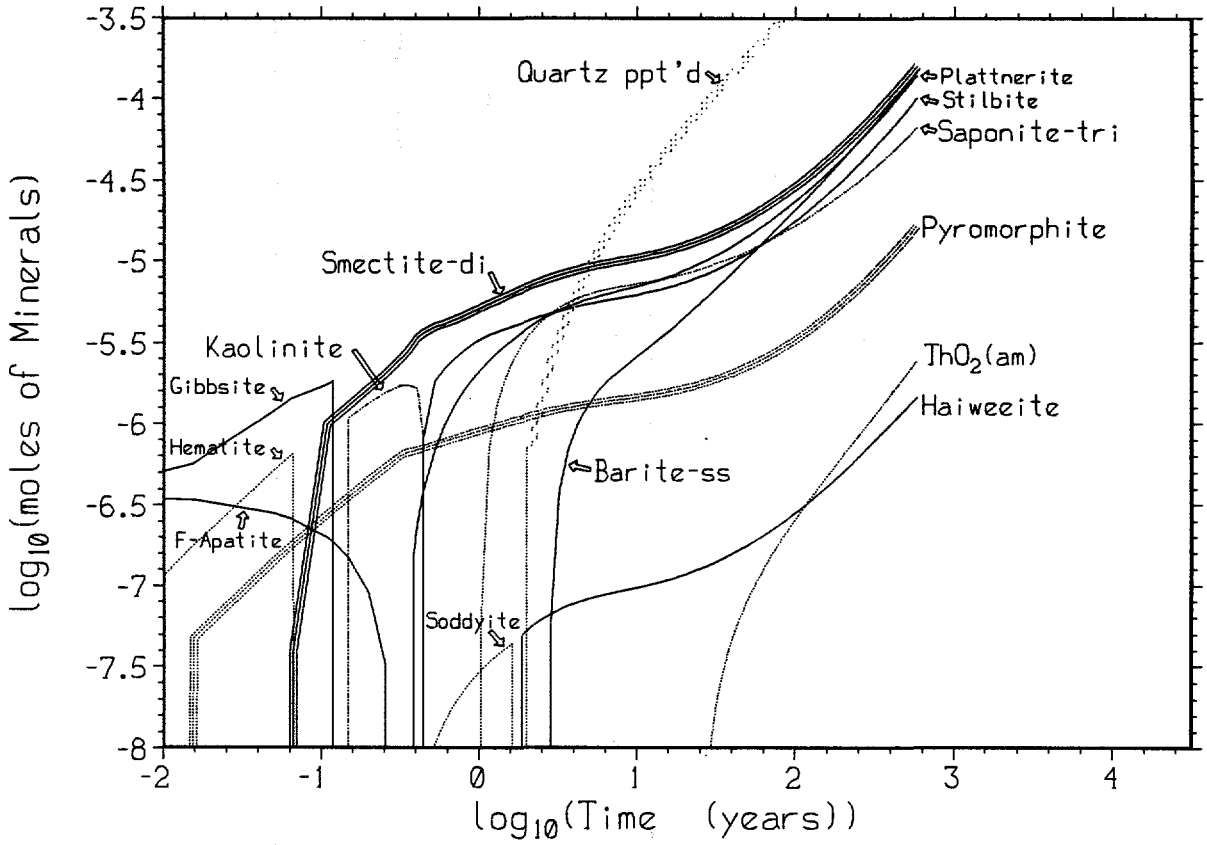

Figure 13. Minerals formed in run (6 CO2), no matrix, TST quartz precipitation, $PCO_2=10^{-3.5}$.

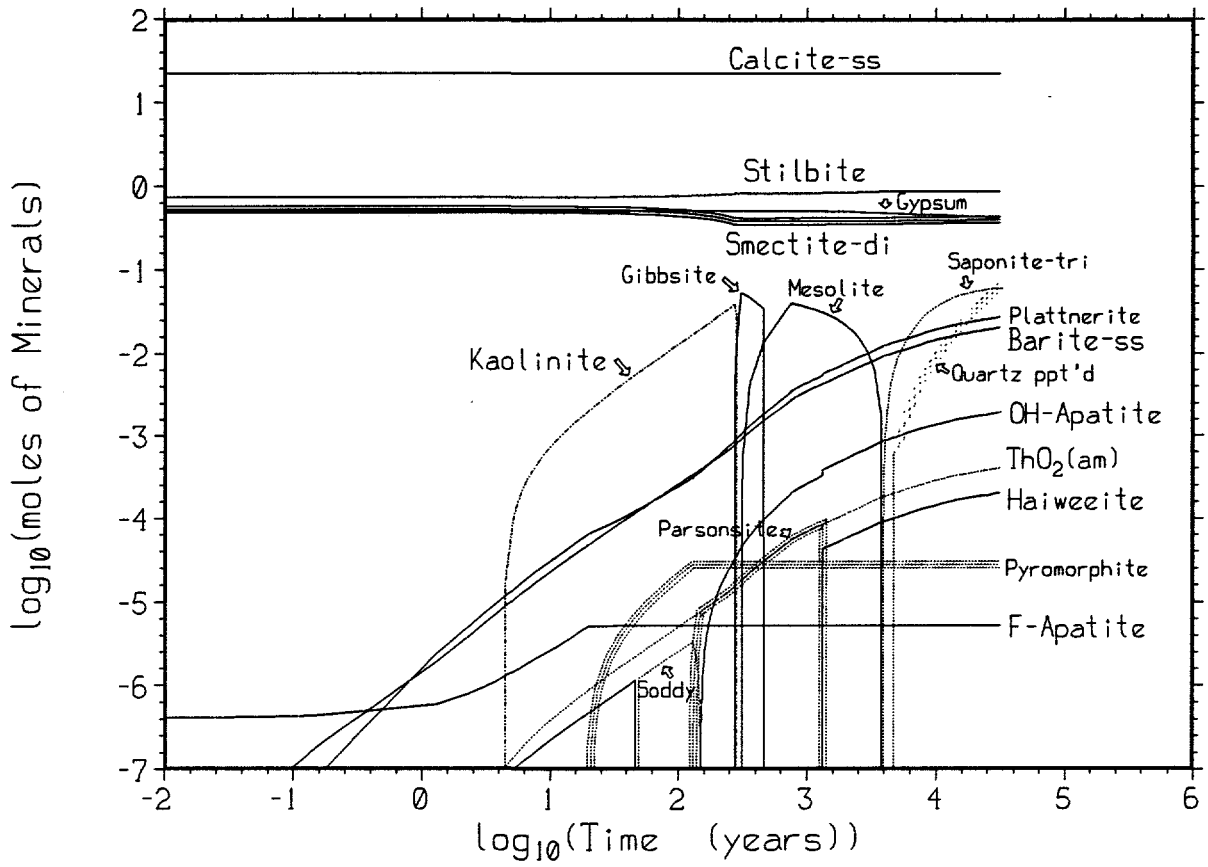

Figure 14. Minerals formed in run (7), carbonated OPC ($PCO_2 = 10^{-3.5}$). "Soddy" is soddyite.

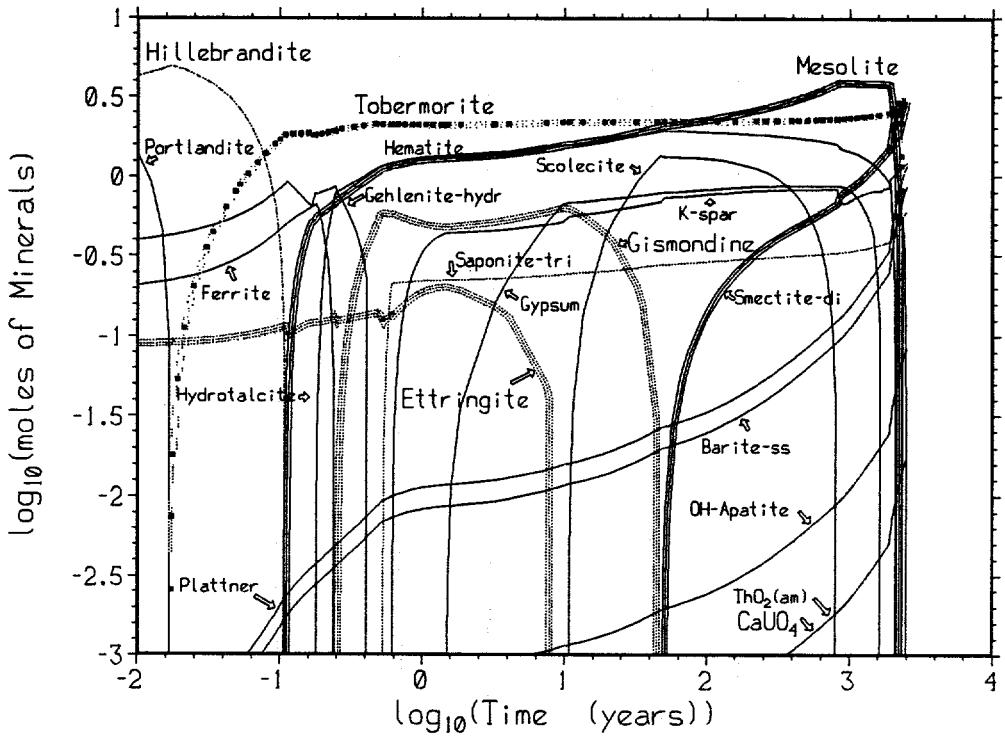

Figure 15. Minerals formed in run (5), matrix is fly ash / OPC / SiO_2 gel.

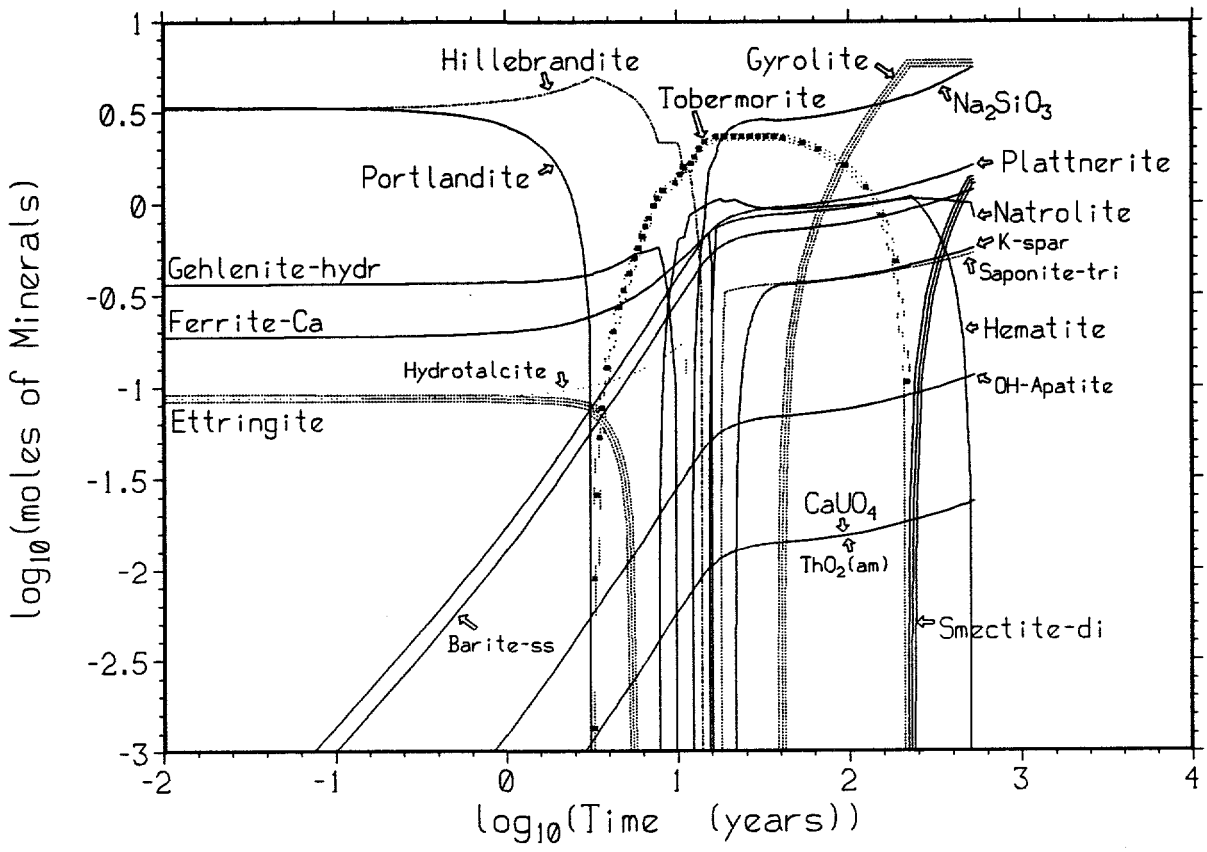

Figure 16. Minerals formed in run (1), matrix is OPC alone.

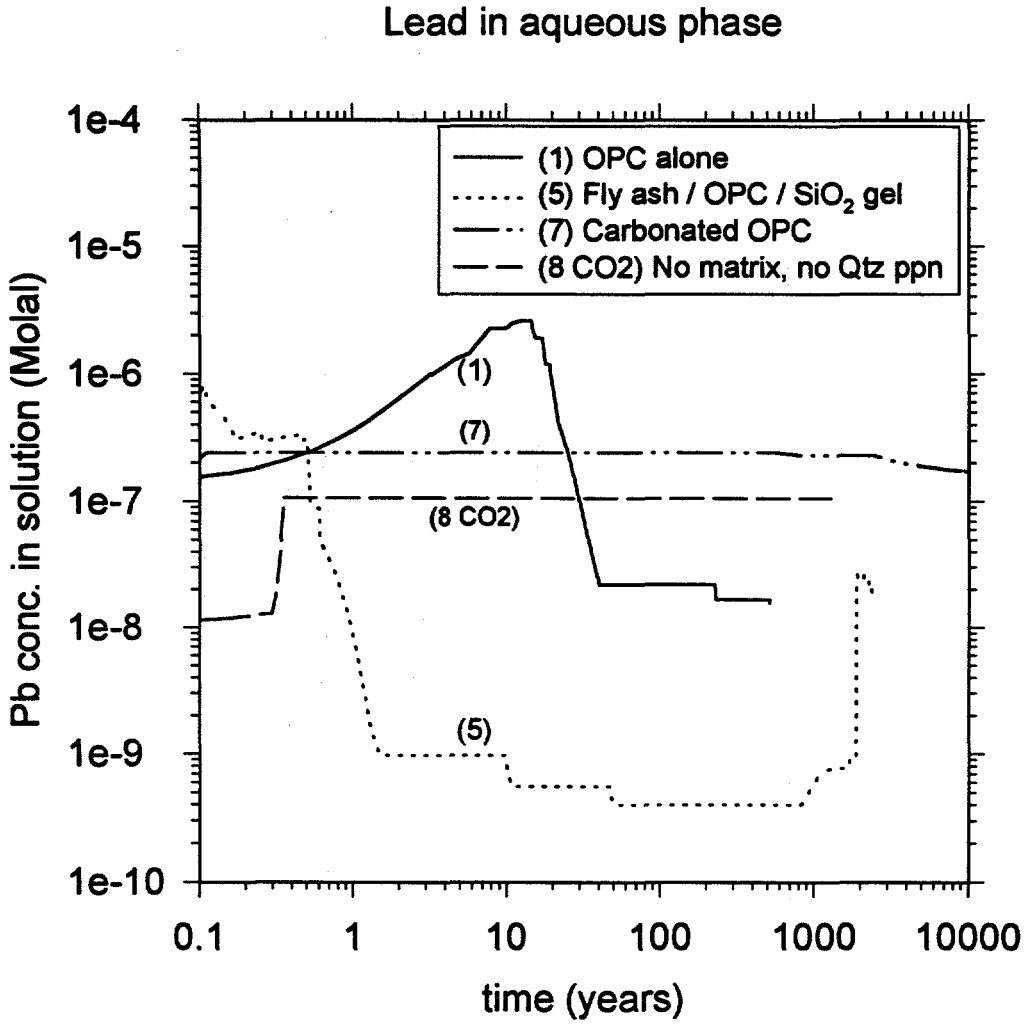

Figure 17. The highest Pb concentrations for run (1) and (5) are from hydroxide complexes; for (7) and (8 CO2), from hydroxyl-carbonate complexes.

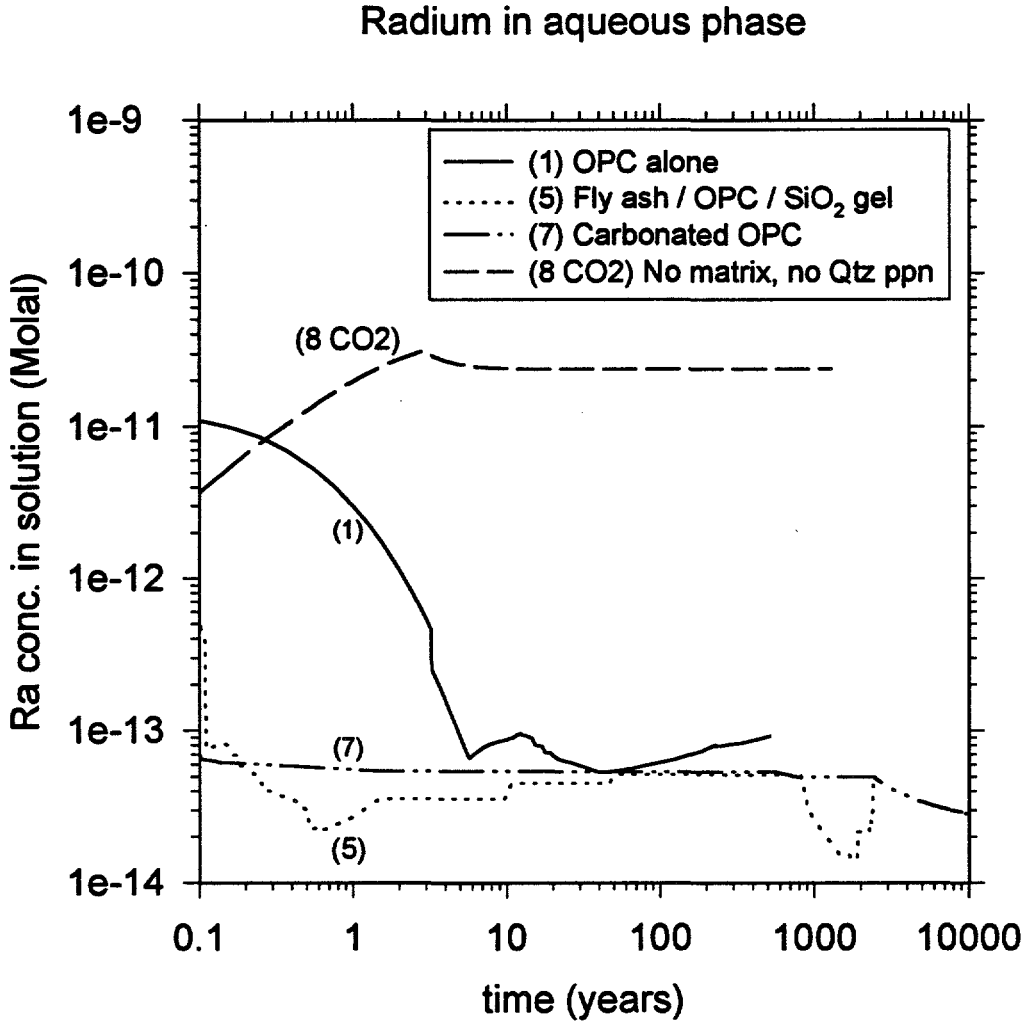

Figure 18. The low Ra concentrations for cases (1), (5) and (7) result from high free sulfate concentrations in the reacted OPC matrix, and precipitation of Ba-Ra sulfate solid solution.

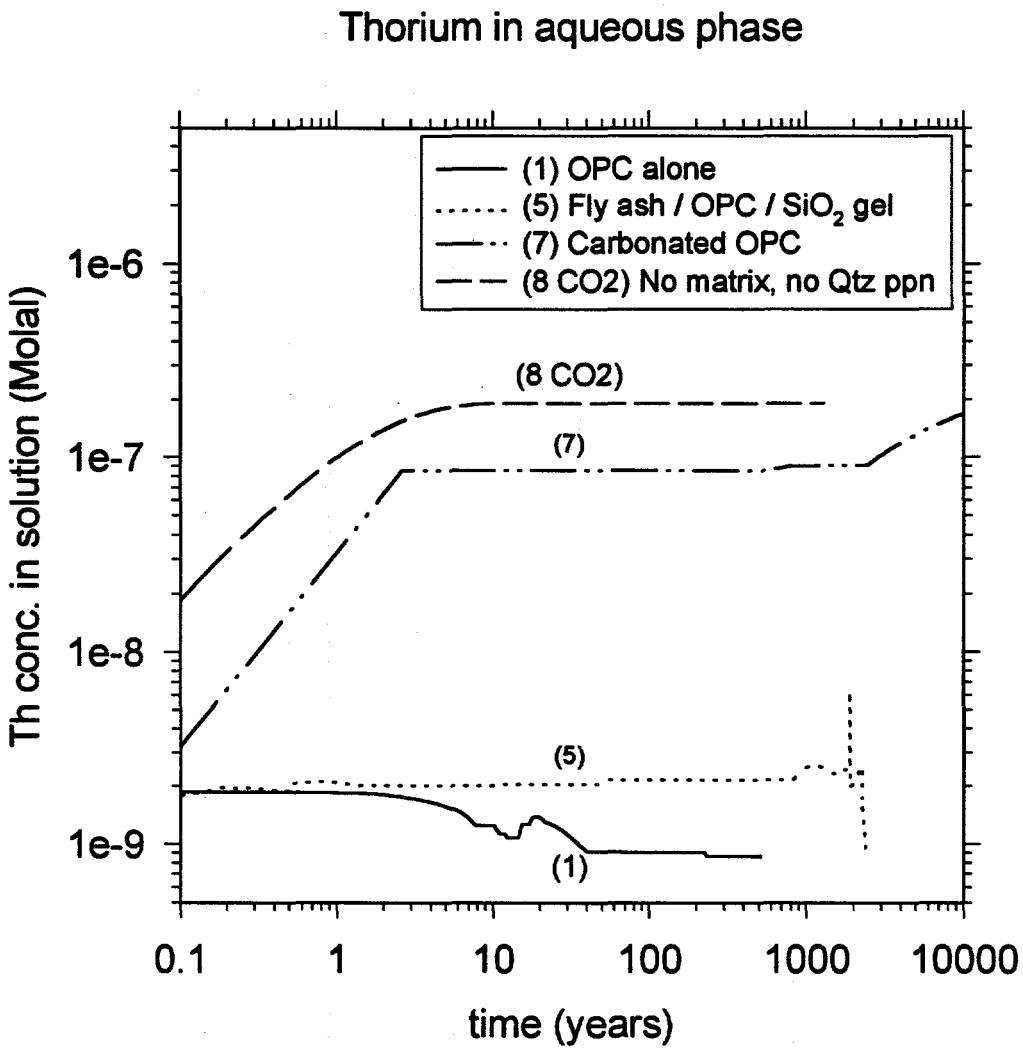

Figure 19. The relatively high Th concentrations in cases (7) and (8 CO2) result from formation of aqueous Th carbonate complexes.

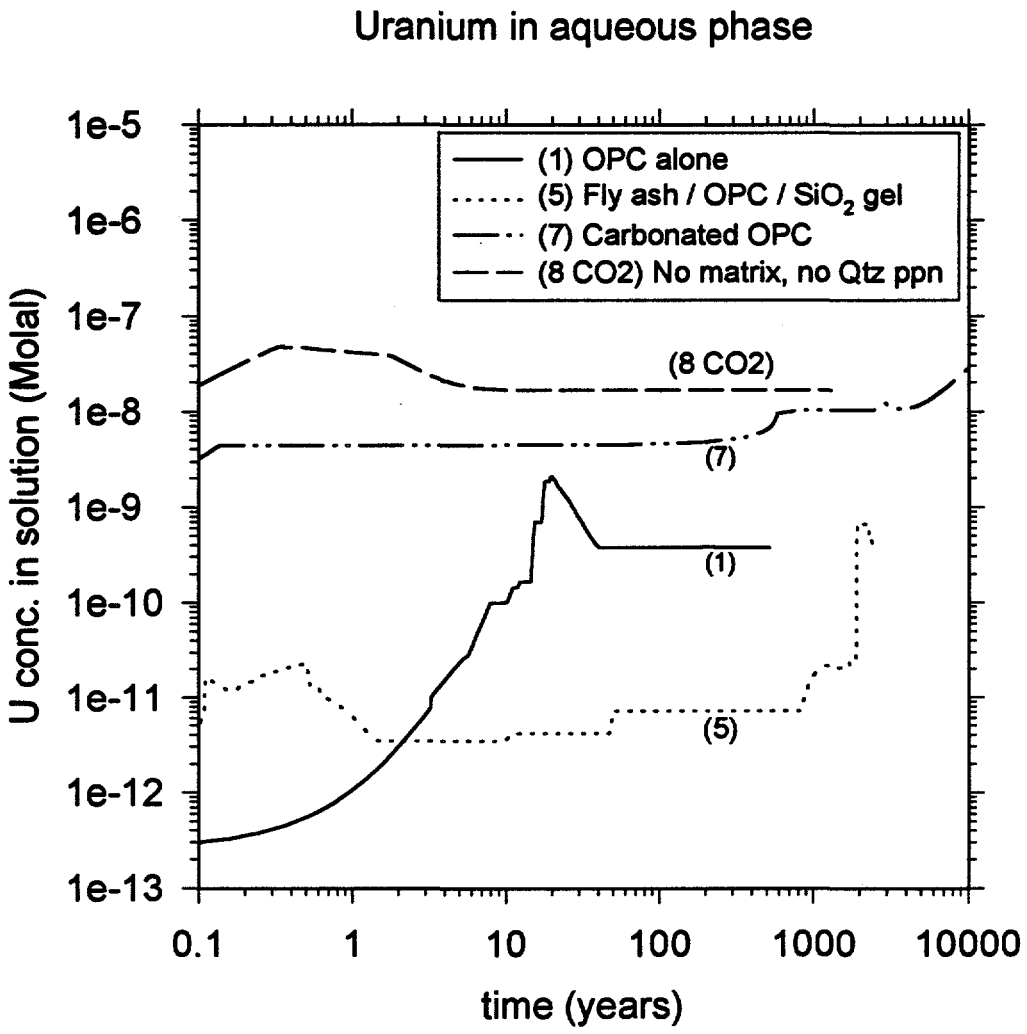

Figure 20. The relatively high U concentrations for cases (7) and (8 CO2) are due to aqueous U carbonate complexes.

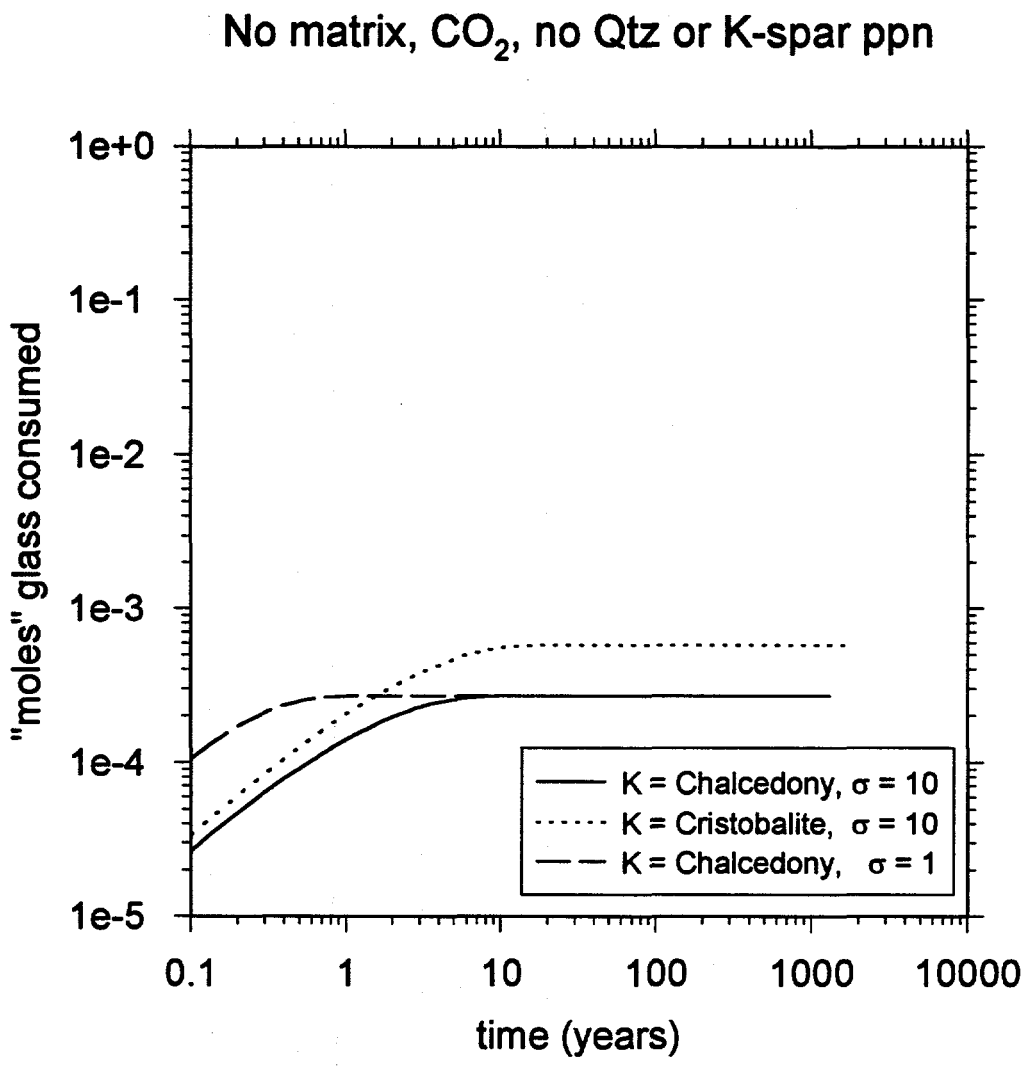

Figure 21. Effect of parameters in affinity term $[1-(Q/K)^{(1/\sigma)}]$ for run (8 CO2).

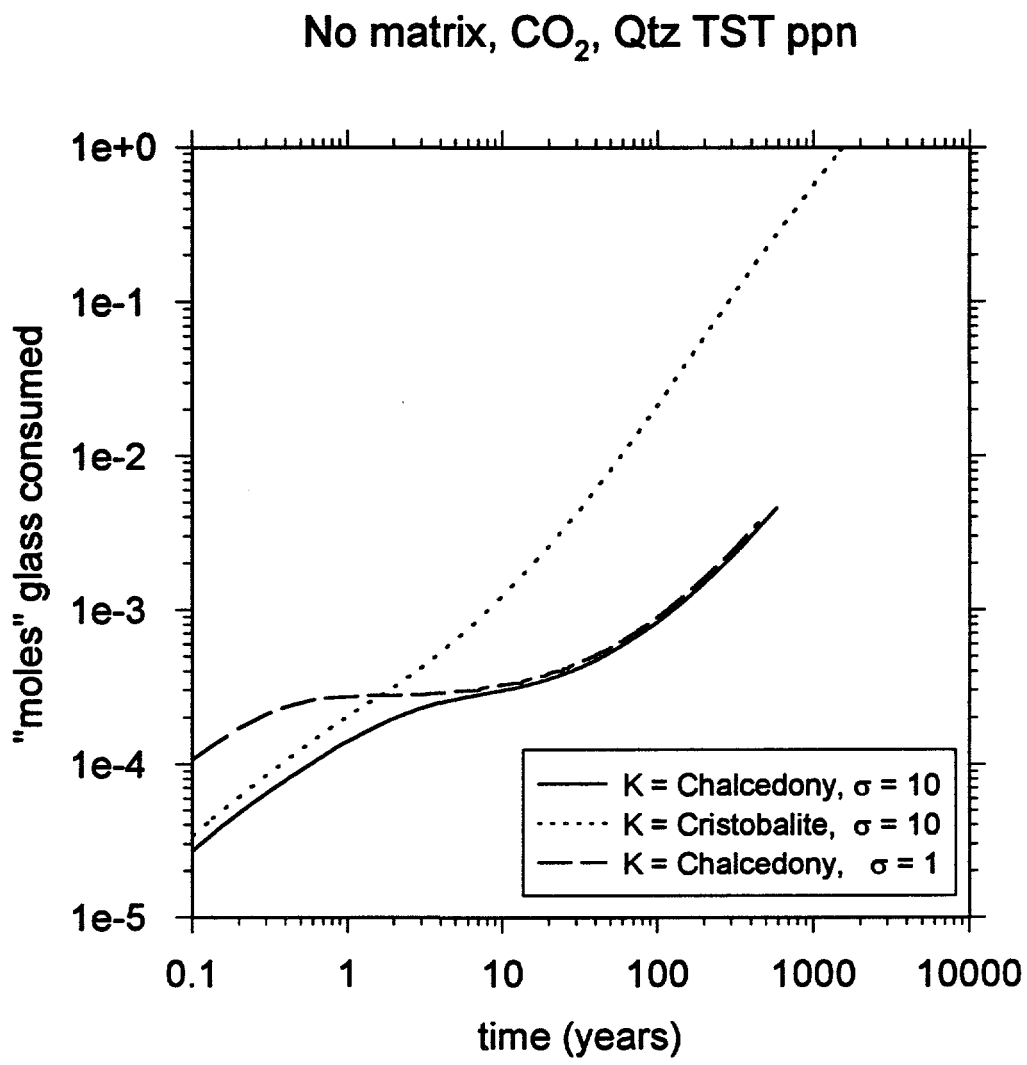

Figure 22. Effect of parameters in affinity term $[1-(Q/K)^{(1/\sigma)}]$ for run (6 CO2), no matrix, half pore space filled with water equilibrated to atmospheric CO_2 pressure ($10^{-3.5}$ atm).

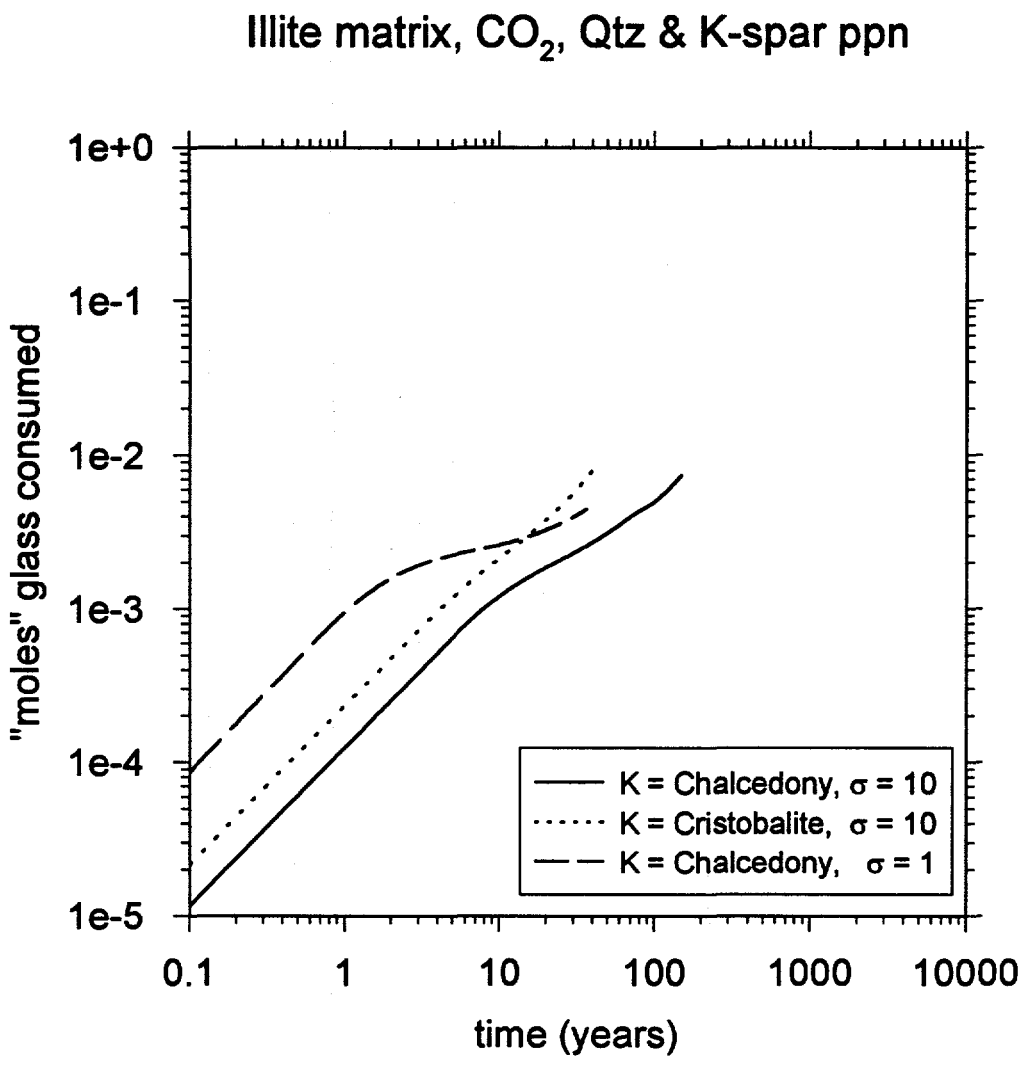

Figure 23. Effect of parameters in affinity term $[1-(Q/K)^{(1/\sigma)}]$ for run (10 CO2), illite matrix, pore water equilibrated to atmospheric CO_2 pressure ($10^{-3.5}$ atm).

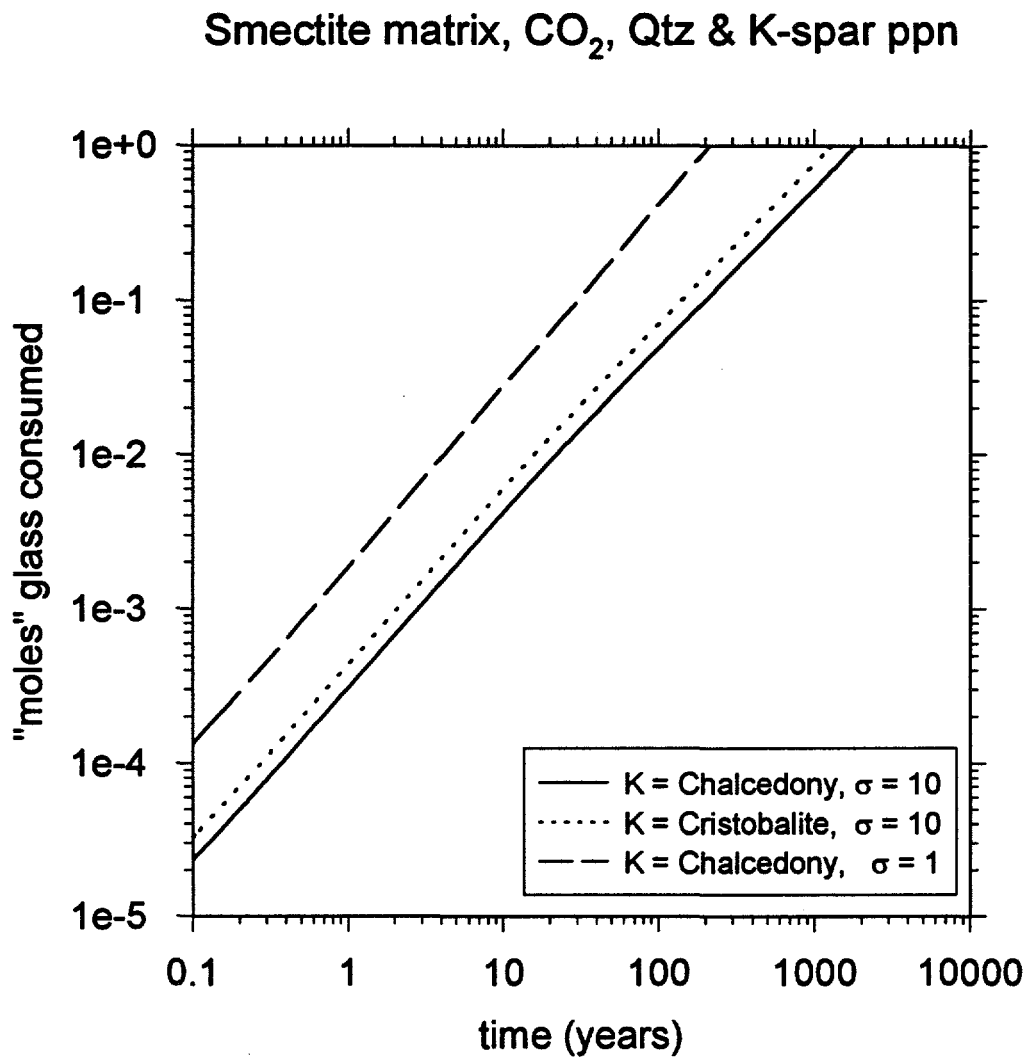

Figure 24. Effect of parameters in affinity term $[1-(Q/K)^{(1/\sigma)}]$ for run (9 CO2), Fe-Mg-rich smectite matrix, half pore space filled with water equilibrated to atmospheric CO_2 pressure ($10^{-3.5}$ atm).

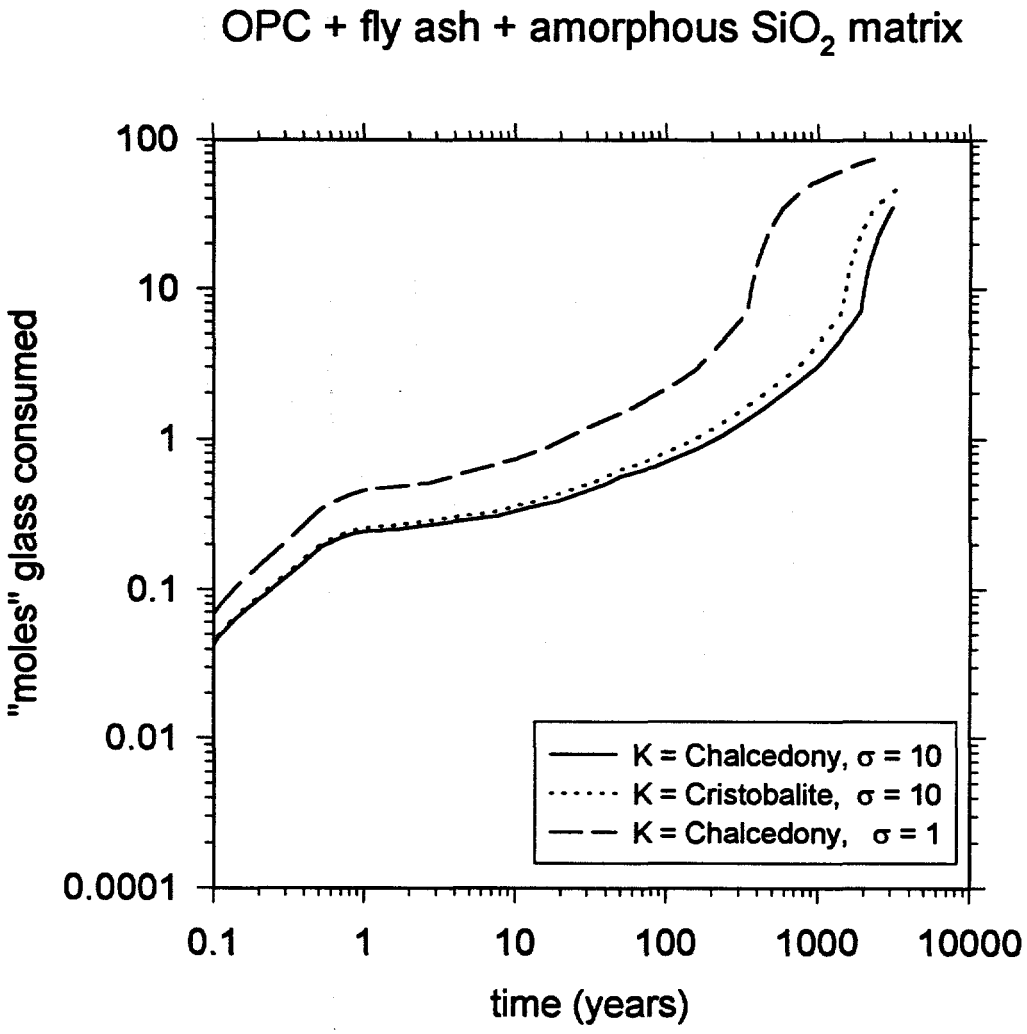

Figure 25. Effect of parameters in affinity term $[1-(Q/K)^{(1/\sigma)}]$ for run (5), OPC-fly ash-silica gel matrix, no CO_2 except that from original pore water (50 ppm HCO_3^-).

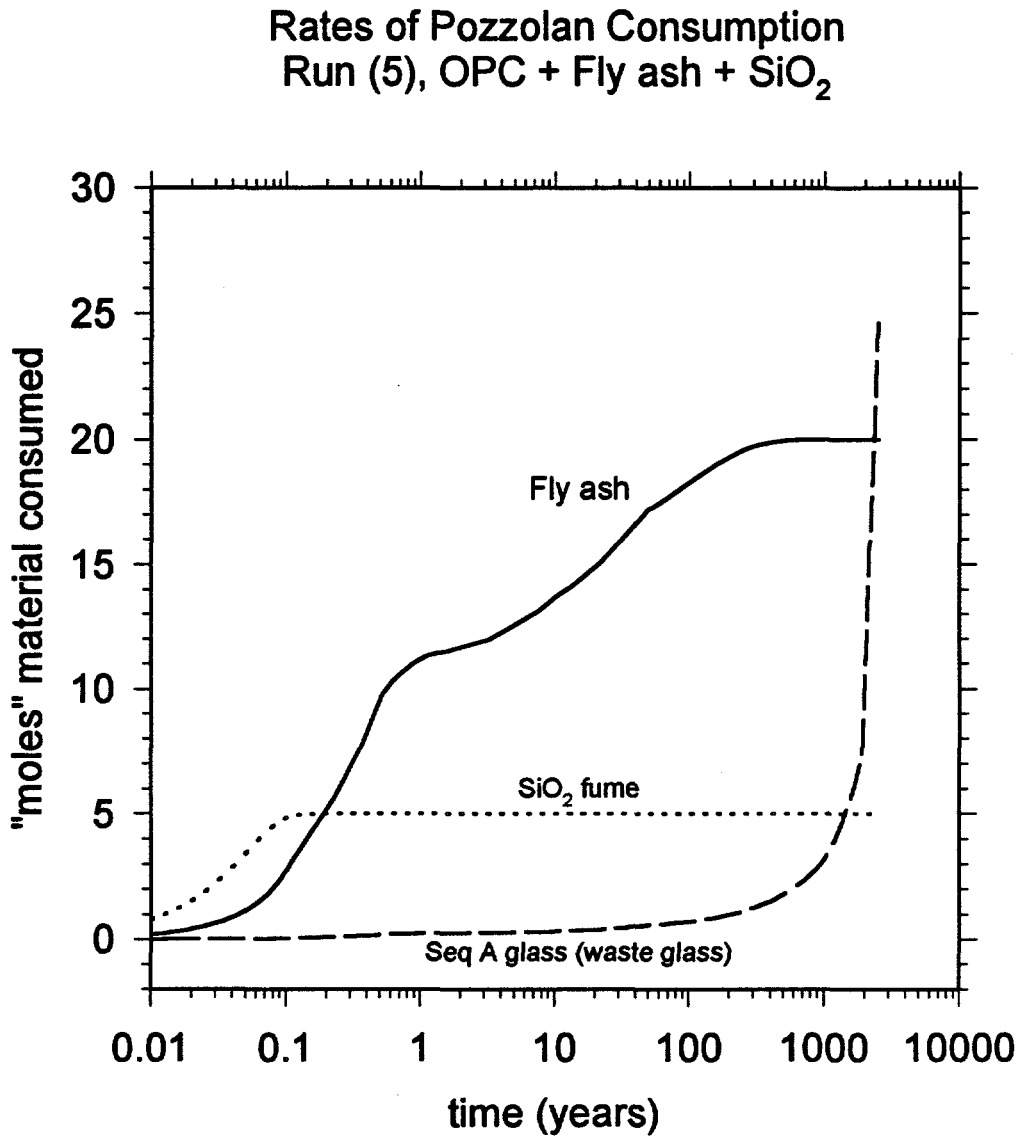

Figure 26. Calculated rate of consumption of the two pozzolanic additives (fly ash and SiO_2 fume), and the sequence A waste glass, for run (5). Fly ash is assumed to be in 10 μm particles, and the fume in 1 μm particles.

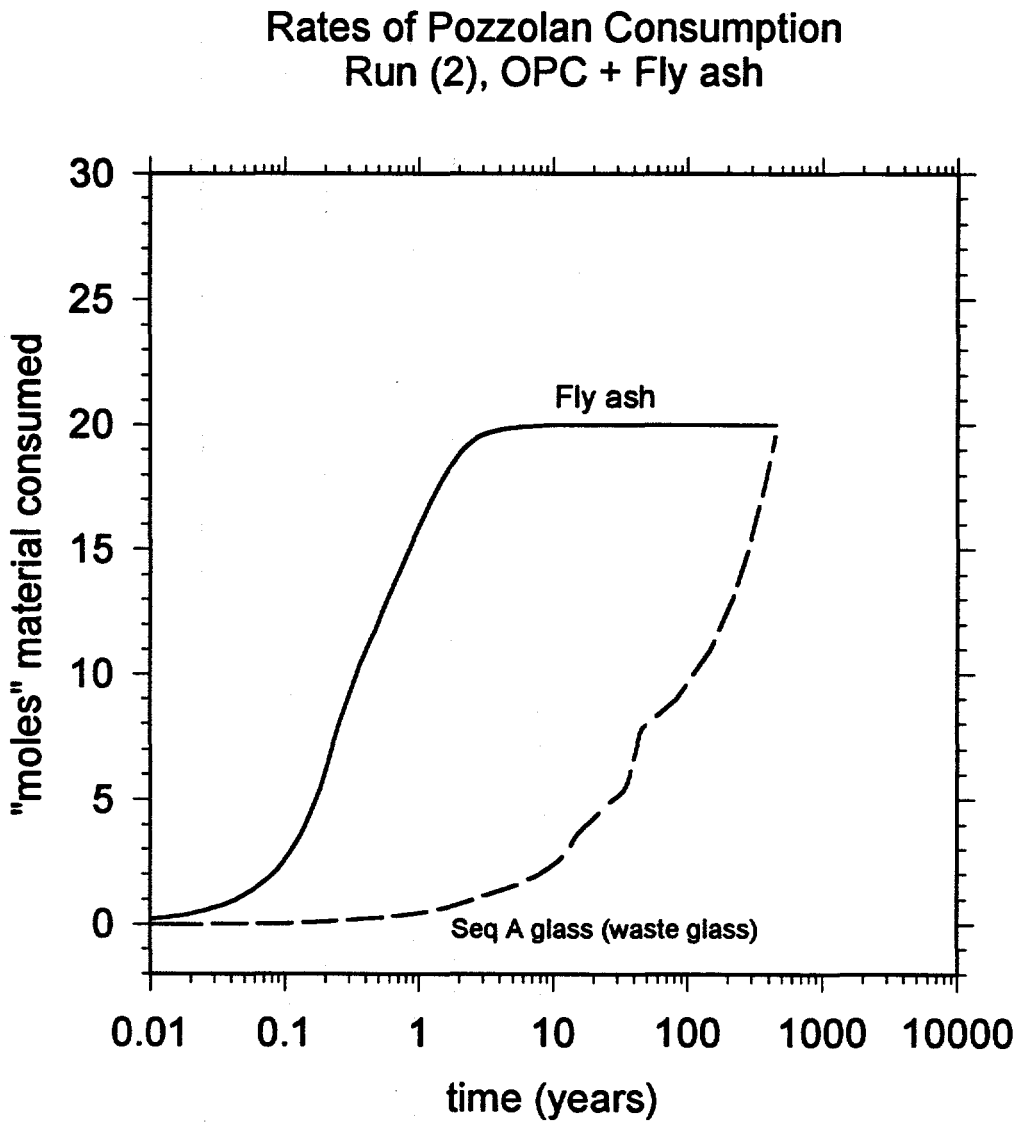

Figure 27. Calculated consumption of fly ash and sequence A glass for run (1). Fly ash is assumed to be in 10 μm particles.

11. Distribution

W.L. Bourcier, L-219
Lawrence Livermore National Laboratory
P.O. Box 808
Livermore, CA 94550

T.J. Wolery, L-219
Lawrence Livermore National Laboratory
P.O. Box 808
Livermore, CA 94550

J.K. Bates
CMT 205 H101
9700 South Cass Ave.
Argonne National Laboratory
Argonne, IL 60439

A. Campbell
ACRS / ACNW
U.S. Nuclear Regulatory Commission
Mail Stop T-2E26
Washington, DC 20555

L.A. Kovach
Waste Management Branch
U.S. Nuclear Regulatory Commission
MS T-9 B-3
Washington, D.C. 20555

E. O'Donnell
Waste Management Branch
U.S. Nuclear Regulatory Commission
MS T-9 B-3
Washington, D.C. 20555

J. Holbrook
Battelle
Pacific Northwest Laboratory
PO Box 999 / MS K9-81
Richland, WA 99352

N. Brown
DOE Richland Operations
P.O. Box 550 S7-53
Richland, WA 99352

R. Woods
Westinghouse Hanford Co.
1835 Terminal Drive
Vitro Building
MS H503
Richland, WA 99352

M. John Plodinec
Westinghouse Savannah River Corporation
Building B-120 Room 773-A
Aiken, SC 29808

C.E. Morris
Dept. of Civil and Mining Engineering
University of Wollongong
Wollongong, NSW
Australia, 2522

MS0734	L.D. Bustard, 6624 (1)
MS0750	P.V. Brady, 6118 (1)
MS0750	J.L. Krumhansl, 6118 (1)
MS0750	K.L. Nagy, 6118 (1)
MS0750	H.W. Stockman, 6118 (1)
MS0750	H.R. Westrich, 6118 (1)
MS1320	E.J. Nowak, 6119 (1)
MS1320	H.W. Papenguth, 6119 (1)
MS1320	M.D. Siegel, 6119 (1)
MS1322	F.D. Hansen, 6121 (1)
MS1335	M.S.Y. Chu, 6705 (1)
MS1342	L.H. Brush, 6348 (1)
MS 1345	D.P. Gallegos, 6331 (1)
MS0899	Technical Library, 4414 (5)
MS0619	Print Media, 12615 (1)
MS0100	Document Processing, 7613-2 (2) For DOE/OSTI
MS9018	Central Technical Files, 8523-2 (1)